UNIVERSITÀ DEGLI STUDI DI CAGLIARI

DOTTORATO DI RICERCA

Scienze e Tecnologie Farmaceutiche
Ciclo XXVII

Exploitation of Ebola Virus VP35 Protein to Identify New Drugs Counteracting its Type I IFN Antagonism

Settore scientifico disciplinare di afferenza
Microbiologia BIO/19

Relatore:
Prof. Enzo Tramontano

Correlatore:
Prof. Elias Maccioni

Presentata da:
Dott.ssa Valeria Cannas

Coordinatore Dottorato:
Prof. Elias Maccioni

Esame Finale Anno Accademico 2013 – 2014

Abstract

Ebolaviruses (EBOVs) are among the most virulent and deadly pathogens ever known, causing fulminant haemorrhagic fevers in humans and non-human primates. The 2014 outbreak of Ebola virus disease (EVD) in West Africa has claimed more lives than all previous EVD outbreaks combined. The EBOV high mortality rates have been related to the virus-induced impairment of the host innate immunity reaction due to two virus-coded proteins, VP24 and VP35. EBOV VP35 is a multifunctional protein, it is essential for viral replication as a component of the viral RNA polymerase and it also participates in nucleocapsid assembly. Early during EBOV infection, alpha-beta interferon (IFN-α/β) production would be triggered upon recognition of viral dsRNA products by cytoplasmic retinoic acid-inducible gene I (RIG-I)-like receptors (RLRs). However, this recognition is efficiently prevented by the double-stranded RNA (dsRNA) binding activity of the EBOV VP35 protein, which hides RLRs binding sites on the dsRNA phosphate backbone as well the 5'-triphosphate (5'-ppp) dsRNA ends to RIG-I recognition. In addition to dsRNA binding and sequestration, EBOV VP35 inhibits IFN-α/β production preventing the activation of the IFN regulatory factor 3 (IRF-3) by direct interaction with cellular proteins. Previous studies demonstrated that single amino acid changes in the VP35 dsRNA binding domain reduce EBOV virulence, indicating that VP35 is an attractive target for antiviral drugs development. Within this context, here we report the establishment of a novel method to characterize the EBOV VP35 inhibitory function of the dsRNA-dependent RIG-I-mediated IFN-β signaling pathway in a BLS2 cell culture setting. In such system, a plasmid containing the promoter region of IFN-β gene linked with a luciferase reporter gene was transfected, together with a EBOV VP35 mammalian expression plasmid, into the IFN-sensitive A549 cell line, and the IFN-induction was stimulated through dsRNA transfection. Through alanine scanning mutational studies with biochemical, cellular and computational methods we highlighted the importance of some VP35 residues involved in dsRNA end-capping binding, such as R312, K282 and R322, that may serve as target for the development of small-molecule inhibitors against EBOV. Furthermore, we identified a synthetic compound that increased IFN-induction only under antiviral response stimulation and subverted VP35 inhibition, proving to be very attractive for the development of an antiviral drug. In conclusion, our results provide the establishment of a new assay as a straightforward tool for the screening of antiviral compounds that target *i)* dsRNA-VP35 or cellular protein-VP35 interaction and *ii)* dsRNA-dependent RIG-I-mediated IFN signaling pathway, in order to potentiate the IFN response against VP35 inhibition, setting the bases for further drug development.

1.0. INTRODUCTION

1.1. Ebola virus

1.1.1. Classification and taxonomy

Ebolaviruses (EBOVs) constitute a group of filamentous, enveloped, non-segmented viruses that owns a single and negative-stranded RNA genome with the characteristic gene order *3´- UTR - core proteins genes - envelope protein genes - polymerase gene - 5´-* UTR. The genus *Ebolavirus*, along with *Marburgvirus* and *Cuevavirus*, belong to the family *Filoviridae,* order of *Mononegavirales*. The family name is derived from "filum", which is Latin for thread, reflecting the agents unique filamentous morphology (Kuhn et al. 2010) (Fig. 1b). Since the discovery, in 1967, of Marburg virus as the first member of the group, classification and taxonomy of filoviruses have changed continuously and the criteria used refer to the most updated terminology with which EBOVs are currently known, named and classified (Kuhn et al. 2010). The family *Filoviridae*, located in the order *Mononegavirales*, is positioned among the *Paramyxoviridae*, *Rhabdoviridae* and *Bornaviride* viral families, which all share similar organization in their negative-sense, single-stranded RNA (ssRNA-) genome. The family *Filoviride* actually comprises three genera, *Marburgvirus*, *Ebolavirus* and *Cuevavirus*, which are all antigenically different. The genera *Marburgvirus* and *Cuevavirus* include each only one single viral species, namely *Marburg marburgvirus* (MARV) and *Lloviu cuevavirus* (LLOV) respectively, while the genus *Ebolavirus* comprises five distinct species: *Bundibugyo ebolavirus* (BDBV), *Zaire ebolavirus* (EBOV), *Reston ebolavirus* (RESTV), *Sudan ebolavirus* (SUDV) and *Taï Forest ebolavirus* (TAFV) (Fig. 1a). According to the rules for taxon naming established by the International Committee on Taxonomy of Viruses (ICTV), the name of the genus *Ebolavirus* is always to be capitalized, italicized, never abbreviated, and to be preceded by the word "genus". The names of its members (ebolaviruses) are to be written in lower case, are not italicized, and used without articles (Kuhn et al. 2010).

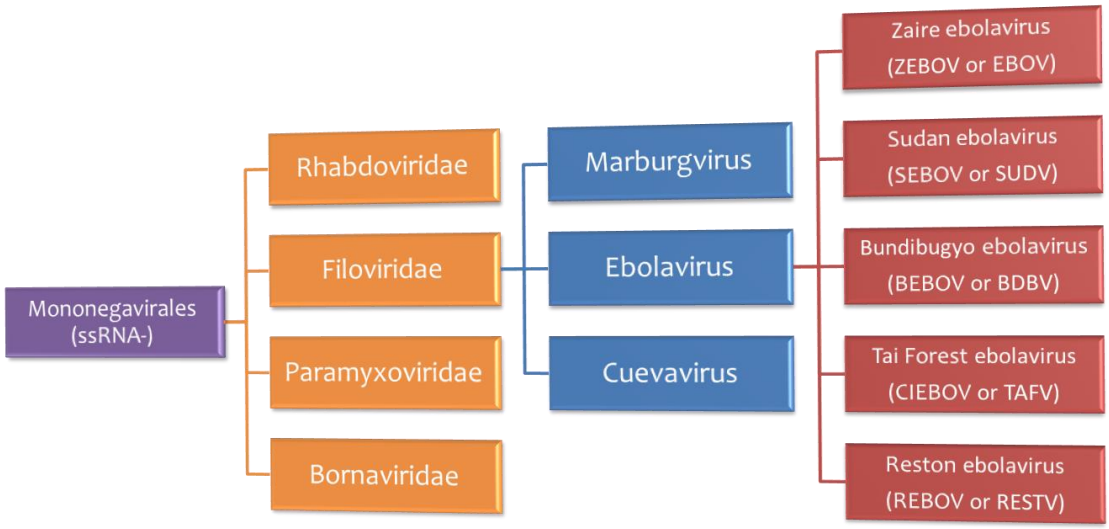

a

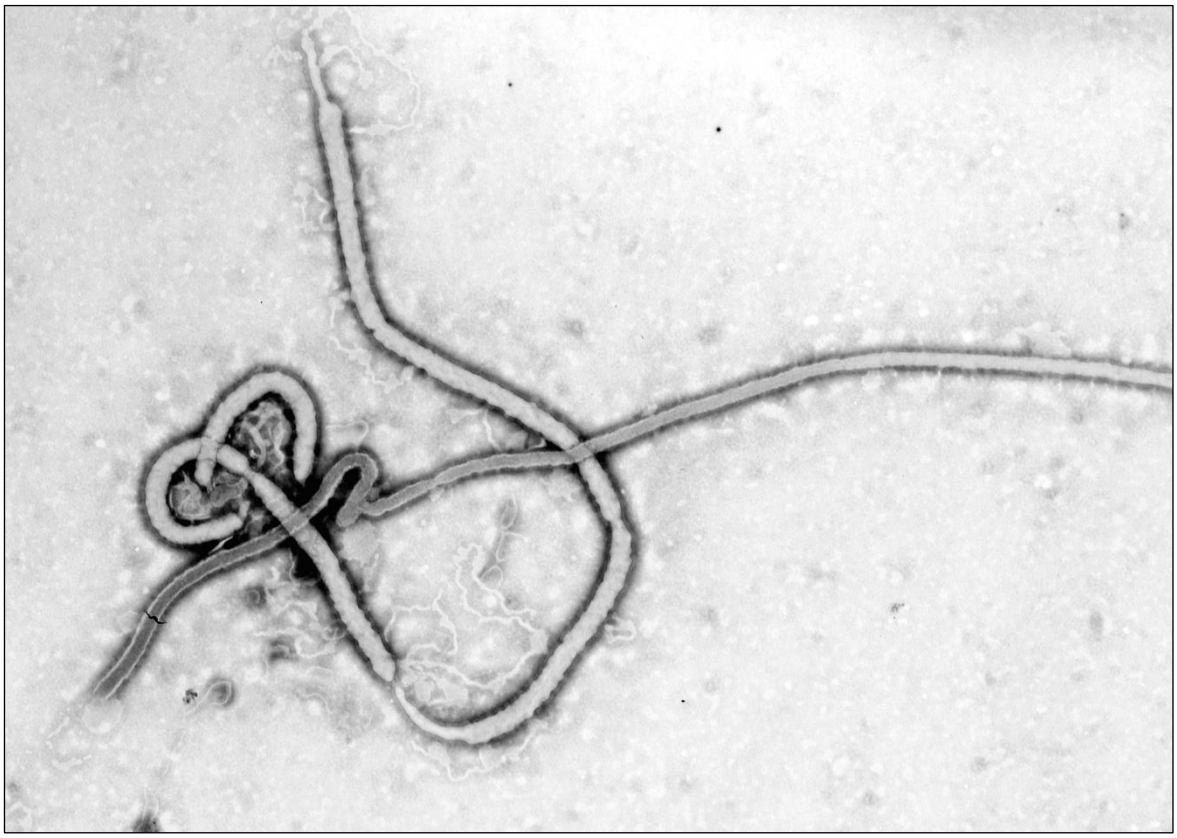

b

Figure 1. Taxonomy and morphology of Ebolaviruses. (a) Current classification of Ebolaviruses according to the 8th Report of the International Committee on Taxonomy of Viruses (ICTV), with the most recently proposed changes in classification and nomenclature (Kuhn et al. 2010) as well as in phylogenetic relationship (Barrette et al. 2011). (b) A transmission electron micrograph shows the ultrastructural morphology displayed by an Ebola virus virion (CDC - Frederick A. Murphy).

1.1.2. Epidemiology of Ebola virus disease

The first recorded outbreaks of Ebola virus disease (EVD), that showed the symptoms of a severe haemorrhagic fever, occurred in June 1976 in southern Sudan (now South Sudan) and in July 1976 in the vicinity of a mission hospital in Yambuku, Zaire (now Democratic Republic of the Congo, DRC) (Deng et al. 1978; Burke et al. 1978; Bres 1978). Although the outbreaks occurred at a similar time and in the same geographical area of central Africa (Yambuku is ~500 km from Nzara), no definite link between them was established, and later virological studies demonstrated differences between the two strains, subsequently described as the Sudan and Zaire strains (McCormick et al. 1983; Richman et al. 1983). The Sudan outbreak began in the town of Nzara, 400 km from the regional capital Juba, and affected workers in a cotton-processing factory. A symptomatic case was transferred to the district hospital of Maridi, where explosive nosocomial transmission occurred. Within four weeks, one-third of the 220 hospital staff had acquired infection, and 41 had died. At this time, there was no knowledge of the mode of transmission of this 'new' disease, and no effective infection control activities or personal protective equipment (PPE) were available. Maridi hospital acted as an amplifier for cases in the community, and by the end of the outbreak in October there had been 284 cases and 151 deaths. Two months after the first case in Nzara, a similar disease became apparent in a mission hospital in Yambuku, Zaire. The initial infections occurred in patients who had attended the outpatient clinic of the hospital. Parenteral injections with syringes not sterilized between patients, from an initial unsuspected index case, were presumed to be the route of transmission. Subsequent transmission then occurred within the hospital and from infected patients into the community. A total of 318 known cases occurred, with 280 deaths, a case fatality rate of 88%. Eleven of the 17 nursing/clinical staff of the hospital died. No patient whose contact was exclusively parenteral injection survived. Investigations indicated that the index case had eaten bush meat during recent forest travel. Because of the dramatic nature of the illness and the clinical symptoms that resembled those

observed during another haemorrhagic fever-like disease, occurred in 1967 in Marburg, Frankfurt (Germany) and in Belgrade (former Yugoslavia), the two African outbreaks were initially suspected to be caused by MARV, the viral agent that had been incidentally transmitted to laboratory workers from tissues of infected monkeys imported from Uganda, causing 31 human infections in Europe, with 7 deaths. The two outbreaks occurred in Sudan and Zaire in 1976, however, were soon found to be caused by two new filoviruses, detected and isolated from clinical samples collected during the outbreaks. Morphologically similar to MARV but antigenically distinct from it, the name "Ebola virus", Sudan and Zaire subtypes, was respectively attributed to them after the small river Ebola, headwater if the Mongala river, a tributary of Congo river (former Zaire), that flows past Yumbuku (Kuhn 2008).

Following the 1976 Sudan and Zaire outbreaks, there have been 18 documented EVD outbreaks in central Africa, and one isolated case in Côte d'Ivoire (in 1974). Epidemiologically, these outbreaks fall into three main groups: those occurring in remote forest areas, linked directly to bush meat consumption, and usually with relatively few cases; those centred around and within regional hospitals, with considerable hospital transmission, spreading into the community; and those occurring in populated rural areas, with mainly community transmission but some transmission in local health facilities. No EVD outbreaks were reported between 1979 and 1994, but after 1994 the number of recognised outbreaks increased. In November 1994, a wave of infections hit three gold-mining camps in Gabon, from which the virus spread with a wave of secondary and tertiary cases among villages along the border with Cameroon. Overall, 52 infections occurred, with 32 deaths (mortality rate of 60%) (Pourrut et al. 2005). An isolated case of Ebola infection occurred in Côte d'Ivoire in 1994 (Formenty et al. 1999) in an expatriate zoologist after undertaking an autopsy on a chimpanzee in the Tai forest area. The zoologist was repatriated and survived. Virology studies showed the strain to be different from those of Sudan and Zaire, and was designated Ebola Tai forest strain (Le Guenno et al. 1995). Forest area outbreaks have occurred in Gabon, Republic of the Congo and DRC (Formenty et al. 2003; Nkoghe et al. 2005; Rouquet et al.

2005; Nkoghe et al. 2011). With the exception of two large, extended, outbreaks in Republic of the Congo and DRC, reported case numbers ranged from 12 to 65, and case fatality rates from 57% to 83%. One outbreak in DRC was closely associated with fruit bat migration and consumption (Leroy et al. 2009; Grard et al. 2011). Two large outbreaks have occurred linked to regional hospitals, in DRC in 1995 and in Uganda, 2000 (Khan et al. 1999; Centers for Disease Control and Prevention (CDC) 2001; Lamunu et al. 2004). The outbreak in DRC occurred in Kikwit, a 350-bed regional hospital, resulting in infection in 80 healthcare workers (though some may have been infected in the community), and subsequent spread to other hospitals following patient transfer (Ndambi et al. 1999; Muyembe-Tamfum et al. 1999). The Uganda outbreak, in Gulu district, was centred on two hospitals and the surrounding communities. There were 425 cases and 224 deaths, including 17 hospital staff. Many of the community cases were associated with attendance at burials. The outbreak spread to another area 150 km distant when a patient was transferred to another hospital (Borchert et al. 2011). Outbreaks in rural communities with some health facilities involvement have occurred in South Sudan and Uganda with case numbers ranging from 6 to 34 except for an extended outbreak in DRC (Baron et al. 1983; Onyango et al. 2007; Shoemaker et al. 2012; Albariño et al. 2013). In 2007 a new strain of Ebola virus was isolated in an outbreak in Bundibugiyo district of Uganda, resulting in 147 reported cases, but a lower case fatality rate than with Zaire or Sudan strains (Wamala et al. 2010; MacNeil et al. 2010; Roddy et al. 2012). An outbreak caused by the same strain (now termed the Bundibugyo strain) occurred in DRC in 2012, though no links were discovered between the two areas (World Health Organization (WHO) 2012).

On March 21, 2014, the Guinea Ministry of Health reported the outbreak of an illness characterized by fever and severe diarrhoea, with a case fatality rate of 59% in the first 49 cases notified. Specimens from 15 of the patients tested were positive for Ebola virus, Zaire strain (Dixon & Schafer 2014). By March 30th, cases were reported in a neighbouring area of Liberia, and in May, the first cases in Sierra Leone occurred. By the middle of June, the outbreak had become the

largest EVD outbreak ever reported, with a total of 528 cases and 337 deaths. By August 8th, there had been a total of 1848 cases and 1013 deaths, spread between the three countries and a small travel-related cluster in Nigeria, and an international public health emergency was declared by WHO (Briand et al. 2014). A number of studies have investigated the possible origin of the outbreak. It was established that the first case, linked through a chain to the cases reported in Guinea on March 21st, was a child in the Gueckedou region of south-eastern Guinea who died on December 6th, 2013 (WHO Ebola Response Team 2014). Virology studies have subsequently confirmed that the virus is the Zaire strain, with 97% homology with earlier strains from DRC and Gabon (Baize et al. 2014). At February 10, 2015, the total reported case number for Guinea, Sierra Leone, and Liberia was 22859, and 9162 deaths (Centers for Disease Control and Prevention (CDC) 2015a). The global dimension of the West Africa outbreak has been demonstrated by the transmission of infection to healthcare workers in hospitals in Europe and the USA, from index cases repatriated from Liberia (Parra et al. 2014; McCarty et al. 2014) (Fig. 2 and Table 1).

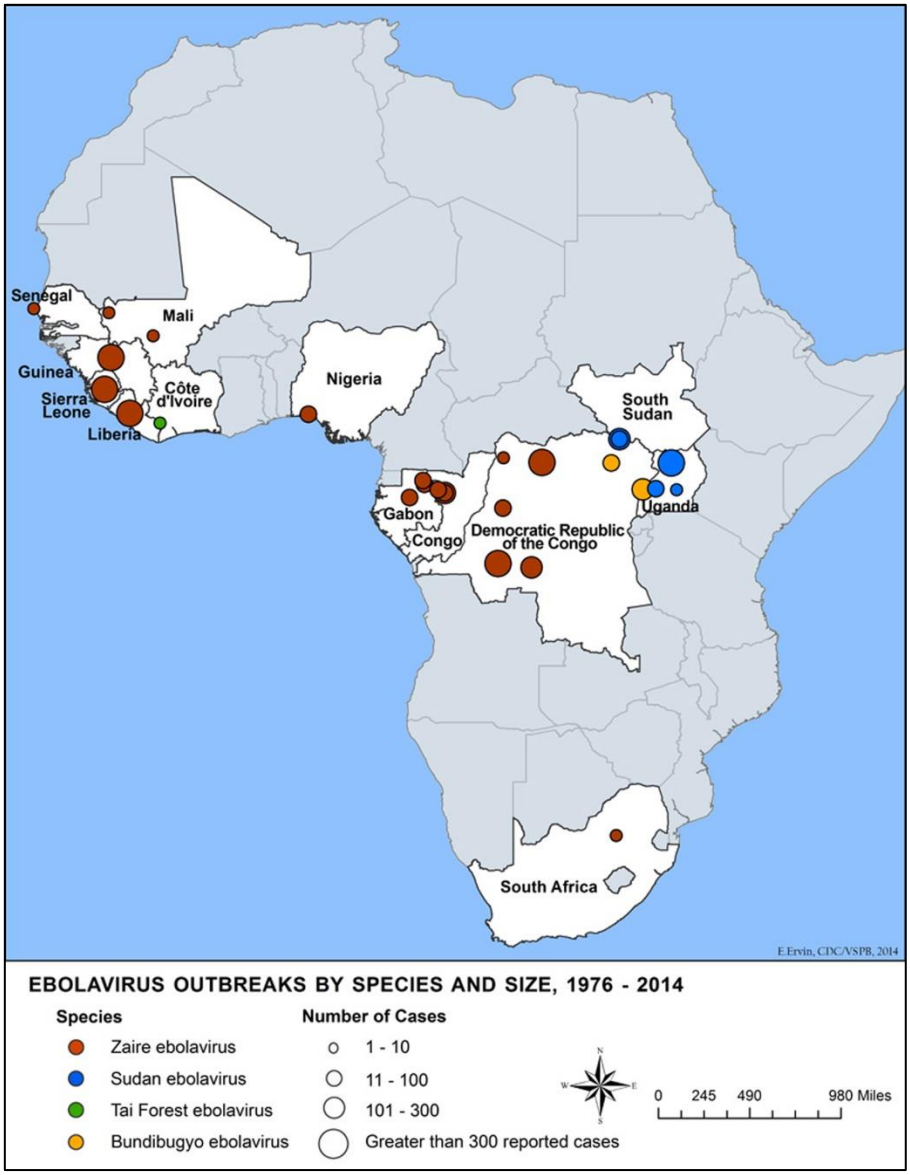

Figure 2. Locations of Ebolavirus infections and outbreaks. Geographic distribution of Ebolavirus natural human outbreaks reported worldwide, as of February 2015. Locations are pointed with pins according to the color-coded and different sizes legend for Ebolavirus species and number of cases, respectively (Centers for Disease Control and Prevention (CDC) 2015b).

Table 1. Outbreaks Chronology: Ebola Virus Disease. Known cases and outbreaks of Ebola Virus Disease, in reverse chronological order (Centers for Disease Control and Prevention (CDC) 2015b).

Year(s)	Country	Ebola subtype	Reported number of human cases	Reported number (%) of deaths among cases
August-November 2014	Democratic Republic of the Congo	Zaire virus	66	49 (74%)
March 2014-Present	Multiple countries	Zaire virus	23406	9457 (40%)
November 2012-January 2013	Uganda	Sudan virus	6*	3* (50%)
June-November 2012	Democratic Republic of the Congo	Bundibugyo virus	36*	13* (36.1%)
June-October 2012	Uganda	Sudan virus	11*	4* (36.4%)
May 2011	Uganda	Sudan virus	1	1 (100%)
December 2008-February 2009	Democratic Republic of the Congo	Ebola virus	32	15 (47%)
November 2008	Philippines	Reston virus	6 (asymptomatic)	0
December 2007-January 2008	Uganda	Bundibugyo virus	149	37 (25%)
2007	Democratic Republic of the Congo	Ebola virus	264	187 (71%)
2004	Russia	Ebola virus	1	1 (100%)
2004	Sudan (South Sudan)	Sudan virus	17	7 (41%)
November-December 2003	Republic of the Congo	Ebola virus	35	29 (83%)
December 2002-April 2003	Republic of the Congo	Ebola virus	143	128 (89%)
October 2001-March 2002	Republic of the Congo	Ebola virus	57	43 (75%)
October 2001-March 2002	Gabon	Ebola virus	65	53 (82%)
2000-2001	Uganda	Sudan virus	425	224 (53%)
1996	Russia	Ebola virus	1	1 (100%)
1996	Philippines	Reston virus	0	0
1996	USA	Reston virus	0	0
1996	South Africa	Ebola virus	2	1 (50%)
1996-1997 (July-January)	Gabon	Ebola virus	60	45 (74%)
1996 (January-April)	Gabon	Ebola virus	37	21 (57%)
1995	Democratic Republic of the Congo (formerly Zaire)	Ebola virus	315	250 (81%)
1994	Côte d'Ivoire (Ivory Coast)	Taï Forest virus	1	0
1994	Gabon	Ebola virus	52	31 (60%)
1992	Italy	Reston virus	0	0
1989-1990	Philippines	Reston virus	3 (asymptomatic)	0
1990	USA	Reston virus	4 (asymptomatic)	0
1989	USA	Reston virus	0	0
1979	Sudan (South Sudan)	Sudan virus	34	22 (65%)
1977	Zaire	Ebola virus	1	1 (100%)
1976	England	Sudan virus	1	0
1976	Sudan (South Sudan)	Sudan virus	284	151 (53%)
1976	Zaire (Democratic Republic of the Congo - DRC)	Ebola virus	318	280 (88%)

1.1.3. Nature reservoirs and life cycle of EBOVs

EVD is a zoonotic disease, and the viruses implicated in human outbreaks are thought to originate in live or dead animals (Pourrut et al. 2005). The circulation of the virus among humans is insufficiently understood, possibly explaining the sporadic nature of the outbreaks (Fauci 2014). Despite advances in understanding the molecular biology and the pathogenesis of filoviruses, identifying the reservoir from where the virus spills into humans and non-human primates, and understanding the factors that facilitate this process, remain challenging (Groseth et al. 2007; Negredo et al. 2011). It was proposed that either the reservoir is a rare species, or that transmission within the reservoir itself is not efficient (Feldmann et al. 2004). In most Ebola virus outbreaks, the source of the infection in the index case has not been determined. Examples are the 1976 outbreaks , the 1995 Mekouka and Kikwit outbreaks, 1996 Bouée outbreak and other subsequent outbreaks from Sudan and Uganda (Pourrut et al. 2005). In several other human Ebola virus outbreaks, such a number from Gabon and the DRC, human infections occurred concomitantly with an increased mortality among non-human primates, such as gorillas and chimpanzees (Rouquet et al. 2005; Muyembe-Tamfum et al. 2012). In 1994, an ethnologist became infected in Côte D'Ivoire after performing an autopsy on a chimpanzee that died during an outbreak in the Taï National Park (Le Guenno et al. 1995; Muyembe-Tamfum et al. 2012). In a 1994 outbreak that affected gold-diggers from Minkebé, Gabon, which was initially confused with yellow fever, people killed a sick gorilla for food (Amblard et al. 1997; Muyembe-Tamfum et al. 2012). Prior to the 1996 Mayibout outbreak in Gabon, children found and butchered a chimpanzee carcass in the forest, and in several subsequent outbreaks it was documented that prior to developing disease, people handled animal carcasses that they found (Pourrut et al. 2005; Le Guenno et al. 1995). Since non-human primates are also susceptible to the infection, they are considered to be intermediate hosts (Georges et al. 1998). Several studies attempted to identify the natural reservoir of the filoviruses. Even though over 8000 vertebrates and 30,000 invertebrates have been captured and tested for the presence of the virus since the first reported

EVD outbreaks in 1976, the reservoir for the infection remains elusive (Pourrut et al. 2007). Small animals, reptiles, arthropods and plants were proposed, at various times and by various authors, as likely reservoirs involved in transmitting the Ebola and Marburg viruses (Feldmann et al. 2004; Ascenzi et al. 2008). Several lines of evidence point towards the possibility that fruit bats could be the natural reservoir of the Ebola virus (Weingartl et al. 2012), and it is conceivable that a different reservoir exists for each of the Ebola virus subtypes (Georges et al. 1998; Feldmann et al. 2004). One of these pieces of evidence is the observation that in some outbreaks, such as the 1995 outbreak from Kikwit (the DRC), the 2007 outbreak from Mweka (the DRC), the 2000 outbreak from Gulu (Uganda) and the 2004 outbreak from Yambio (Sudan), the hunting and eating of fruit bats was linked to the human outbreaks (Muyembe-Tamfum et al. 2012). As a result of these observations, several studies proposed to examine evidence of Ebola virus infection in bats and in other species. Although Ebola virus has never been isolated from bats in the wild, the detection of the virus in bats by PCR and serologic evidence indicates that they may be a reservoir for the Ebola virus (Takada 2012; Bausch & Schwarz 2014). The possibility that bats may be a reservoir for the virus is also supported by many studies on the Marburg virus infections (Towner et al. 2009; Amman et al. 2012). Demonstrating direct transmission from putative reservoirs, such as bats, is difficult because of the nature of bat bites, which are often invisible and painless, but evidence for this route, even though circumstantial, is powerful (Feder et al. 1997; Oczkowski 2007; Edson et al. 2011; Johnson et al. 2014). Bats, also known as 'flying foxes', the only known flying mammals in the world, and among the most ancient of the mammals, inhabit all continents except Antarctica, and represent almost 25% of the recognised mammal species (Calisher et al. 2006; Omatsu et al. 2007). Bats live on average 3.5-times longer than a mammal of similar size, promoting the persistence of the virus in the host and increasing the likelihood of transmission (Hayward et al. 2013; Smith & Wang 2013). This, along with other characteristics, such as bat migration and their population structure and migration patterns, make them particularly suitable reservoirs for viruses (Calisher et al. 2006; Stein 2015).

EBOVs transmission likely begins unidirectionally (Fig. 3), with reservoirs bats chewing and sucking the pulp of certain fruits, thereby contaminating them with their saliva. Masticated fibres or urine and feces may then contaminate the ground as bats feed, and such partially eaten fruits and wastes may be consumed in the tree canopy or in the ground by highly susceptible secondary hosts, including gorillas, chimpanzees, monkeys, duikers and rodents. Once infected, accidental hosts can sustain virus transmission through both intra-specific and inter-specific direct contacts. Human infection may occur after hunting, butchering and consumption of bushmeat from one of these hosts, or, alternatively, through contaminated fruits by bats excreta. Hence, human-to-human transmission can be repeatedly sustained within the wave-like spread of an outbreak (Pourrut et al. 2005; Groseth et al. 2007; Gonzalez et al. 2007).

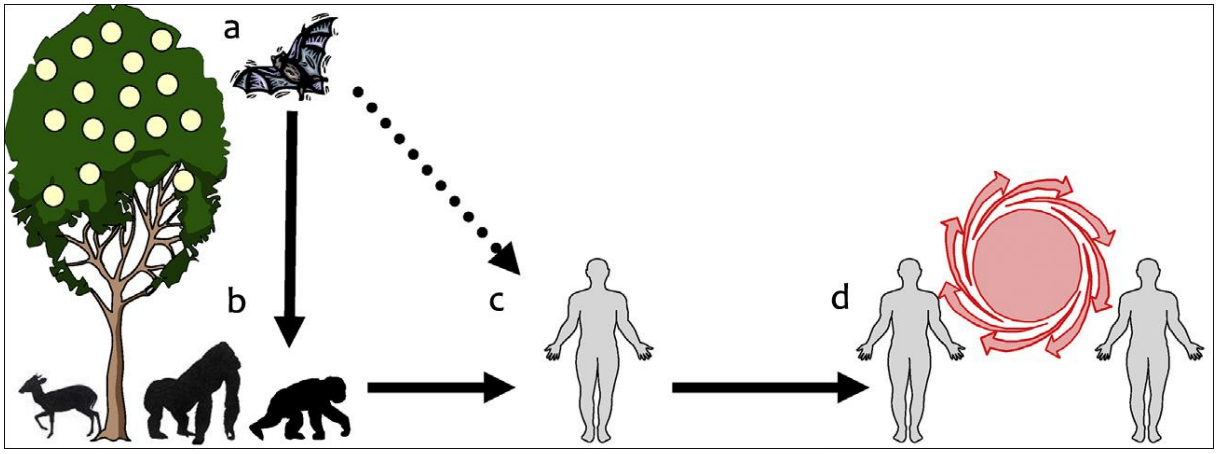

Figure 3. Mechanism of Ebolavirus transmission in nature. (a) Proposed virus reservoir: fruit bats. The virus maintains itself in fruit bats. The bats spread the virus during migration. (b) Epizootic in primates. Infected fruit bats enter in direct contact with other animals and pass on the infection, sometimes causing large-scale epidemics in gorilla, chimpanzees and other monkeys or mammals (e.g. forest antelopes). (c) Primary human infection. Humans are infected either through direct contact with infected bats (rare event), or through handling infected dead or sick animals found in the forest (more frequent). (d) Secondary transmission. Secondary human-to-human transmission occurs through direct contact with the blood, secretions, organs or other body fluids of infected persons. High transmission risk when providing direct patient care or handling dead bodies (funerals).

1.1.4. Clinical manifestation of EVD

The clinical manifestations of EVD were described during the initial outbreaks in DRC and Sudan in 1976; more details were reported for a large number of patients after the 1995 Kikwit epidemic, and shorter descriptions have appeared for subsequent outbreaks (Bwaka et al. 1999; Kortepeter et al. 2011). It seems that different species of EBOV might cause somewhat different clinical manifestations. Generally, EVD is a severe acute viral illness often characterized by the sudden onset of fever followed by a 2-3-day initial period with non-specific symptoms: fever, severe headache, muscle pain, intense weakness, sore throat, and sometimes conjunctive injection. This is followed by a 2-4-day deteriorating period with severe sore throat, chest and abdominal pain, maculopapular skin rash on the trunk and shoulders, diarrhoea, vomiting, impaired kidney and liver function, and in some cases both internal and external bleeding (Fig. 4). During this phase the lab results show low counts of white blood cells and platelets as well as elevated liver enzymes. For fatal cases, the 2-4-day terminal period is characterized by hemorrhage, hiccups, somnolence, delirium, and coma. Bleeding is manifested as maculopapular skin rash, petechiae, ecchymosis, uncontrolled bleeding from venepuncture sites, and postmortem evidence of visceral hemorrhagic effusions. Abortion is a common consequence of infection, and infants born from mothers dying of Ebola infection are fatally infected. Death in shock usually occurs 6-9 days after onset of clinical disease. During the EVD initial period, blood sampling shows that all sick individuals have circulating viral antigen. However, recent reports of EBOV and SUDV have shown that fatal illness is associated with high and increasing amounts of virus in the bloodstream. Conversely, patients who survive infection show a decrease in circulating virus with clinical improvement around day 7-10. In most cases, this improvement coincides with the appearance of EBOV-specific antibodies (Towner et al. 2004; Sanchez et al. 2004). Although EBOV disappears quickly from the bloodstream of recovering patients, it was isolated from seminal fluid of a few patients up to the 61st day after onset of illness in a laboratory acquired case. The EVD incubation period varies between 2 and 21 days. During EVD outbreaks, the case-fatality rate has varied from

outbreak to outbreak between 25 and 90% (Mahendradhata 2005), while in the current outbreak is around 50% (World Health Organization (WHO) 2014).

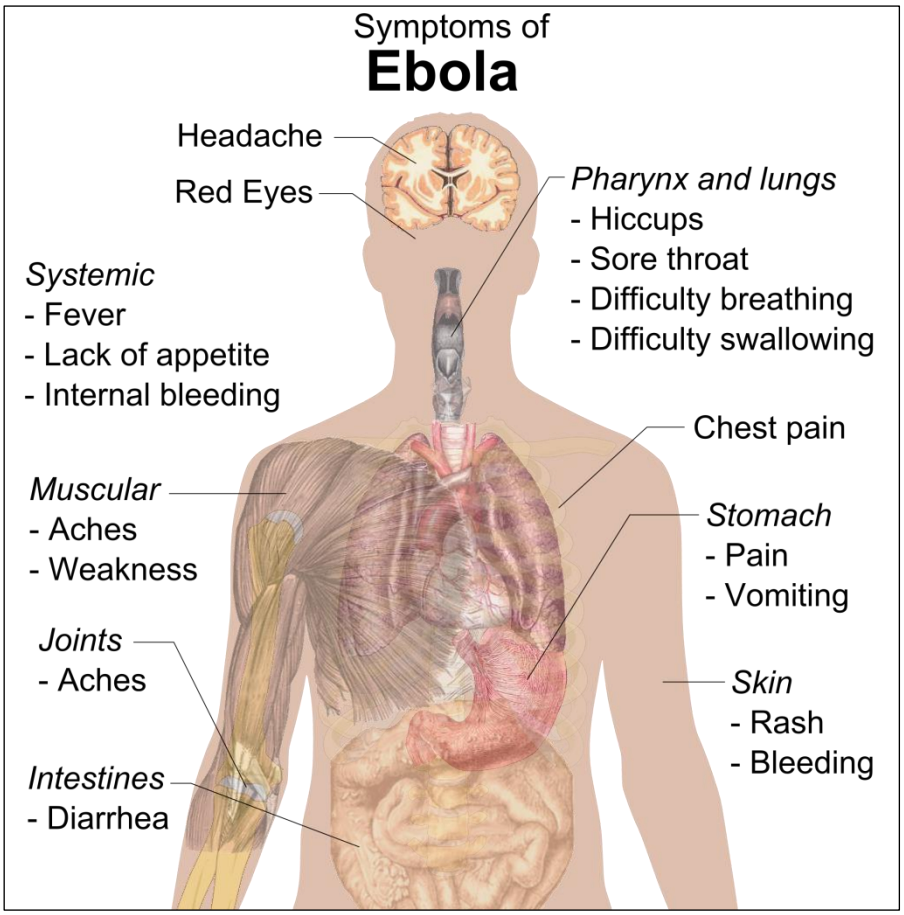

Figure 4. Signs and symptoms of EVD. Symptoms of EVD include fever, severe headache, muscle pain, weakness, fatigue, diarrhea, vomiting, abdominal (stomach) pain and unexplained hemorrhage (bleeding or bruising). Symptoms may appear anywhere from 2 to 21 days after exposure to EBOV, but the average is 8 to 10 days. Recovery from EVD depends on good supportive clinical care and the patient's immune response. People who recover from EBOV infection develop antibodies that last for at least 10 years.

1.1.5. Pathology and pathogenesis of EVD

Filoviruses enter the body through mucosal surfaces or skin abrasions or through the use of contaminated needles (Zaki & Goldsmith 1999) (Fig. 5a). The uncontrolled EBOV replication is important to its pathogenesis due both to its cytopathic effects and the prominent induced dysregulation of the host immune response. Virally-induced immune system impairment occurs

through a variety of mechanisms. Studies in nonhuman primates as well as guinea pigs raise the possibility that monocytes, macrophages and dendritic cells are early and preferred sites of viral replication (Connolly et al. 1999; Geisbert, Hensley, et al. 2003), though it remains possible that virus is present on these cells through binding to lectin receptors. It has been suggested that these cells act as vehicles for the transport of virus through the lymphatic system (Hensley et al. 2002). A further viral replication and systemic spread to other organs and tissues follows (Fig. 5b). Infection of monocytes and macrophages leads to the release of proinflammatory cytokines and chemokines, including tumor necrosis factor, interleukin-1β, macrophage inflammatory protein-1α and reactive oxygen and nitrogen species (Feldmann et al. 1996; Bray & Geisbert 2005). The expression of these mediators attracts more monocytes and macrophages to the sites of infection and may also attract neutrophils. Although recent data suggests that they are not productively infected, human neutrophils treated with filovirus in vitro show rapid activation of triggering receptor expressed on myeloid cells-1 (TREM-1) (Mohamadzadeh et al. 2006) that results in the release of further inflammatory cytokines and chemokines that contribute to vasodilation and increased vascular permeability. In addition, infected monocytes and macrophages express cell surface tissue factor, which may be involved in the development of coagulopathies (Geisbert, Young, et al. 2003). After infection, macrophages undergo cell lysis and apoptosis in large numbers (Gupta et al. 2007) contributing to viral dissemination by supporting viral replication or by transporting virus bound to cell surface lectin binding proteins within the lymphatic system. Like neutrophils, monocytes and macrophages may also secrete soluble factors that exacerbate pathogenic manifestations of the disease (Mohamadzadeh et al. 2006). Similarly to monocytes and macrophages, immature dendritic cells (DCs) are EBOV 'targets', either by means of attachment of viral particles interacting with DC-expressed C-type lectin DCSIGN or by means of infection interacting with other DC expressed cell-surface receptors (Fig. 5c). DCs EBOV infected are severely compromised in critical functions: they do not become mature or activated and are unable to up-regulate major histocompatibility complex (MHC) molecules and thus to

stimulate T cells (Bosio et al. 2003; Mahanty et al. 2003). The consequences of non-functional DCs include a diminished ability to stimulate humoral or cell-mediated immune responses, which may contribute to the lack of control of viral replication. A principal determinant of the inhibitory effect on innate immune function is EBOV resistance to the antiviral effects of interferon (IFN), which is likely to be due to interruption of critical IFN response pathways by the virus itself (Harcourt et al. 1998; Jahrling et al. 1999; Kash et al. 2006). In addition, the expression of ISGs important in the type I IFN response is decreased in EBOV infected cells (Harcourt et al. 1998; Kash et al. 2006; Harcourt et al. 1999). Like some other viruses, EBOV encodes specific viral proteins that antagonize the IFN response. In particular, 2 virally encoded proteins, VP24 and VP35, have been shown to interfere with the IFN response induction (Basler et al. 2003; Reid et al. 2006; Cárdenas et al. 2006). The virus-induced inhibition of the IFN pathway not only decreases ISGs transcription to prevent an antiviral response state, but also contributes to lower the number of mature and activated myeloid DCs, which in turn hinders the activation of the adaptive immune response. Surprisingly, patients who succumb to EBOV infection show little evidence of an activated adaptive immune response. Adaptive immunity is severely compromised also because lymphocytes undergo massive apoptosis in infected humans and nonhuman primates (Gupta et al. 2007; Baize et al. 1999; Reed et al. 2004). As a result, the number of CD4+ and CD8+ T cells is substantially reduced in fatal human and nonhuman primate infections before death (Baize et al. 1999; Reed et al. 2004; Sanchez et al. 2004) (Fig. 5d). The pathological changes seen in patients dying of EVD include coagulation abnormalities, vascular permeability, haemorrhage and organ necrosis and failure. The current hypothesis is that the fundamental mechanism of EBOV pathogenesis is vascular injury and damage secondary to coagulation abnormalities and increased vascular permeability, due to the release of inflammatory cytokines and chemokines by infected and activated monocytes and macrophages, and to direct endothelial cell damage from viral replication late in infection (Mahanty & Bray 2004; Mohamadzadeh et al. 2007). The direct viral damage of tissues and organs may lead to organ failure and shock. The infection of certain cell

types plays an important role in EBOV pathogenesis. Infection of innate immune cells is thought to be pivotal to the systemic dissemination of the virus during human infection (Geisbert, Hensley, et al. 2003; Connolly et al. 1999). In addition, infection and necrosis of hepatocytes cause impairment of liver function. Liver enzymes are elevated in most filovirus infections (Fisher-Hoch et al. 1992; Johnson et al. 1995; Ryabchikova et al. 1999), and decreased liver functions could account for the decreased synthesis of coagulation factors and development of coagulation disorders prominent during fatal infection. Finally, the development of shock at later stages of the disease is multifactorial and, along with haemorrhage, may be due in part to the infection and resulting necrosis of cells of the adrenal cortex that are important in the regulation of blood pressure (Ryabchikova et al. 1999). Although filoviruses are among the most virulent and fatal pathogens known, some patients infected with Ebola virus recover from the infection. In fact, it is evident that an early and robust, but transient, innate immune response and the subsequent activation of adaptive immune response are necessary to protect against fatal infection. If such a host immune response is not generated, the virus evades immune control and the infection progresses to end-stage disease (Zampieri et al. 2007).

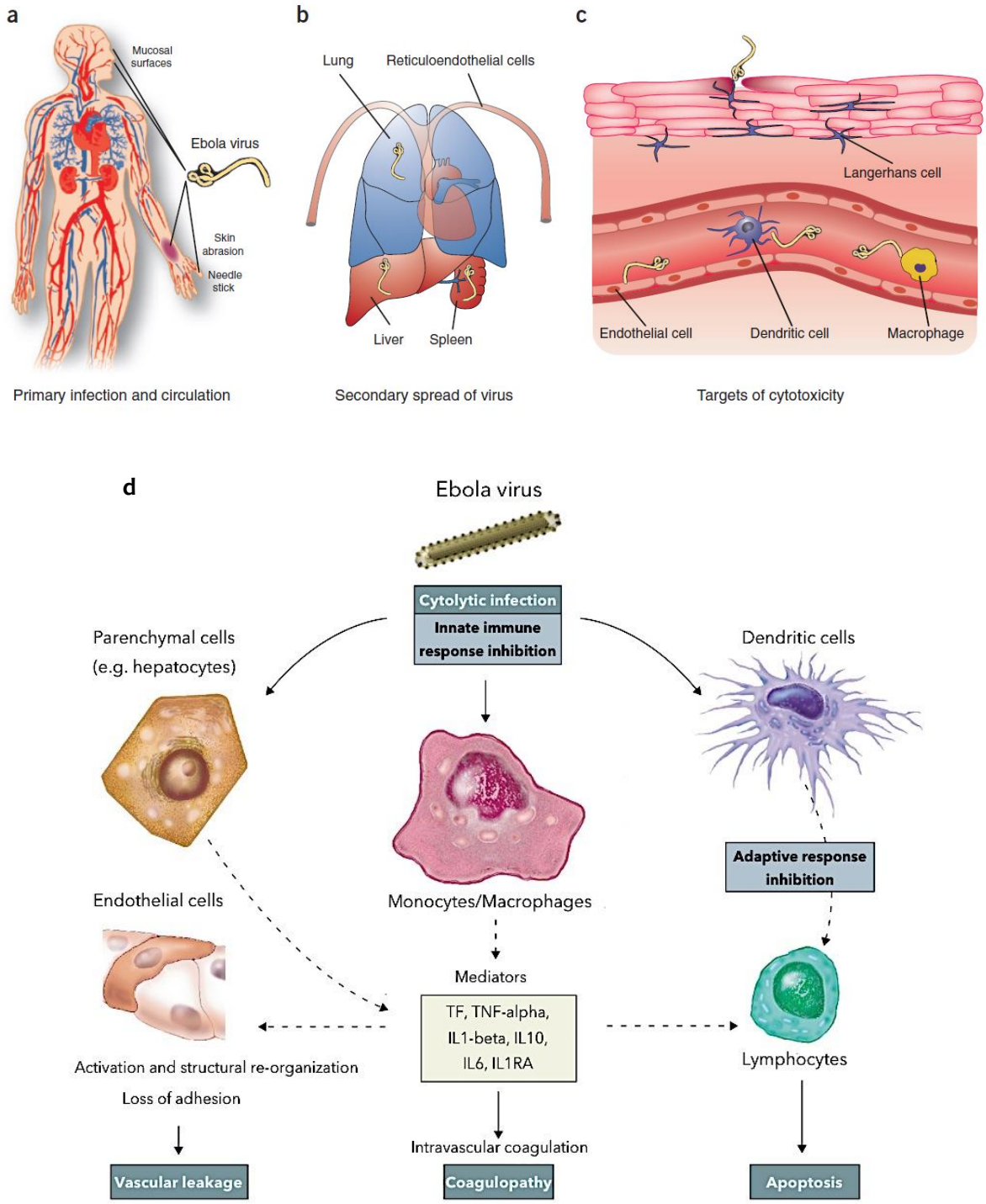

Figure 5. Infection, spread and target cell destruction by Ebola virus. (a) Ebola virus (yellow) infects subjects through contact with body fluid or secretions from an infected patient and is distributed through the circulation. Entry can occur through abrasions in the skin during patient care, burial rituals and possibly contact with infected bushmeat, or across mucosal surfaces. Accidental needle stick is the primary route of occupational exposure. (b) Early targets of replication are reticuloendothelial cells, with high replication in several cell types within the lungs, liver and spleen. (c) Dendritic cells, macrophages and endothelium appear to be susceptible to cytopathic effects of EBOV gene products through disruption of cellular signaling pathways affected by virus binding, phagocytic uptake or both. Indirect damage may also be inflicted by circulating factors such as tumour necrosis factor and nitric oxide. (d) Virus infection and uncontrolled replication causes lysis of monocytes/macrophages, DCs, and hepatocytes and suppresses innate immune response in these cells. Direct injury to infected cells is accompanied by indirect effects mediated by pro-inflammatory and anti-inflammatory cytokines and chemokines.

1.1.6. Structure of Ebola virus

EBOV virions produced in tissue culture are pleomorphic, appearing as either U-shaped, six-shaped, or circular (torus) configurations, or as elongates filamentous forms (Kuhn 2008). A typical EBOV virion contains one viral nucleocapsid (NC) that runs through a cylindrical axis of ~80 nm in diameter and is enwrapped by an envelope acquired from the host cell membrane during virus budding. The average virion length is ~982 nm, with a molecular mass of about 3.82 x 10^5 kDa. In addition to this common form, other viral particles are observed, such as "continuous-virions" containing 2 NCs or more in multiples by an integer of 2, and "linked-virions" composed of single NCs that are connected by short sections of an empty envelope (Beniac et al. 2012). EBOVs NC is a tubular, ~50 nm-wide, cross-striated and double-layered helix. The inner layer is 22 nm in diameter and consists of a 18.9 kbp ssRNA genome that is tightly associated in its entire length by regular repeats of the viral nucleoprotein NP, which, in turn, are connected each other and run along the NC axis at a pitch of ~7 nm with a periodicity of 12 subunits per helical turn (Bharat et al. 2012). The NP-RNA structure is then stabilized and protected by a 37 nm-wide outer layer, that consists of a series of "boomerang-shaped" protrusions, formed by repeats of the heterodimeric association between the viral minor matrix VP24 and the viral polymerase co-factor VP35, each one of these being bridged to different sites of two NP subunits (Bharat et al. 2012). Finally, in the interior of such double-layered NC, there are copies of the other viral polymerase co-factor VP30 and of the viral RNA-dependent RNA polymerase L protein, which are bound to NP and VP35 subunits, respectively. The described RNA-NP-VP24-VP35-VP30-L complex forms a loose soluble-layered helix that must be condensed into a rigid tubular structure to form the mature EBOV NC (Bharat et al. 2012). To this purpose, this helix is further surrounded by a 5 nm-wide lattice composed by regular repeats of the matrix protein VP40, which, associating with VP35 and the C-terminus of the NP subunits, provide the required stabilization to condensate the NC helix. Such tubular architecture is then enwrapped by an envelope originating from cellular membrane, in which are mounted repeats of the viral glycoprotein GP, necessary for cellular attachment and

fusion of EBOV virions. GPs form spikes that extend 10 nm from the envelope surface, with 3.5 nm stalk and 6.5 club-shaped head (Beniac et al. 2012). These are 15 nm centre-to-centre spaced and have an irregular-clustered distribution on EBOV virion surface. Every spike is typically composed by a trimeric association of GP subunits, each one consisting of a transmembrane GP2 domain and GP1 mucin-like domain, the latter being the putative receptor binding domain for a cell surface ligand that has not yet been definitively identified (Beniac et al. 2012; Bharat et al. 2012) (Fig. 6).

1.1.7. EBOV genome and proteins

EBOVs have a linear, non-segmented, ssRNA- genome of approximately 19 kb in length and an average molecular mass of 4 x 10^3 kDa (Kuhn 2008). EBOVs genome is organized in 7 linear genes which encode up to 9 viral proteins, 7 of which are structural proteins found in mature virions, while 2 additional proteins are secreted and do not participate to the formation of viral particles (Fig. 7). Such organization is almost identical among the five EBOV species, very similar with that of the closely related filoviruses MARV and LLOV and it is also shared, among *Mononegavirales*, between *Filoviridae* and the other three families in the order, such as *Paramixoviridae*, *Rhabdoviridae* and *Bornaviridae* (Barrette et al. 2011). *EBOV* genome is not polyadenylated at its 3' terminus and is uncapped at its 5' termini. At both genomic ends there are two brief extragenic regions, namely leader (*l*) and trailer (*t*) regions (Fig. 7), which contain sequences of *cis-acting* signals for the genome endcapsidation, replication and transcription. These regions appear to be highly conserved in the *Filoviridae* family, slightly varying in length among EBOV species. Typically, *l* region comprehends the first 49-55 nucleotides at the 3' termini, that immediately precedes the initiation transcription signal of the first gene. At the 5' termini, *t* region consists of a variable number of nucleotides (from 25 up to 676) following the termination transcription signal of the last gene. The 2 untranslated *l* and *t* regions show a certain degree of self-complementarity and are also complementary each to other at both respective ends. Owing to this reciprocal base pairing, *l* and *t* regions may lead to the formation of secondary structures that are typically found

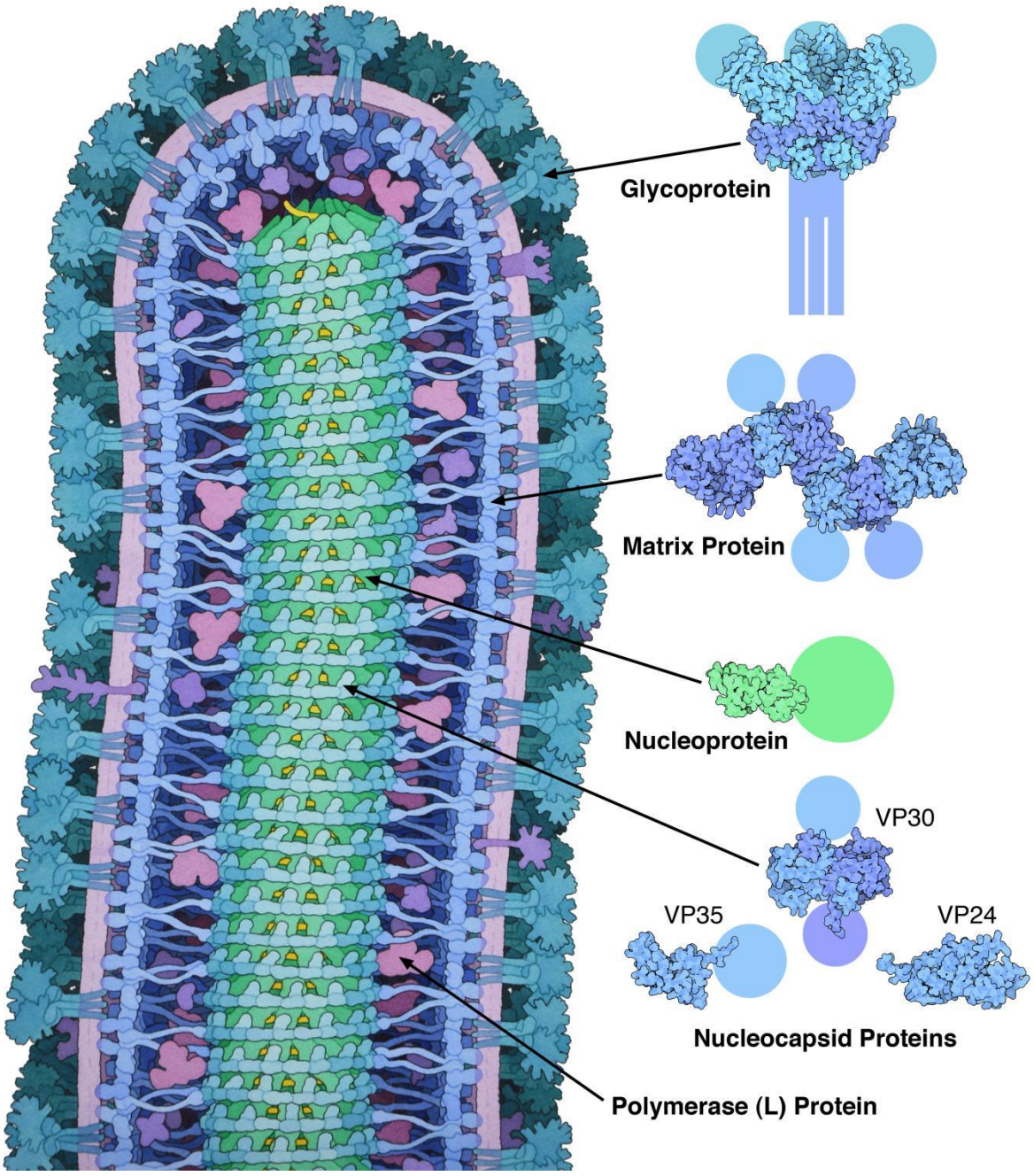

Figure 6. Structure of Ebolavirus virion. Ebola virions consist on filamentous-shaped particles enwrapped onto a host cell membrane-derived envelope with peplomers of the viral glycoprotein GP trimeric complexes. Under the envelope, an outer matrix layer is formed by the two VP40 and VP24 proteins shroud the viral NC. Immature NC consists on a ribonucleoprotein complex formed by a ssRNA (-) encapsidated by protomers of the NP and associated to the viral proteins VP30 and VP35-L complex, which represent the viral RNA-dependent RNA polymerase holoenzyme (Goodsell 2014).

in EBOV genome ends, including the *stem loop*, the *hairpin loop* and the *panhandle* structure (Crary et al. 2003; Mühlberger 2007). The 7 *EBOV* genes are tandemly arranged in the following linear order: NP, VP35, VP40, GP, VP30, VP24 and L. The first EBOV gene codes for the NP, a nucleoprotein of 739 amino acid residues and a predicted molecular mass of 83.3 kDa that is as major component of the EBOV NC by tightly encapsidating both viral RNA genome and antigenome. The second gene codes for the viral protein VP35, a 340 amino acid long protein of a 35 kDa mass which acts as a component of the replication and transcription holoenzyme and is also an assembly factor of EBOV viral particles. Moreover, VP35 is a determinant of EBOVs virulence, being an antagonist of the host antiviral innate immune response. The third gene along EBOV genome encodes for the viral protein VP40, a major protein consisting of 326 residues and a molecular weight of 35 kDa. VP40 forms the viral matrix in which EBOV NCs are assembled into mature virions and also plays a critical role during virus budding. The GP protein is the only EBOV structural glycoprotein and is encoded by the homonymous fourth gene after a process of mRNA editing. GP is translated as a 676 amino acid precursor and then processed by host enzyme furin into the two disulphide-linked heterodimer that decorates the EBOV envelope. The same, unedited transcript of GP gene encodes for two non-structural glycoproteins, the 291 amino acid residues sGP and the amino acid residues ssGP, which are secreted as soluble glycoprotein from infected cells. The fifth EBOV gene codes for the viral protein VP30, a 288 amino acid residues protein with a molecular mass of 32 kDa that acts as a component of the EBOV NC and is a polymerase co-factor important for EBOV transcription. The sixth gene codes for VP24, a matrix protein of 251 amino acid residues and a molecular weight of 28.2 kDa. The viral protein VP24 plays a structural role in viral assembly and also in an antagonist of the host innate immune response to viral infection. Finally, the seventh and last gene of EBOV genome encodes for the L protein, a large protein of 2212 amino acids and a molecular weight of 252.7 kDa that constitutes the catalytic site of the EBOV RNA-dependent RNA polymerase complex. The coding region of each ebolaviral gene consists of a central *open reading frame* (*ORF*) with highly-conserved

transcription initiation and termination sequences that contain the pentameric sequence 3'-UAAUU-5'. For 1 EBOV gene, the *GP*, there are 3 different *ORFs* in the *GP* gene, which code, through a process of mRNA editing, for 3 distinct forms of the viral glycoprotein, one of which is a structural (GP) and two are non-structural secreted proteins (sGP and ssGP). The ORF of each EBOV gene is flanked at both sides by long non-translated sequences, termed *intergenic regions* (*IR*), which vary in length (from 57 up to 684 bp) and nucleotide composition among EBOVs species and are seemingly not essential for viral transcription. EBOV genes also share *overlapping regions* (*OR*), that reside between *VP35* and *VP40* genes and between *VP24* and *L* genes in the RESTV species, while EBOV, SUDV, TAFV and BDBV species possess an additional third *OR* between *GP* and *VP30* genes (Kuhn 2008) (Fig. 7).

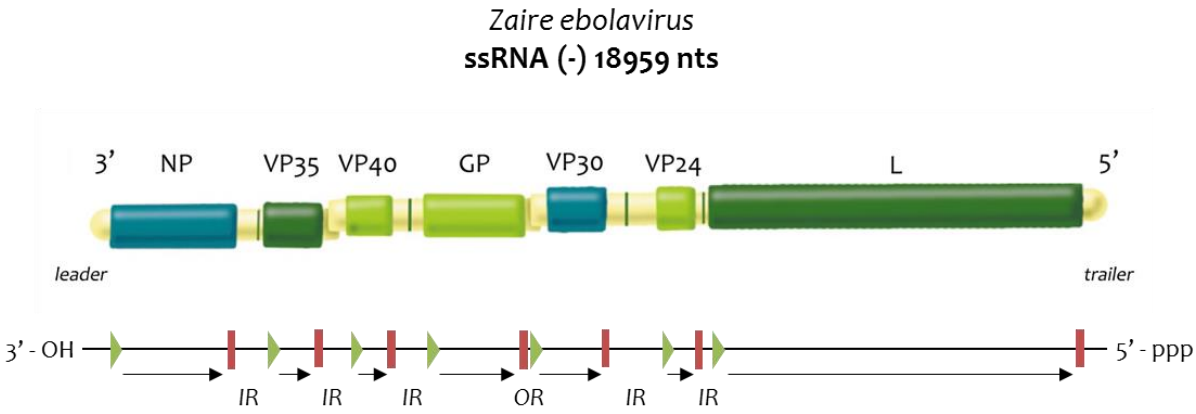

Figure 7. Organization of EBOV genome. Schematic diagram of the EBOV ssRNA (-) genome with its coding regions. Transcription start signals are depicted as green triangles and stop signals as red bars. *leader*, *trailer*, intergenic (*IR*) and overlapping regions (*OR*) are indicated.

1.1.8. EBOV cellular cycle

While having a preference for monocytes, macrophages, DCs, endothelial cells and hepatocytes, EBOVs are pantropic in infecting multiple cell types and exploit their enzymatic machineries through a replication cycle that is entirely cytoplasmatic (Takada 2012). EBOVs entry into target cells occurs by macropinocytosis and requires attachment of EBOV GP protein to a receptor

molecule that has not yet been identified (Olejnik et al. 2011). In fact, none of the cellular proteins implicated in ebolaviral entry totally match with EBOVs tropism and it remains allusive whether these molecules act as functional receptors mediating both viral attachment and membrane fusion or are rather co-receptors required only to enhance these processes (Takada 2012). According to the model currently proposed (Fig. 8), trimers of GPs on EBOV virion surface interact with members of the C-type lectin family (such as DC-SIGN, L-SIGN and hMGL) that concentrate virions on permissive cells before receptor engagement. Next, viral particle is internalized into an endosomal vesicles, likely as a consequence of the interaction between GP and the T-cell immunoglobulin and mucin domain 1 (TIM-1) protein with the participation of members of the Tyro3/Axl/Mer (TAM) co-receptors family (Olejnik et al. 2011). Following internalization, acidification of the endosomal lumen triggers cellular proteases Cathepsin L and B to trim the EBOV GP into a smaller form that, with the cooperation of at least one as yet undetermined factor, elicits fusion of viral envelope with host endosomal membrane. Cleavage of GP by endosomal cathepsins removes heavily glycosylated regions in GP1 subunits, thereby exposing a region that acts as ligand for the Niemann-Pick C1 (NPC1) protein, an endosomal cholesterol transporter that has been found essential for filovirus infection (Takada 2012). NCP1 likely mediates fusion of EBOV GP2 loop into endosomal membrane, this step being followed by the collapse of GP into a six-helix bundle that allows for lipid mixing and hemifusion of the host and viral membrane lipids. The hemifused membranes finally resolve forming a pore through which the EBOV NC is released in the cytoplasm, allowing viral replication cycle to continue. After the fusion, the viral particles uncoating takes place and EBOV antigenoma is transcribed into mRNA using viral proteins associated with NC. The genome transcription is mediated by VP30, VP35 and viral polymerase L complex bound to the genome coated by NP (Hartlieb et al. 2003; Bharat et al. 2012). VP30 phosphorylation leads to dissociation of the VP35/L complex and is the signal for the transition from transcription to replication process (Martinez et al. 2011; Biedenkopf et al. 2013). Therefore, the viral genomes are replicated and coated with NP, VP24, VP30 and VP35

(Muhlberger et al. 1999). During assembly, L binds to the ribonucleoprotein complex through interaction with VP35. Subsequently, ribonucleoproteins bind to the matrix protein VP40, which mediates the transport of immature viral particles up to the plasma membrane through the COPII transport system (Yamayoshi et al. 2008). After reaching the plasma membrane, the virion moves through lipid rafts, in which the final assembly takes place and through which the extrusion of mature viral particles occurs (Fig. 8) (Stahelin 2014).

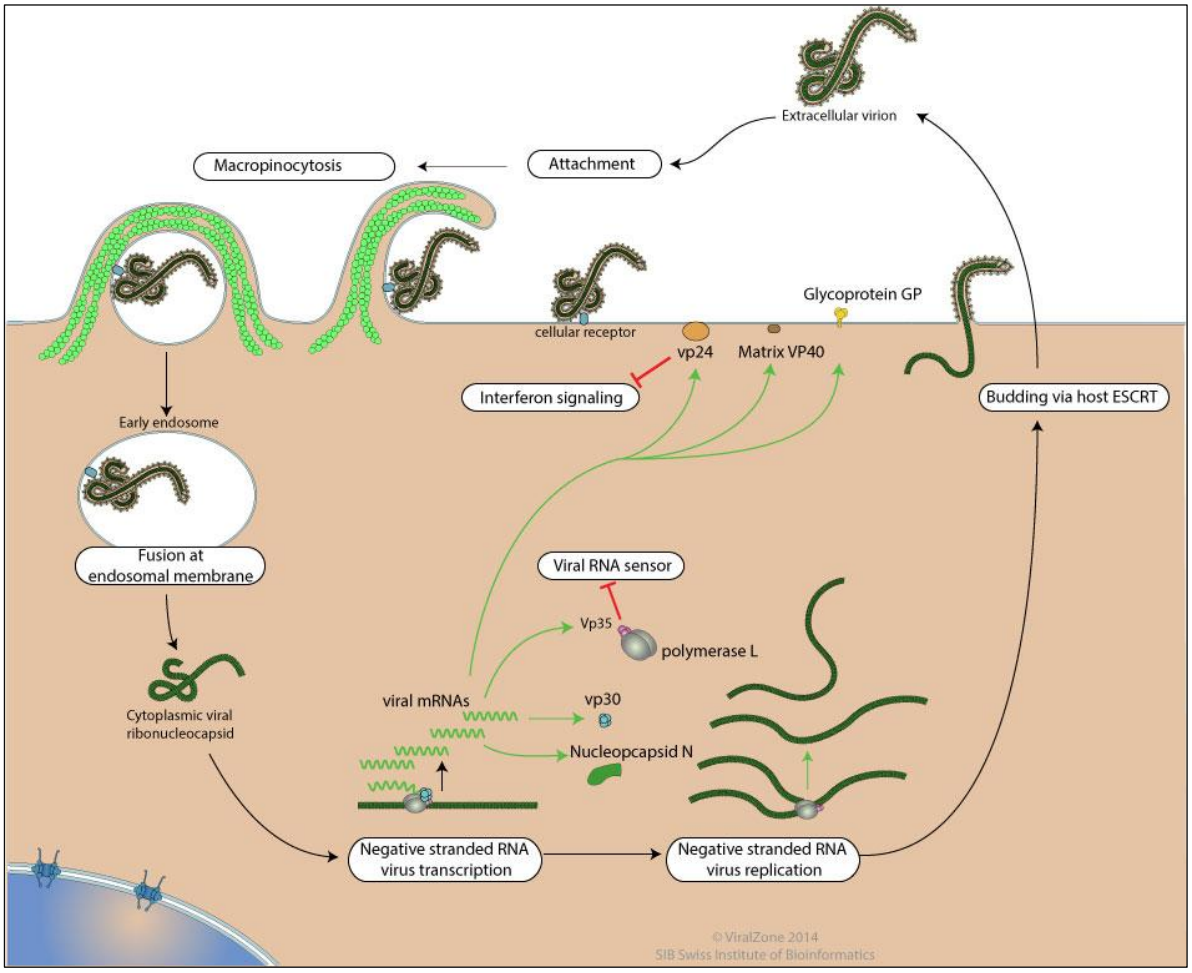

Figure 8. EBOV replication cycle. Attachment of the GP virion to an unidentified host surface receptor results in receptor-mediated macropinocytosis. The virion is acidified within the endocytic vesicle leading to the uncoating of the NC and release of the viral RNA genome into the cytoplasm of the host cell. Polyadenylated monocistronic mRNAs are synthesized from the negative-sense genomic RNA template by the replicase-transcriptase VP35-L-VP30 holoenzyme and translation of the viral mRNA genome yields the filoviral structural proteins. Viral replication of the positive-sense antigenome serves as template for the generation of the negative-sense progeny genomes. Prolonged replication produces excessive amounts of viral proteins, which facilitates transition from transcription/translation to replication within host cells. The concentration of NP is the primary trigger that induces this transition between mRNA transcription/translation and genomic replication. Binding of NP to progeny genomic RNA with VP35, VP30 and L result in the formation of immature ribonucleocapsids which, in turn, are enwrapped by VP24 and VP40 onto a matrix layer. Following assembly, virions are released from the host cell by budding of membrane-inserted GP peplomers.

1.1.9. Countermeasures against EVD

Identify patients with symptoms consistent with the case definition as outlined by the WHO and the Centers for Disease Control and Prevention (CDC), is the first step of clinical management, especially for patients in geographical areas where EBOV infections have previously been reported and/or patients in other countries with similar symptoms who have travelled to these countries within the past 21 days. These patients need to be rapidly isolated, the patient contacts identified and appropriate containment and preventive measures instituted. Blood samples need to be immediately obtained and submitted to the nearest clinical laboratory certified to conduct diagnostic evaluation for EBOV (Goeijenbier et al. 2014). Currently, the treatment of EVD includes the administration of 'supportive care' and treatment strategies. EVD patients benefit most from managing the haemodynamics and haemostasis. It was established that fluid replacement therapy drastically increases the chance of survival when started in the early phase of the disease (Fowler et al. 2014). Ribavirin, the only known antiviral that is effective against certain VHF pathogens such as Lassa fever, is not effective against Ebolaviruses (Jahrling et al. 1999; Huggins 1989). Various drugs with a potential effect in EVD are in the experimental phase and have shown beneficial effects against EBOVs (mainly EBOV and SUDV) in animal models and have been used in small numbers to treat EVD patients. The WHO declared that, considering the magnitude and severity of the current outbreak, it is ethical to use experimental drugs for treatment and prevention of EVD. ZMapp is a cocktail of monoclonal antibodies and is being used to treat some victims of the current EBOV outbreak. Its role in EVD treatment still needs to be established, since efficacy data in humans have not been published yet. The strongest evidence that ZMapp is indeed effective in EVD comes from experiments in non-human primates in which ZMapp was able to revert advanced EVD when administered up to five days post infection (Qiu et al. 2014). Unfortunately, there is a limited supply of ZMapp at this moment. Of the non-antibody based antiviral preparations, only the nucleoside analogue favipiravir has been tested extensively in humans. Recently the drug gained approval in Japan for use in humans infected with novel and re-

emerging influenza viruses. Besides activity against influenza virus infection, this drug also has documented activity against a wide variety of RNA viruses including EBOVs (Furuta et al. 2013; Smither et al. 2014). Favipiravir prevented death in mice infected with EBOV when treatment was started six days post infection (Oestereich et al. 2014). These results are promising, but need to be confirmed in a non-human primate model. BCX-4430 is also a nucleoside analogue with broad spectrum activity against RNA viruses and has proven to be effective against the Marburg virus in a non-human primate model and Ebola virus in a mouse model (Warren et al. 2014). Finally, TKM-ebola and AVI-6002 are under development for the treatment of EVD and exert their action via gene silencing. Both drugs have proven to be effective in mouse and primate models, and some safety and pharmacokinetic data in humans are available for AVI-6002 (Geisbert et al. 2010; Warren et al. 2010; Heald et al. 2014).

In earlier outbreaks attention was paid to potential treatment of EVD patients with blood transfusion from EVD survivors. For instance, in the EVD outbreak in Kikwit (Democratic Republic of Congo) in 1995, patients receiving convalescent serum from EVD survivors showed a much lower CFR (Mupapa et al. 1999). However, these results were based on a small number of patients with a potential treatment bias. Furthermore, this passive immunotherapy did not seem to be effective in a non-human primate model (Jahrling et al. 2007). Due to the potential for antibodies to enhance viral infections via antibody-enhancement mechanisms, a note of caution is in placement for the use of passive immunotherapeutic strategies. In addition, since antivirals are small molecules, increasing their production to a larger scale should be easier than it would be for monoclonal antibodies, resulting in a more effective strategy against EVD.

1.2. Antiviral Innate Immune Response

Defense mechanisms against infectious pathogens are regulated in concert with innate and adaptive immunity. The innate immune system, in particular, is essential to initiate these anti-pathogen immune activities in both peripheral and lymphoid tissues. Viral infections in children and young adults are common and generally uneventful. In most instances, the patients recover and either eliminate the virus or incorporate it in a latent or persistent form without further problems. Although viruses are obligate intracellular parasites and rely entirely on the metabolic machinery of the host cell, they usually do not cause much harm. The main reason is that our body is not defenseless but makes use of numerous measures to keep viruses at bay. The type I IFN system is a major player in antiviral defense against all kinds of viruses. Virus-infected cells synthesize and secrete type I IFN (IFN-α/β) which warns the body of the dangerous intruders. Secreted IFNs circulate in the body and cause susceptible cells to express potent antiviral mechanisms which limit further viral growth and spread (Haller et al. 2006; Yoneyama & Fujita 2010).

1.2.1. IFN system

IFNs are a group of secreted cytokines that elicit distinct antiviral effects. They are grouped into three classes called type I, II and III IFNs, according to their amino acid sequence. Type I IFNs (discovered in 1957; Isaacs & Lindenmann 1957) comprise a large group of molecules; mammals have multiple distinct IFN-α genes (13 in man), one to three IFN-β genes (one in man) and other genes, such as IFN-ω, -ε, -τ, -δ and -κ. The IFN-α and -β genes are induced directly in response to viral infection, whereas IFN-ω, -ε, -δ and -κ play less well-defined roles, such as regulators of maternal recognition in pregnancy (Randall & Goodbourn 2008). Type III IFNs have been described more recently and comprise IFN-λ1, -λ2 and -λ3, also referred to as IL-29, IL-28A and IL-28B, respectively (Ank et al. 2006; Uze & Monneron 2007). These cytokines are also induced in

direct response to viral infection and appear to use the same pathway as the IFN-α/β genes to sense viral infection (Onoguchi et al. 2007). Type II IFN has a single member, also called IFN-γ or 'immune IFN', and is secreted by mitogenically activated T cells and natural killer (NK) cells, rather than in direct response to viral infection (Randall & Goodbourn 2008). IFN-α/β acts through a common heterodimeric receptor, which appears to be expressed ubiquitously, to activate a signal-transduction pathway that triggers the transcription of a diverse set of genes that, in total, establish an antiviral response in target cells. These genes are referred to as IFN-inducible genes or IFN-stimulated genes (ISGs). A subset of ISGs can also be induced directly (in an IFN-independent manner) by viral infection, perhaps offering a degree of protection in the primary infected cells, although the dramatic viral sensitivity of IFN-α/β receptor-knockout mice suggests that this is much less effective than the IFN response itself. In addition to the cell-autonomous activities of IFN-α/β, these cytokines modulate the immune system by activating effector-cell function and promoting the development of the acquired immune response. The type I IFN system is indispensable for vertebrates to control viral infections. The importance of type I IFNs is further demonstrated in instances where disruption of a single IFN effector gene causes a complete loss of innate immunity against a particular type of virus, leading to overwhelming infection and rapid death (Haller et al. 2006).

Before an appropriate immune response can be generated, the virus needs to be recognized. For this, immune cells are equipped with different groups of receptors, which are able to sense microbial intruders including viruses. These pattern recognition receptors (PRRs) recognize pathogen associated molecular patterns (PAMPs), which are fundamentally different from host structures (Gaajetaan et al. 2012). However, major viral PAMPs are viral nucleic acids, which are structurally similar to the host's; therefore, the process by which PRRs distinguish self from non-self nucleic acids has to be strictly regulated. Three PRR families have been identified as nucleic acid-sensing PRRs; endosomal Toll-like receptors (TLRs), cytoplasmic retinoic acid inducible gene (RIG-I)-like receptors (RLRs) and uncharacterised DNA sensor molecules. These PRRs commonly

activate type I IFNs in addition to pro-inflammatory cytokines. TLRs are transmembrane receptors, which detect PAMPs on the outer membrane or in the endosomal compartment (Kawai & Akira 2007). On the other hand, RLRs are involved in the recognition of cytoplasmic PAMPs (Takeuchi & Akira 2008). Viral nucleic acids are specifically recognised by endosomal TLRs, RLRs and DNA sensors. Taken together, the innate immune system is equipped with a large variety of PRRs and this extended array is essential to sense the various microbial components and to prevent or limit viral spread as much as possible (Yoneyama & Fujita 2010).

1.2.1.1. RIG-I-like Receptors (RLRs)

RLRs, DExD/H-box-containing RNA helicases, are sensor molecules for the detection of viral RNA in the cytoplasm of infected cells. RLR genes are found only in the genome of higher vertebrates, therefore it is believed that RLRs have evolved as specialised receptors for the type I IFN system (Sarkar et al. 2008). In mammals, three family members have been identified, retinoic acid inducible gene I (RIG-I), melanoma differentiation associated gene 5 (MDA5) and laboratory of genetics and physiology 2 (LGP2) (Yoneyama & Fujita 2009). All three RLRs contain a typical RNA helicase domain with RNA-dependent ATPase activity. In the N-terminal portion of RIG-I and MDA5, two caspase recruitment domains (CARDs) are encoded; however LGP2 is completely devoid of CARDs. Since the CARD of RLR is implicated in the activation of downstream signalling via homotypic interaction with a CARD-containing adaptor molecule, mitochondrial antiviral signalling (MAVS) (also known as, IFN-promoter stimulator 1 (IPS-1), virus-induced signalling adaptor (VISA), and CARD adaptor inducing IFN (Cardif)) (Seth et al. 2005), both RIG-I and MDA5 are positive regulators in antiviral innate immunity. On the other hand, the function of the CARD-less LGP2 remains unclear. Another functional domain of RLRs is the C-terminal domain (CTD), also termed the repressor domain (RD). The CTD/RD of RIG-I and LGP2 is known to have dual functions; repression of RIG-I activity in the absence of a viral infection and recognition of specific viral RNA after an infection. The expression profile of RLR contrasts strikingly with that of TLRs.

RLRs are exclusively expressed in the cytoplasm, therefore RLRs detect viral RNA inside of the cytosol (Yoneyama et al. 2004). Moreover, since RLRs are ubiquitously expressed in most cell types, they are responsible for the eradication of viruses via the innate antiviral activity of IFNs. All three RLRs are typical ISGs, therefore positive feedback regulation of the signalling is provoked after a viral infection (Fig. 9) (Yoneyama & Fujita 2010).

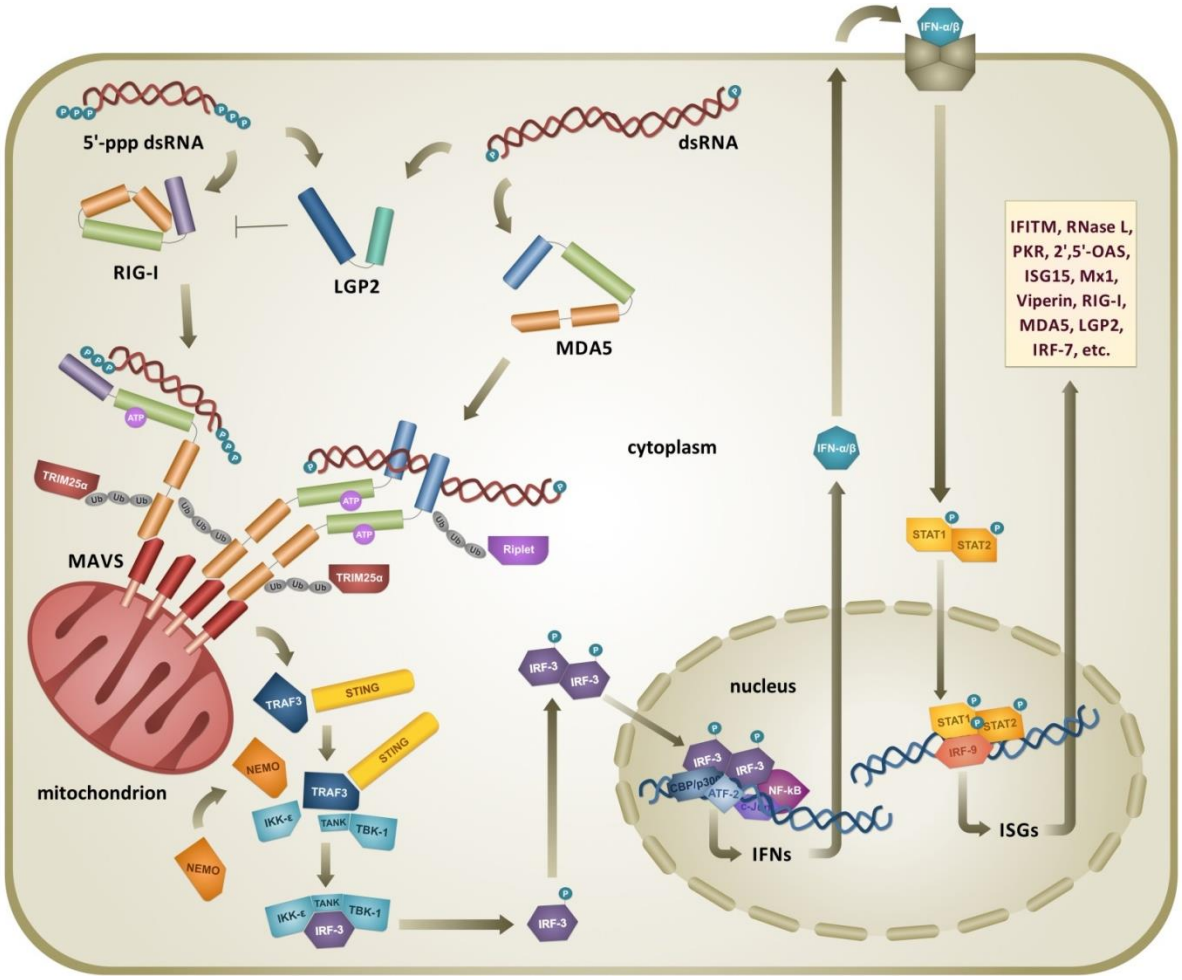

Figure 9. Activation of the type I IFN antiviral response triggered by the RLRs pathway upon dsRNA detection. Viral short 5'-ppp dsRNA and long dsRNA are preferentially recognized by the CTD of RIG-I (violet) and of MDA5 (azure) respectively, with LGP2 modulating the activity of RIG-I helicase. Upon dsRNA binding to their Hel domain (green), ATP-mediated homo-oligomerization, translocation onto dsRNA, ubiquitination, and TRIM25- or Riplet-mediated ubiquitination, RLRs interact through their CARDs (orange) with the CARD of mitochondrion-associated MAVS (red). Signaling prosecution involves recruitment of TRAF3, NEMO and STING adaptors and the assembly of TBK1- IKK-ε complex, which phosphorylates IRFs. Activated IRF dimers translocate to the nucleus and, together with other transcription factors, induce the expression of IFN-α/β. Type I IFNs are secreted and bind to their cognate receptor, activating STAT transcription factors for the induction of several ISG products with antiviral activity and the overexpression of RLRs pathway components (Zinzula & Tramontano 2013).

RIG-I. RIG-I is a key sensor of RNA virus infections and activator of the signaling cascade leading to production of type I IFN. Through a number of studies, RIG-I has been demonstrated to be the main recognition receptor for multiple RNA viruses including Newcastle disease virus (NDV), vesicular stomatitis virus (VSV), Sendai Virus, HCV, Japanese encephalitis virus (JEV), influenza A virus, rabies virus, measles virus, and respiratory syncytial virus (RSV) (Foy et al. 2005; Kato et al. 2005; Melchjorsen et al. 2005; Hornung et al. 2006; Liu et al. 2007). RIG-I mediated signaling cascade leads to activation of IRF-3 and NF-κB (Yoneyama et al. 2004). The critical adaptor for RIG-I signaling was identified as a mitochondrially located, CARD containing protein, MAVS. This adaptor is activated via CARD-CARD association with RIG-I and initiates a signaling cascade leading to activation of IFN-β transcription factors and subsequent production of IFN (Seth et al. 2005). RIG-I preferentially binds to short (<300 bp) ssRNAs and dsRNAs that have blunt ends and a 5' triphosphate (5'-ppp) (Reikine et al. 2014). Since RIG-I-dependent viruses expose a 5'-ppp signature in the process of viral entry or replication, the RNA genome of these viruses is recognised by RIG-I. This specificity also explains the strict discrimination between self and non-self RNA by RIG-I, because most endogenous RNAs lose their 5'-ppp group in the process of maturation, and escape detection by RIG-I (Yoneyama & Fujita 2010). RIG-I can be divided into three basic domains, the N-terminal CARD, central helicase domain, and C-terminal regulatory domain (Fig. 10). The N-terminal tandem CARD domains are required for interaction with the MAVS CARD domain and downstream signaling. The carboxy-terminal CTD/RD of RIG-I has proven to contain multiple diverse functions critical to RIG-I activity. Through mutational analysis, this domain was identified to possess the repressor activity responsible for self-inhibition. The repression of signaling likely occurs through intramolecular association between the CTD/RD and both the CARD and helicase domains (Takahasi et al. 2008). A conformational change induced by RNA binding leads to the unfolding of the molecule and exposure of the CARD allowing for downstream signaling. In addition to signaling repression and RNA recognition, the CTD/RD domain has also been characterized as being required for RIG-I dimerization. The exact role of the

helicase domain in RIG-I activity has been the most challenging to elucidate. The biochemical roles of this domain can be separated into two related but separate enzymatic functions, ATPase activity and helicase/translocase activity. The helicase domain also appears to have an important role in RNA binding (Baum & García-Sastre 2010). Formation of the RIG-I-MAVS complex on mitochondria induces the assembly of protein complexes to initiate downstream signalling. As signalling molecules, TRAF3/6, caspase-8/10, RIP1, Fas-associated death domain (FADD) and TNF receptor-associated death domain (TRADD) were demonstrated to be involved in the signalling. These molecules induce kinase activities of both IKKα/IKKβ and TBK1/IKK-ε complexes to activate NF-κB and IRF-3, respectively, leading to the production of proinflammatory cytokines and type I IFNs. Several ubiquitinating or deubiquitinating enzymes have been identified as regulators for RIG-I and related signalling molecules, as Tripartite motif protein (TRIM) 25, which is an E3 ubiquitin ligase and specifically interacts with RIG-I CARD and conjugates Lys-63-linked ubiquitins, which are required for interaction between RIG-I and MAVS (Yoneyama & Fujita 2010).

MDA5. MDA5 was identified as a DExD/H helicase family member during a screening of genes, which were upregulated by IFN treatment and at the same time involved in growth suppression of melanoma cells. Similar to RIG-I, MDA5 contains two N-terminal CARD domains, a dsRNA-dependent ATPase motif within a central helicase domain, and a regulatory C terminal domain (Fig. 10) (Kang et al. 2002). In contrast to RIG-I, MDA5 preferentially binds internally to long dsRNA (> 1000 bp) with no end specificity and cooperatively assembles into a filament on the dsRNA. Unlike RIG-I, the CARDs of MDA5 are not sequestered in the absence of ligand. The forced proximity of the CARDs upon MDA5 filament formation induces oligomerization of MDA5 CARDs, forming a scaffold for binding and oligomerization of MAVS CARD. Notably, the atomic structures of the MDA5 CARDs have not yet been determined. A crystal structure of the MDA5 helicase domains and CTD/RD bound to dsRNA revealed how MDA5, despite having a similar domain architecture as RIG-I, recognizes dsRNA in a different manner. The helicase domains of MDA5 wrap around dsRNA similarly to the helicase domains of RIG-I. However, consistent with the

observation that MDA5 is not preferentially activated by 5'-ppp dsRNA (Kato et al. 2006), the MDA5 CTD/RD is rotated by 20°, bringing it closer to the dsRNA, as compared to the RIG-I structure. This orientation of the CTD promotes cooperative filament formation along dsRNA, initiated from internal sites in the dsRNA rather than from one of the ends (Berke & Modis 2012). The molecular machinery of MDA5-mediated signal transduction is known to be almost identical to the one of RIG-I-mediated signal transduction. However, a MDA5-specific negative regulator, dihydroacetone kinase (DAK) has been identified (Diao et al. 2007). DAK associates with MDA5, but not RIG-I, and inhibits polyI:C-induced IFN production. Further analysis will be necessary to determine the physiological function of MDA5 in the regulation of adaptive immunity.

LGP2. The third member of the RLR family, LGP2, has been implicated as a negative regulator of RIG-I and a positive regulator of MDA5; however, the exact role of this molecule in viral infection remains controversial. Like RIG-I and MDA5, LGP2 contains a DExH/D box helicase domain and a carboxy-terminal CTD/RD (Fig. 10). However, unlike those receptors, it lacks the CARD domain, and therefore, it is unable to signal through MAVS. Since LGP2 recognises RIG-I ligands, such as short dsRNA, with greater affinity than RIG-I, the sequestration of RNA from RIG-I could be the reason for the inhibitory effect of LGP2. Since LGP2 CTD can function as RD (Saito et al. 2007), it may directly interact with RIG-I and inhibit its activation. Alternatively, it has been shown that LGP2 can interact directly with MAVS and competes in the binding between MAVS and IKKε, leading to inhibition of RIG-I-mediated signalling (Komuro & Horvath 2006). On the other hand, analyses of LGP2 knockout mice indicated that LGP2 positively regulates EMCV-induced antiviral activity. Although the precise molecular mechanism of this positive effect of LGP2 has been uncharacterised, one possible explanation is the cooperative recognition of viral dsRNA with MDA5. Further analysis will be necessary to address this issue (Yoneyama & Fujita 2010).

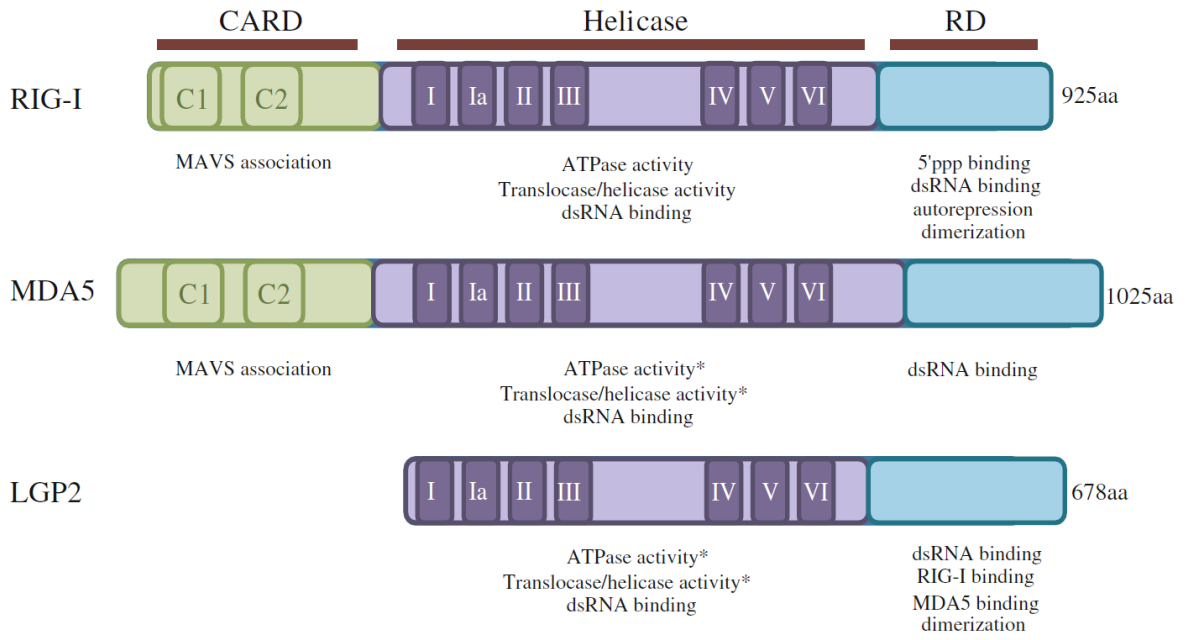

Figure 10. RLR domains and their function. The RLR proteins can be divided into three basic domains. (1) The N-terminal CARD domain, composed of two tandem CARDs. (2) The central helicase domain, belonging to the DExD/H family of RNA helicases. (3) The unique C-terminal domain containing multiple regulatory functions (RD). The CARD domain, present in RIG-I and MDA5 but absent in LGP2, is required for interaction with MAVS and downstream signaling. CARD1 (C1) is involved in physical interaction with the CARD domain of MAVS, whereas CARD2 (C2) of RIG-I undergoes ubiquitination required for RIG-I activation. The helicase domain contains six conserved DExD/H helicase motifs and is involved in translocation/unwinding of RNA and ATP hydrolysis required for RLR function. The helicase domain is also implicated in RNA binding for all three RLR members. The RD is required for recognition and binding of RNA substrates. This domain provides specificity for either 5'-ppp containing RNA (RIG-I) or dsRNA (MDA5, LGP2). RD is also required for homo- (RIG-I, MDA5) and hetero- (LGP2) dimer formation, necessary for signaling by these receptors. The RD of RIG-I additionally provides a unique function of auto-repression, and RIG-I constructs lacking the RD domain constitutively induce IFN in the absence of RNA stimuli (Baum & García-Sastre 2010). *Activity has not been shown directly and is assumed based on sequence similarity to the helicase domain of RIG-I.

1.2.1.2. Toll-like Receptors (TLRs)

TLRs are a family of single-transmembrane proteins expressed predominantly in immune cells, such as macrophages and DCs (Kawai & Akira 2007). Characteristic features of TLRs are the extracellular leucine-rich repeat (LRR), which is involved in the recognition of specific PAMPs, and an intracellular signal-transduction domain known as the Toll/IL-1 receptor (TIR) domain. Among the TLR family members, TLR1, 2, 4, 5 and 6 are expressed on the cell surface and responsible for the detection of bacterial and fungal cell wall components as PAMPs, whereas TLR3, 7, 8 and 9 recognise viral nucleic acids in the endosomal compartment. The signal transmitted through these TLRs commonly induces the production of proinflammatory cytokines, such as IL-6 and

tumour necrosis factor (TNF)-α, via the activation of NF-κB; however, the endosomal TLRs specifically activate type I IFNs in addition to proinflammatory cytokines. These endosomal TLRs commonly require an endoplasmic reticulum protein, UNC-93B, which is responsible for delivering them to the endosomal compartment (Kim et al. 2008).

TLR3. TLR3 detects dsRNA, which is found in the genome of dsRNA viruses or replication- or transcription- intermediates of ssRNA of RNA or DNA viruses (Fig. 11a). Expression of TLR3 is predominantly observed in the intracellular compartments of cDCs and macrophages, while some fibroblasts also express TLR3 on their cell surface. A dsRNA ligand is recognised by TLR3 via its N-terminal ectodomain (ECD), which consists of an N-terminal-specific LRR (LRR-NT), 23 LRRs, and a C-terminal-specific LRR (LRR-CT). TLRs are known to utilise specific adaptor molecules to transmit downstream signalling. In the case of TLR3, the essential adaptor is TIR domain-containing adaptor inducing IFN-β (TRIF) (also known as TIR domain-containing adaptor molecule 1 (TICAM1)). TRIF directly interacts with TLR3 via TIR-TIR homotypic interaction and recruits a set of signalling molecules, including TNF receptor-associated factors (TRAF)3, TRAF6, receptor interacting protein 1 (RIP1), and transforming growth factor-alpha activated kinase 1 (TAK1), leading to the activation of transcription factors NF-κB, IRF-3 and IRF-7.

TLR7/TLR8. TLR7 and TLR8 are structurally homologous and are sensors of ssRNA. In the human system, TLR7 is predominantly expressed in pDCs and involved in the robust expression of IFN-α, whereas the expression of TLR8 is observed in myeloid DCs and monocytes. Since both TLR7 and TLR8 are expressed in the intracellular endosomal compartment, the endosomal degradation of viral particles to expose viral ssRNA is required for the recognition by TLR7/8. TLR7/8 transmits signals via a specific adaptor molecule, MyD88, which contains a TIR domain and a death domain. Upon the binding of a ligand, the TIR domain of TLR7/8 interacts with MyD88, and recruits downstream signalling molecules, IRAK1/2/4, TRAF3/6 and Osteopontin. IRF-7, which is constitutively expressed in pDCs, is recruited to this signalling complex, and directly activated by

IRAK1 via phosphorylation at specific C-terminal serine residues (Fig. 11b) (Yoneyama & Fujita 2010).

TLR9. TLR9 is predominantly expressed in the endosomal compartment of pDCs and B cells, and implicated in the detection of CpG-containing DNA. TLR-9-mediated signalling, which leads to the production of both proinflammatory cytokines and IFN-α, is almost identical to the TLR7/8 pathway (Fig. 11b) (Yoneyama & Fujita 2010).

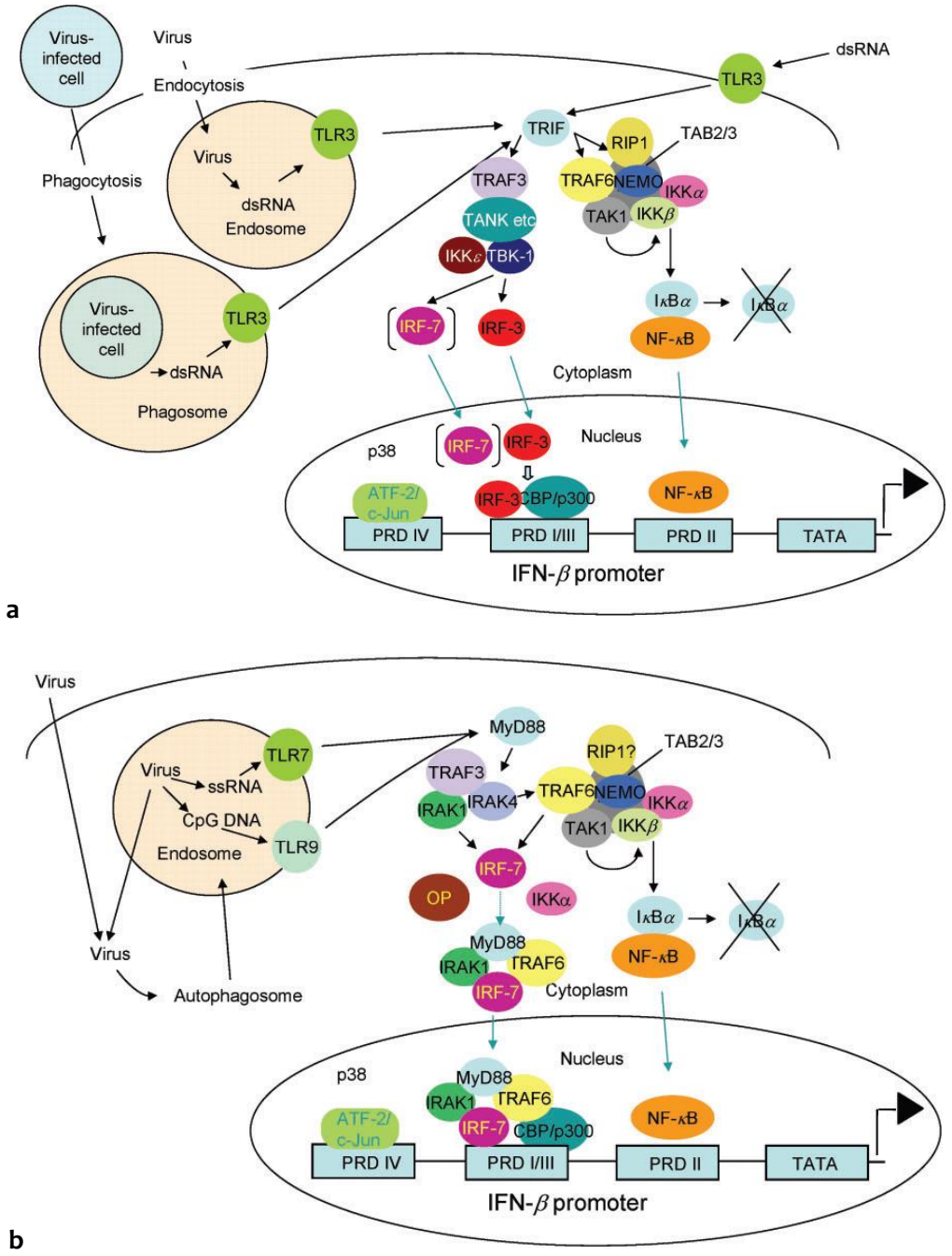

Figure 11. TLR3-, TLR7- and TLR9-dependent signalling. (a) dsRNA binds to TLR3. Activated TLR3 recruits the adaptor TRIF that, in turn, acts as a scaffold to recruit signalling components that feed into either the IRF-3 or the NF-κB pathways. NF-κB activation requires TRAF6 and RIP1 recruitment to TRIF and their co-operation in recruiting the IKK complex and TAK1. TAK1 phosphorylates the IKKβ subunit of the IKK complex, leading to its activation and phosphorylation of IκB. Phosphorylated IκB is ubiquitinated and subsequently degraded by proteasomes, releasing NF-κB for migration to the nucleus (green arrow) and assembly on the IFN-β promoter. IRF-3 activation requires recruitment of TRAF3 to TRIF. TRAF3 binds to TANK, which then binds to TBK-1 and/or IKKε, which are activated in an uncharacterized manner and can phosphorylate IRF-3 directly. IRF-7 is activated by TBK-1 and IKKε in a similar manner. The activated IRFs also migrate to the nucleus (green arrows) and assemble on the IFN-β promoter with NF-κB and ATF-2/c-jun, leading to the recruitment of co-factors such as CBP/p300 and RNA polymerase II and, ultimately, stimulation of transcription. (b) ssRNA or CpG DNA bind to TLR7 or TLR9. Activated TLRs recruit the adaptor MyD88 that recruits IRAK-4 and IRAK-1. This complex acts as a scaffold to recruit signalling components that feed into either the IRF-7 or NF-κB pathways. IRF-7 recruitment to the MyD88 adaptor complex requires polyubiquitination by TRAF6 in a RIP1-dependent manner. IRF-7 is phosphorylated by IRAK-1 and a complex containing IRF-7, MyD88, TRAF6, IRAK-1 and possibly IRAK-4 is released and migrates to the nucleus (green arrows). Here, it assembles on the IFN-β promoter with NF-κB and other factors, leading to the stimulation of transcription.

1.2.2. Signalling responses to type I IFN

The basic signalling pathway activated in response to IFN α/β has been characterized in detail (Platanias 2005) (Fig. 12). IFN-β and the multiple IFN-α subspecies activate a common type I IFN receptor (IFNAR) which sends a signal to the nucleus through the JAK-STAT pathway. The STAT proteins are latent cytoplasmic transcription factors which become phosphorylated by the Janus kinases JAK-1 and TYK-2. Phosphorylated STAT-1 and STAT-2 recruit a third factor, IRF-9, to form a complex known as IFN-stimulated gene factor 3 (ISGF-3) which translocates to the nucleus and binds to the IFN-stimulated response element (ISRE) in the promoter region of ISGs. Specialized proteins serve as negative regulators and inhibitors of the JAK-STAT pathway. The suppressor of cytokine signaling (SOCS) proteins prevents STAT activation (Kubo et al. 2003) whereas protein inhibitor of activated STAT (PIAS) family members function as small ubiquitin-like modifier (SUMO) E3 ligases and inhibit the transcriptional activity of STATs (Shuai & Liu 2005). Type I IFNs activate the expression of several hundred ISGs some of which code for antiviral proteins. To date, three antiviral pathways have been firmly established. These comprise the protein kinase R (PKR) (Williams 1999), the 2'-5' OAS/RNase L system (Silverman 1994) and the Mx proteins (Haller & Kochs 2002; Haller et al. 2006).

Protein kinase R (PKR). PKR is synthesized in inactive form and, in response to the dsRNA, produced during viral replication, undergoes dimerization and activation. In addition to activation by dsRNA, PKR is activated by protein kinase R (PKR)-activating protein (PACT) (Patel et al. 2000). The best-characterized substrate for PKR is the α subunit of the eukaryotic translational initiation factor 2 (eIF2α). Phosphorylation by PKR prevents recycling of eIF2α such that initiation is halted. Additionally, eIF2α phosphorylation can activate autophagy, by which the contents of a cell can be degraded and, for HSV-1, this limits viral replication (Talloczy et al. 2006). The involvement of PKR has been invoked in a number of other antiviral mechanisms, including the induction of apoptosis and cell-cycle arrest (Randall & Goodbourn 2008).

2'5' OAS. 2', 5' Oligoadenylate synthetase was discovered and characterized as an enzyme that in the presence of dsRNA converts ATP into 2'5'-linked oligomers of adenosine that bind to and activate RNase L, which degrades cellular and viral RNAs. The OAS/RNase L system has been linked to the induction of IFN and may also affect apoptosis (Silverman 1994).

Mx. Mx and the Mx family of genes encode large GTPases related to dynamin; the precise functions of Mx and the superfamily of GTPases are unknown, but they show antiviral activity against a wide range of RNA viruses. The Mx proteins act by recognizing nucleocapsid-like structures and restricting their localization within the cell, thereby restricting virus replication. For example, human MxA recognizes the viral nucleoprotein of Thogoto virus (THOV) and prevents transport of the incoming viral nucleocapsids into the nucleus (Weber et al. 2000; Randall & Goodbourn 2008).

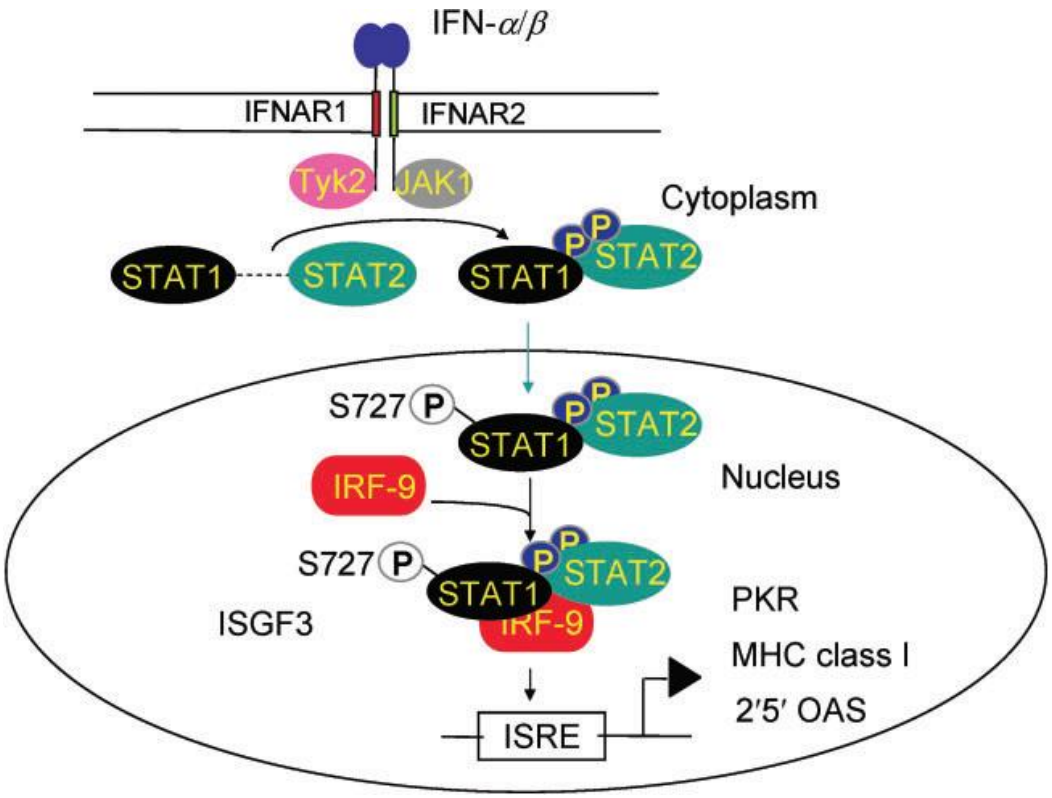

Figure 12. Signalling pathway activated by IFN-α/β. The biological activities of IFN-α/β are initiated by binding to the type I IFN receptor. This leads to the activation of the receptor associated tyrosine kinases JAK1 and Tyk2, which phosphorylate STAT1 on tyrosine 701 and STAT2 on tyrosine 690. Phosphorylated STAT1 and STAT2 interact strongly with each other by recognizing SH2 domains, and the stable STAT1–STAT2 heterodimer is translocated into the nucleus, where it interacts with the DNA-binding protein IRF-9. The IRF-9-STAT1-STAT2 heterotrimer is called ISGF3 and it binds to a sequence motif (ISRE) in target promoters and brings about transcriptional activation. In addition to the phosphorylation of tyrosine, STAT1 also requires phosphorylation on serine 727 for function.

1.3. Inhibition of Innate Immune Response

Because of the strong antiviral and immunoregulatory role of type I IFN, viruses developed a large variety of anti-type I IFN mechanisms. Consequently, nearly all steps of the type I IFN pathway can be blocked or manipulated by different viruses for their own benefit. There are five main ways by which viruses circumvent the IFN response, such as *i)* interfering globally with host cell gene expression and/or protein synthesis, *ii)* minimizing IFN induction by limiting the production of viral PAMPs and/or by specifically blocking IFN-induction cascades, *iii)* inhibiting IFN signalling, *iv)* blocking the action of IFN-induced enzymes with antiviral activity and *v)* having a replication strategy that is (largely) insensitive to the action of IFN. Within each of these strategies, different viruses have evolved a great diversity of molecular mechanisms to achieve similar ends. Since RNA viruses tend to accumulate nucleic acid intermediates and byproducts in the host cytoplasm during their replication cycle, preventing recognition by host PRRs of such PAMPs is of crucial importance. Therefore, most RNA viruses encode proteins that display IFN-antagonism properties aimed to circumvent the host innate immune system. Among those proteins, most have been revealed as involved in targeting the RLR pathway at several levels (Versteeg & García-Sastre 2010). The impact of this counteraction becomes particularly evident for those RNA viruses that cause severe diseases in humans, since in several cases the fatal outcome has been related to their ability to subvert the type I IFN-mediated innate immune response (Bray 2005). It is therefore not surprising that, among the different viral proteins identified as inhibitors of IFN-α/β production and signaling, most are also molecular determinants of virulence and pathogenesis (Bowie & Unterholzner 2008; Versteeg & García-Sastre 2010). To this category belongs EBOV, whose extreme lethality is the result of uncontrolled viral replication associated with a total impairment of the innate immune system, related, at least in part, to the properties displayed by three determinants of virulence and pathogenicity: VP24, VP35 and VP40 proteins. However, only the multifunctional polymerase cofactor VP35 acts by suppressing IFN-α/β production, while VP24

and VP40 matrix proteins are involved in inhibiting the type I IFN signaling pathway (Basler & Amarasinghe 2009; Ramanan et al. 2011). Within RNA viruses also human infections by highly pathogenic Influenzaviruses (IAVs) may typically result in acute respiratory distress syndrome with fatal pneumonia, due, at least in part, to the ability of IAVs to efficiently suppress the host innate immune response (Ramos & Fernandez-Sesma 2012). In particular, regarding interference with the dsRNA-induced production of IFN-α/β, IAVs exert their antagonism through the properties of at least three proteins, namely NS1, PB2 and PB1-F2, which target the RLR pathway at several levels and with different mechanisms. Particularly, NS1 plays a central role in virus replication and block of the host innate immune response through several distinct molecular mechanisms that are triggered by interactions with dsRNA or specific cellular proteins (Benjamin G. Hale et al. 2008; Ehrhardt et al. 2010). VP35 and NS1 proteins, that present similar structure and a IFN-antagonist function that targets the RLR pathway, are presented here in detail (Fig. 13) (Zinzula & Tramontano 2013).

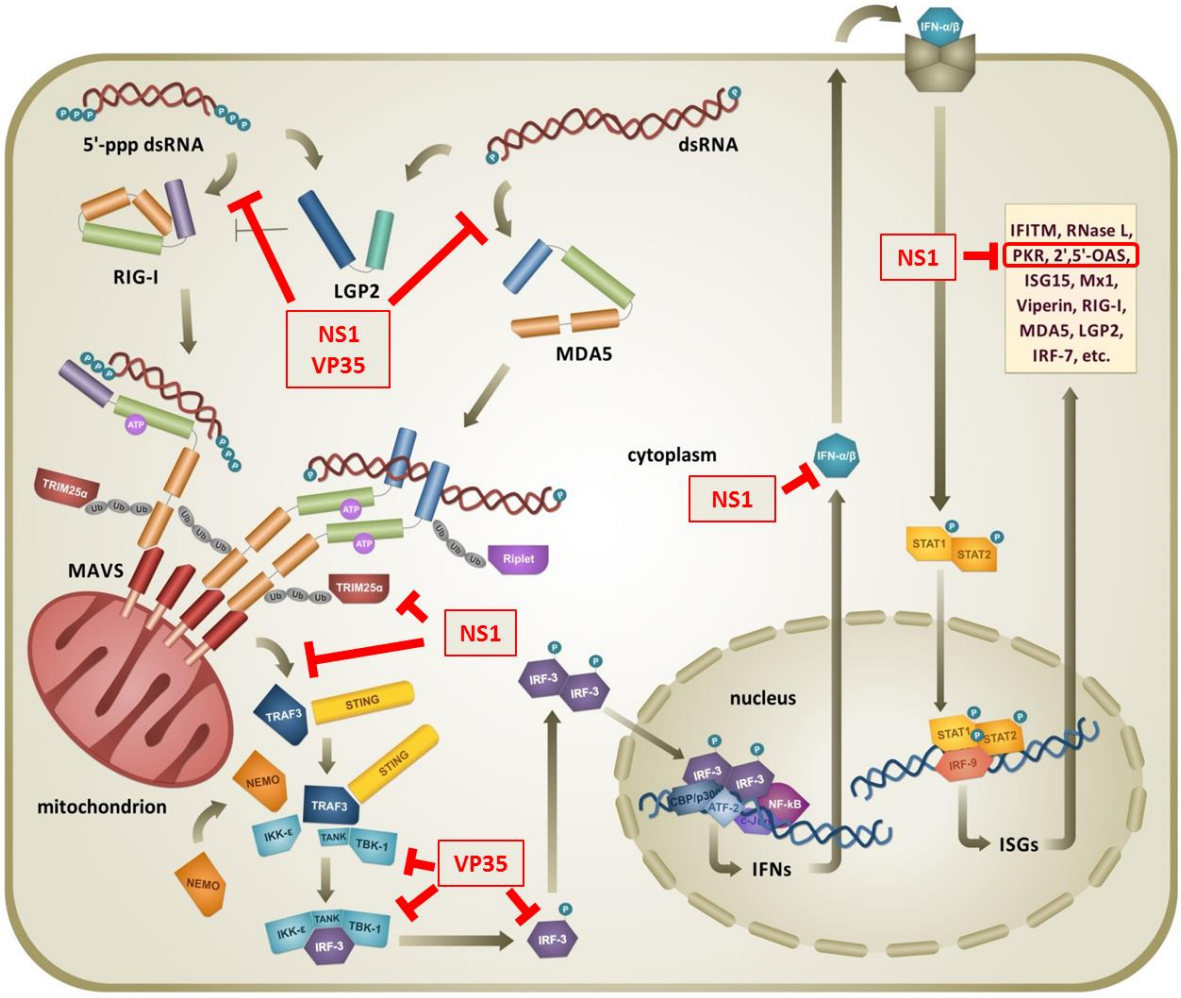

Figure 13. RLRs pathway inhibition by VP35 and NS1 proteins. VP35 and NS1 inhibit the RIG-I pathway-mediated production of IFN-α/β. VP35 acts upstream by sequestering dsRNA to RIG-I recognition and downstream by interacting with the IRF-3 kinases IKK-ε and TBK-1. This prevents efficient phosphorylation of IRF-3, blocking activation of the IFN-β promoter. NS1 hides dsRNA to RIG-I recognition and interact directly with TRIM25 inhibiting RIG-I ubiquitination/activation preventing the IFN synthesis. NS1 also blocks cellular pre-mRNAs processing and prevents their nuclear export, including IFN mRNAs synthesized in response to viral infection. Moreover it sequesters viral dsRNAs from detection by 2'-5' OAS and inhibits the activity of PKR.

1.3.1. EBOV VP35 protein

In EBOV infections, recognition of viral RNA by the cytoplasmic PRR RIG-I is prevented through the dsRNA binding properties of the EBOV VP35 that mimics 5'-ppp dsRNA ends recognition performed by RIG-I (Schlee et al. 2009). EBOV VP35 also interferes with the activation of IRF-3 (Hartman, Bird, et al. 2008) and inhibits PACT-induced RIG-I ATPase activity preventing PACT interaction with and activation of RIG-I (Luthra et al. 2013), allowing EBOV to evade innate immunity activation. As stated before, the multifunctional viral protein VP35 is also an essential component of the viral RNA polymerase complex and a nucleocapsid assembly factor (Basler et al. 2000; Basler et al. 2003; Cárdenas et al. 2006; Daisy W. Leung et al. 2010; Prins, Binning, et al. 2010; Ramanan et al. 2012), and is critical for RNA silencing suppression (Haasnoot et al. 2007) and PKR inhibition (Schümann et al. 2009). These features highlight the viability of VP35 as an important target for therapeutic development.

1.3.1.1. EBOV VP35: the gene and the protein

Among the nine viral products encoded by the EBOV genome, the multifunctional VP35 protein is a key determinant of virulence and pathogenesis, which plays critical roles in several steps of the EBOV lifecycle, including genome replication and transcription, NC assembly and inhibition of the innate immune response to viral infection (Basler & Amarasinghe 2009). The VP35 protein is the product of a homonymous gene of ~ 1000 nucleotides in length whose locus represents the second ORF in the EBOV genome, located between the NP and VP40 genes (Fig. 14a). This ORF encodes for a protein that in Zaire subtype is 340 amino acid residues long (329 residues in SUDV and RESTV, 341 in TAFV and BDBV) with a molecular mass of ~ 35 kDa, from which the name. The amino acid sequence of VP35 consists of at least two domains (Fig. 14b). The N-terminal region is essential for replication and transcription of the EBOV genome. Spanning the first 220 residues, this region is composed of two flexible and disordered regions that flank a putative coiled-coil

domain (CCD) required for VP35 homo-oligomerization. This process leads to the formation of presumed homo-trimers and/or tetramers and was demonstrated to be indispensable for the role of VP35 as a polymerase co-factor (Moller et al. 2005). The C-terminal domain is instead important for the capability of VP35 to suppress the host innate immune response, and, given that this domain alone was found sufficient to exert such property, the tentative name of interferon inhibitory domain (IID) was proposed for it (Leung et al. 2009). Encompassing the last 120 C-terminal residues the IID is the only one portion of VP35 that has been structurally solved so far (Leung et al. 2009) (Fig. 14c). VP35 IID estimated molecular mass is ~ 16 kDa and it appears as a monomer in solution. It is further divided into two independently folded units, an N-terminal α-helical subdomain and a C-terminal β-sheet subdomain, connected one to the other by a short, flexible, 10 residues-long linker region. The α-helical subdomain is a bundle of four α-helices spanning residues 221-283, arranged in two layers that pack against the C-terminal β-sheet. This second subdomain comprises residues 294-340 and is folded into four stranded β-sheet and a brief, fifth α-helix (Leung et al. 2009) (Fig. 14d). Overall, the VP35 IID reveals a high degree of sequence similarity among filoviruses, with the most conserved residues belonging to two distinct basic patches, namely the first basic patch (FBP) and the central basic patch (CBP). The CBP is located at the very C-terminus, encompassing amino acids 304-340 and has been found essential for binding of VP35 to dsRNA, a property of the protein that is strongly correlated with its innate immune antagonism. This feature led to term VP35 IID also as RNA binding domain (RBD) and to consider it as a novel, unique fold that does not follow the α-β-β-β-α organization observed for canonical RBDs. Notably, a stretch of amino acid residues (304-313) within the CBP shares a very high degree of sequence similarity with the RBD of the multifunctional IAV NS1 protein, which is a dsRNA binding protein and known antagonist of the innate immune system (Kimberlin et al. 2010). EBOV replication and transcription are primer-independent processes and synthesis of viral RNA during these phases starts with a single nucleoside triphosphate, resulting in production of genomes, antigenomes and viral transcripts that bear 5'-ppp ends (Hastie et al.

2012). Given that this feature might be a potent inducer for RLRs-mediated IFN-α/β response, viral mRNAs are capped shortly after their initiation, while 5'-ppp motifs in genomes and antigenomes are immediately and tightly bound by NP-protein protomers. Also, such encapsidation of EBOV genomes and antigenomes within NC has the effect to avoid annealing of template and de novo synthesized viral RNAs into dsRNA, which is a major ligand of RLRs (Gerlier & Lyles 2011). However, even though EBOV RNAs are unlikely to be found naked in infected cells, the RNA-dependent RNA polymerase machinery is not perfect and might produce a variety of defective interfering (DI) RNA particles, such as read-through transcripts that remain uncapped or abortive genomes, antigenomes and small non-coding RNAs that fail to be encapsidated. These may undergo self-hybridization to form secondary structures or could anneal to complementary sequence resulting in dsRNA with blunt ends or exposed 5'-ppp, thus representing perfect agonist for the RIG-I pathway (Gerlier & Lyles 2011). To mask such DI particles and prevent recognition of EBOVs nucleic acids by RLRs, VP35 protein binds dsRNA in a sequence-independent manner, wrapping about its blunt or 5'-ppp-exposing ends (Hastie et al. 2012). As revealed by the two solved structures of Zaire EBOV IID in complex with 8 bp dsRNA (Daisy W Leung et al. 2010) and RESTV IID bound to a 18 bp dsRNA (Kimberlin et al. 2010), VP35 uses a bimodal strategy in which one VP35 monomer binds terminal nucleotides and the RNA phosphate backbone, while a second monomer binds only the phosphate backbone of dsRNA. These two modalities, termed as "end-capping" and "backbone-capping" respectively, lead the two VP35 monomers to assemble into an asymmetric dimer that creates a continuous, positively charged pocket for receiving dsRNA (Kimberlin et al. 2010) (Fig. 14e). The end-capping VP35 packs against the terminal bases of dsRNA with a non-polar face of hydrophobic residues as well as by a hydrogen bond from the carboxyl group of the very C-terminal I340 and, at the same time, it binds to the dsRNA phosphate backbone with basic residues K282, R312 and R322, which all lie within the highly conserved CBP of VP35 RBD. By contrast, two of those CBP residues (R312 and R322) and a third one (K339) do not bind dsRNA in the backbone-binding VP35, but rather form the dimer interface with the end-

capping VP35, while residues I340, S272, R305 and Q274 are among those that make hydrogen bonds with the dsRNA backbone in this VP35 monomer (Daisy W Leung et al. 2010). Notably, amino acid residues involved in both dsRNA and dimer-interface interaction, such as R312, R322 and K339 are those that were previously found as critical for EBOV immune suppression and VP35 dsRNA binding (Hartman et al. 2004; Cárdenas et al. 2006; Leung et al. 2009). However, such unique bimodal strategy adopted by VP35 seems to efficiently compete with RLRs by exactly mimicking their way to approach and bind to dsRNA. Therefore, by binding and sequestering key recognition motifs on dsRNA, VP35 blocks recognition and signaling by RIG-I and MDA-5 and prevents initiation of the type I IFN innate immune response (Kimberlin et al. 2010; Daisy W Leung et al. 2010).

1.3.1.2. EBOV VP35 function as antagonist of the innate immune system

The multifunctional VP35 protein has been implicated in a variety of molecular mechanisms by which EBOVs counteract the type I IFN antiviral response (Basler & Amarasinghe 2009). According to the current knowledge, EBOVs strategies seem to mainly consist in targeting RLRs pathways. The first indication that the VP35 protein could antagonize the host IFN response came from the discovery that this protein was able to functionally complement the impaired growth of delNS1 Influenza virus, a mutant virus lacking the gene that codes for the IFN antagonist NS1 protein (Basler et al. 2000). Follow-up experiments also demonstrated that VP35 abolishes the phosphorylation, dimerization and nuclear translocation of IRF-3, thereby connoting the IFN antagonism of VP35 in the suppression of the signaling pathway that originates from the activation of RIG-I upon stimulation by non self RNA (Basler et al. 2003). The search for a functional domain responsible of the inhibition of IRF-3 activation led to identify a dsRNA binding domain in the C-terminal half of VP35 that was sufficient, alone, to exert its anti-IFN properties (Hartman et al. 2004; Cárdenas et al. 2006). Notably, sequence alignment revealed that this domain of VP35 has high degree of similarity with N-terminal dsRNA binding domain of the IAV

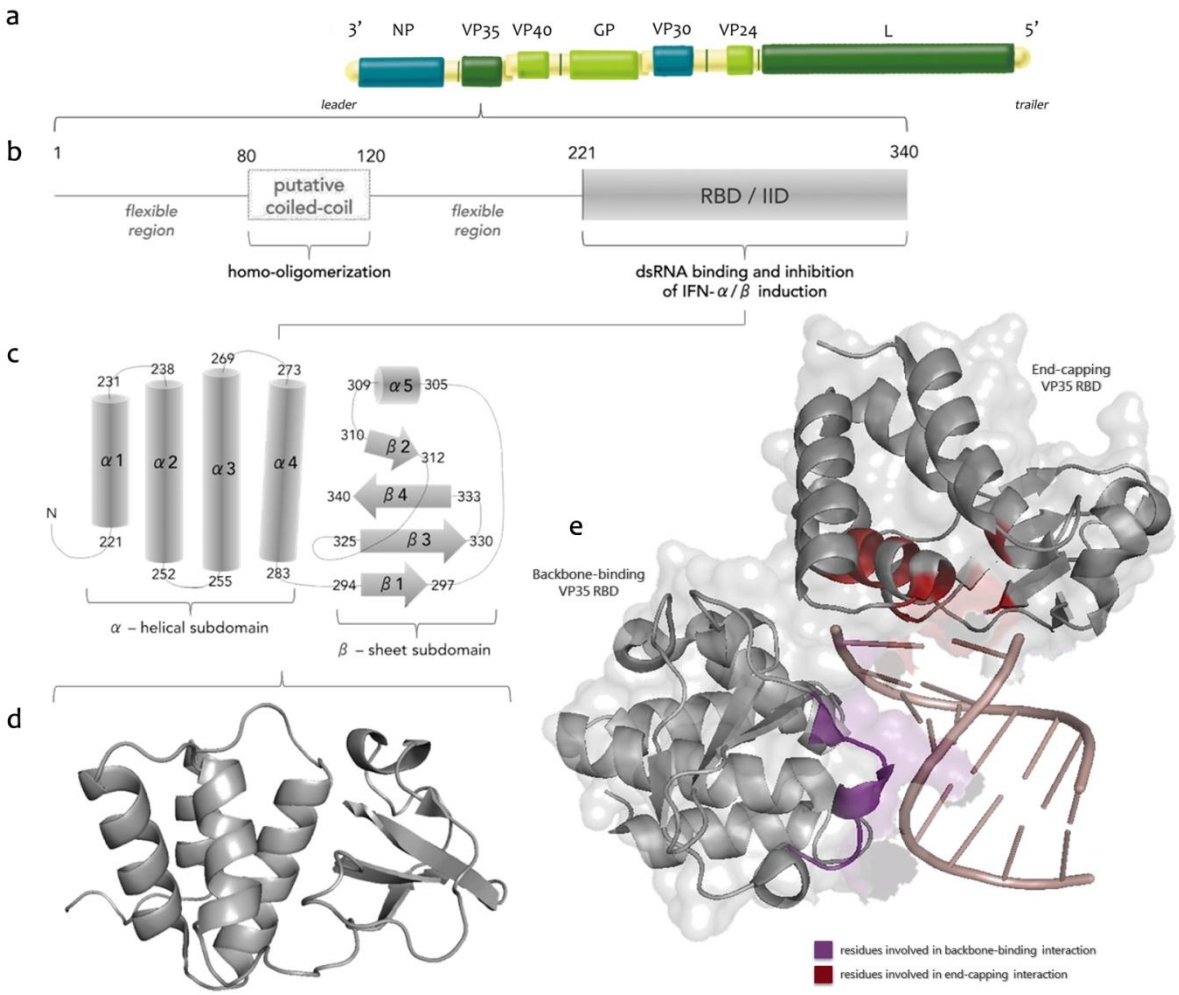

Figure 14. EBOV VP35 protein. Encoded by the second ORF within the EBOV genome (a), VP35 is a multifunctional protein of 340 amino acid residues and a molecular weight of ~ 35 kDa (b) consisting on an unsolved N-terminal region with a coiled-coil domain (CCD) essential for its homo-oligomerization and replicative function, and a structurally solved C-terminal region that is essential for its anti-IFN properties (c). Consisting of two alpha-helical and beta-sheet subdomains, this interferon inhibitory domain (IID) also contains a dsRNA binding domain (d) whose core sequence, named as central basic patch (CBP), is highly conserved among all ebolaviral species and displays a high degree of identity with the dsRNA binding domain if the influenza virus NS1 protein, a known IFN-antagonist. (e) VP35 binds to blunt-ended or 5'-ppp dsRNA with a bimodal strategy consisting of a monomer binding the nucleic acid phosphate backbone (backbone binding strategy) and another monomer binding to the terminal bases of dsRNA duplex (end-capping strategy).

NS1 protein (Hartman et al. 2004). In this regard, given that VP35 is able to bind dsRNA, it is not surprising that the major functional contribution to the IFN antagonism displayed by this protein resides in its C-terminal IID, where the dsRNA binding domain in also located (Cárdenas et al. 2006). As stated above, according to the proposed model, VP35 would block the induction of IFN-α/β by sequestering viral dsRNA to RIG-I recognition, and several observations strongly support the reliability of this interpretation. In fact, the mutation into alanine of basic residues R305, K309

and R312, which are located within the RBD, caused failure of dsRNA binding as well as loss of IFN inhibition without affecting VP35 replicative function (Hartman et al. 2004; Hartman et al. 2006; Hartman, Ling, et al. 2008). Upon infection with these mutant viruses, animals became protected by subsequent exposure by wild type EBOV, to which normally would have succumbed (Prins, Delpeut, et al. 2010). VP35 exerts its inhibition of RIG-I-mediated induction of IFN-α/β also by molecular mechanisms that are independent by its dsRNA binding function. In fact, given that this protein was found able to interact with the kinase domain of the TBK-1/IKK-ε complex and that it suppressed the activation of IFN-β promoter mediated by the overexpression of these two kinases (Prins et al. 2009), it is likely that VP35 may act as an alternate substrate for IFN kinases, thereby hampering the phosphorylation of IRFs. VP35 was also recently shown to hijack the host Small Ubiquitin-like Modifier (SUMO) machinery to accomplish extensive SUMOylation of IRFs (Chang et al. 2009). Through direct interaction with SUMO E2, Ubc9, PIAS1 and E3 ligase, and subsequent recruitment onto this complex of IRF-7 and IRF-3, VP35 promotes SUMOylation of these IRFs which, in turn, results in the transcriptional repression of type I IFN (Chang et al. 2009). In addition to suppression of the RLRs activation and RLR-mediated production of IFN-α/β, it is emerging that EBOV VP35 antagonizes the host cell defence targeting a variety of other antiviral mechanisms. In fact, VP35 was found to abolish the PKR-induced shutdown of protein translation, probably inhibiting the phosphorylation of its eIF2-α (Feng et al. 2007; Schümann et al. 2009). Moreover, VP35 has been shown to act as a suppressor of the RNA interference (RNAi) pathway. During EBOV infection RNAi is activated by the production of virus-specific dsRNAs, which are processed into 21 nucleotide long small interfering RNAs (siRNAs) by Dicer, an RNAse III-like endonuclease. Subsequently, siRNA is unwound, and one strand of this duplex, the guide-strand, is incorporated into the RNA-induced silencing complex (RISC). This complex, formed by TRBP and PACT proteins, uses the siRNA guide-strand to target viral mRNAs bearing complementary sequences. According to the model proposed, VP35 would overcome antiviral RNAi response by suppressing the RISC processing of siRNAs. In particular, VP35 interacts with Dicer and its two

partners TRBP and PACT, thereby subtracting RISC from approaching to siRNAs. Notably, given that these two members of the RISC also interact with and activate PKR, their sequestration might explain how VP35 suppresses PKR activity, given that a physical interaction between this kinase and VP35 was not detected (Fabozzi et al. 2011).

1.3.2. IAV NS1 protein

IAV replication, spread and pathogenesis are highly dependent on the function of NS1 protein (Basler & Aguilar 2008). Among the key features of NS1 is its capacity for RNA binding, including to dsRNA (Chien et al. 2004). One of the consequences of NS1 binding to dsRNA is to bind and sequester viral dsRNAs from detection by 2'-5' OAS (Min & Krug 2006). Activated OAS synthesizes 2'-5' oligoadenylates, which in turn stimulate latent RNase L, leading to viral RNA degradation (Silverman 2007). NS1 also binds and inhibits the activity of protein kinase R (PKR), inhibiting the PKR-dependent phosphorylation of eIF-2α and thereby avoiding shutdown of viral protein synthesis by PKR (Min et al. 2007). Other important roles of NS1 include binding to the 30 kDa subunit of cleavage and polyadenylation specificity factor (CPSF30), and also to poly(A)-binding protein II (PABPII) (Chen et al. 1999; Kuo & Krug 2009). These activities lead to inhibition of 3'-end processing of cellular pre-mRNAs and prevention of their nuclear export, including IFN mRNAs synthesized in response to viral infection. Further inhibition of cellular mRNA export is achieved by the interaction of NS1 with components of the nuclear pore complex (Satterly et al. 2007). Finally, NS1 has been shown to interact directly with TRIM25, an E3 ubiquitin ligase responsible for activation of RIG-I, which normally leads to downstream signalling and stimulation of the IFN response (Ludwig & Wolff 2009). NS1 binds to TRIM25, inhibits RIG-I ubiquitination and thus prevents the synthesis of cellular IFN (Gack et al. 2009).

1.3.2.1. IAV NS1: the gene and the protein

The IAV genome consists of eight single-stranded negative sense RNA segments that encode 10 or 11 viral proteins, depending on the strain. All of the proteins are structural proteins except for NS1 and PB1-F2. The NS1 protein is designated as non-structural protein because it is synthesized in infected cells, but is not incorporated into virions (Palese & Shaw 2007). This protein is coded by segment 8, which also encodes nuclear export protein (NEP, previously termed NS2) from a spliced mRNA. (Lin et al. 2007). Regulation of splicing is controlled, in part, by the viral NS1 protein itself and may represent a mechanism for auto-regulation of protein levels within infected cells.

NS1 has a strain-specific length of 230–237 aa and an approximate molecular mass of 26 kDa (Palese & Shaw 2007). NS1 is divided into two distinct functional domains: an N-terminal RNA-binding domain (residues 1– 73) (Fig. 8a), which in vitro binds with low affinity to several RNA species in a sequence independent manner, and a C-terminal 'effector' domain (residues 74–230) (Fig. 8b, c), which predominantly mediates interactions with host-cell proteins, but also functionally stabilizes the RNA-binding domain (Wang et al. 2002). The RNA-binding domain alone is a symmetrical homodimer with each monomer consisting of three α-helices. Dimerization is essential for binding dsRNA and the stoichiometry of dimer:dsRNA is 1:1 (Chien et al. 2004). Two identical helices from each NS1 monomer contribute towards dsRNA-binding by forming antiparallel 'tracks' on either side of a deep cleft. The 'tracks' consist of conserved basic and hydrophilic residues that appear to form complementary contacts with the polyphosphate backbone of dsRNA (Fig. 8d) (Yin et al. 2007). Residues in NS1 that mediate this interaction include T5, P31, D34, R35, R38, K41, G45, R46 and T49 (Yin et al. 2007). It should be noted that alanines are commonly substituted for both R38 and K41 in many experimental studies in order to abrogate the RNA-binding activity of NS1 (Fig. 8a). Crystallographic studies revealed that the C-terminal effector domain of both a human and avian NS1 protein (residues 74–230) can independently homodimerize, with each monomer consisting of seven β-strands and three α-helices (Benjamin G Hale et al. 2008). Within each monomer, the β-strands form a twisted,

crescent-like, anti-parallel β-sheet around a long, central α-helix. There is currently no structure available for the C-terminal ~25 amino acids of NS1, a region which is involved in many strain-specific functions. The precise dimeric assembly of the NS1 effector domain has yet to be fully established, as two dimer conformations have been proposed: strand–strand (Bornholdt & Prasad 2006), and helix–helix (Benjamin G Hale et al. 2008) (Fig. 8b, c). Amino acids involved at both dimer interfaces appear reasonably well-conserved; however, biochemical evidence indicates that W187 (a residue located at the helix–helix interface) is essential for dimerization of an avian NS1 effector domain in solution (Benjamin G Hale et al. 2008). This suggests that the helix–helix dimer, at least for the avian NS1 protein used, is likely to be biologically relevant (Fig. 8b, c). Interestingly, recent data suggest that a third dimeric state of the NS1 effector domain also probably exists (PDB ID: 2RHK). As a full-length NS1 protein structure has yet to be determined, the actual conformation of the complete NS1 dimer may differ significantly from that already published for the two individual domains (Benjamin G. Hale et al. 2008).

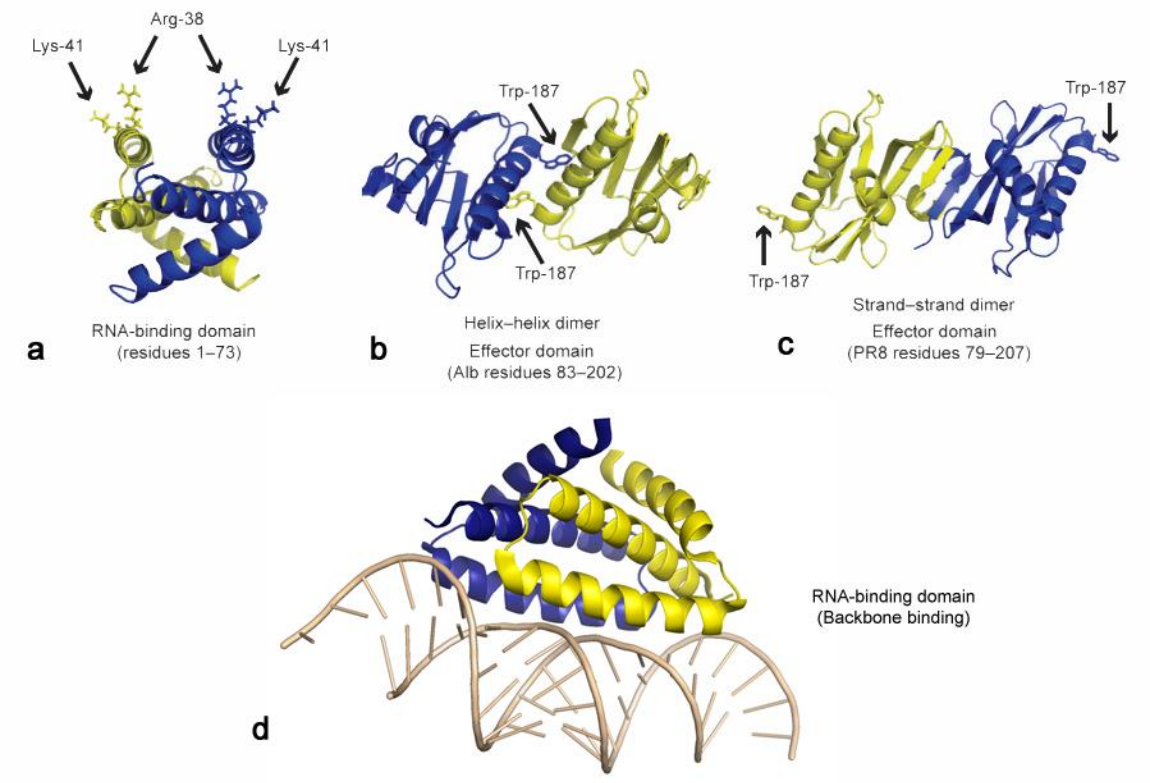

Figure 15. Structure of the IAV NS1 protein. (a) Cartoon ribbon representation of the dimeric RNA-binding domain (residues 1–73). R38 and K41, which are critical for RNA-binding, are highlighted. (b) and (c) Cartoon ribbon representations of the two proposed effector domain dimerization conformations. (b) Residues 83–202 (helix–helix dimer). (c) Residues 79–207 (strand–strand dimer). W187, which has been shown experimentally to be essential for dimerization of the avian NS1 protein effector domain, is highlighted in both structures. (d) Structure of NS1 RNA-binding domain (residues 1-70) bound to dsRNA phosphate backbone. For all structures (a–d), monomers are coloured blue and yellow. Images were prepared using PyMol (PDB files: 1NS1, 2GX9, 3D6R, 2ZKO).

1.3.2.2. IAV NS1 function as antagonist of the innate immune system

Several studies have attempted to demonstrate how NS1 acts to limit the production of IFN-β. Current evidence indicates that NS1 proteins limited IFN-β induction by both pre-transcriptional (cytoplasmic) and post-transcriptional (nuclear) processes (Benjamin G. Hale et al. 2008). Studies using NS1 of Influenza A/Puerto Rico/8/34 (IAV PR8) demonstrated that this protein prevents dsRNA- and virus-mediated activation of the IRF-3, NF-κB and c-Jun/ATF-2 transcription factors, which are otherwise essential for IFN-β induction (Talon et al. 2000; Ludwig et al. 2002). Such inhibition was shown to occur pre-transcriptionally, and to require two residues in NS1 that strongly contribute to RNA-binding: R38 and K41 (Talon et al. 2000) (Fig. 8a). Recent work indicates that PR8 NS1 may mediate its pre-transcriptional block on IFN-β induction by forming a

complex with RIG-I (Pichlmair et al. 2006; Mibayashi et al. 2007). Co-precipitation of RIG-I with PR8 NS1 is dependent upon R38 and K41 in PR8 NS1, suggesting that these two residues are involved in a potential protein–protein interaction, or that RNA acts as an intermediary component (Pichlmair et al. 2006). General inhibition of nucleo-cytoplasmic transport of all poly(A)-containing mRNAs was one of the first functions ascribed to NS1 and it was suggested that direct binding of NS1 to the 3' poly(A) tail of mRNAs was the mechanism by which this inhibition occurred (Qiu & Krug 1994). However, viral mRNAs are not prevented from leaving the nucleus of infected cells, despite them having a poly(A) tail. Therefore, interactions between NS1 and proteins directly involved in mRNA maturation and nucleo-cytoplasmic transport may play the greater and more specific role in cellular mRNA export inhibition (Benjamin G. Hale et al. 2008). Influenza virus A/Udorn/72 (Ud) has been extensively used to model the nuclear inhibition of cellular pre-mRNA processing by NS1. The C-terminal effector domain of Ud/ NS1 binds directly to two zinc-finger regions in the 30 kDa subunit of cleavage and polyadenylation specificity factor (CPSF30) and interacts with poly(A)-binding protein II (PABPII) (Chen et al. 1999; Kuo & Krug 2009). The Ud/NS1–CPSF30 complex is thought to prevent CPSF30 from binding cellular pre-mRNAs, thereby inhibiting normal cleavage and polyadenylation of the 3'-end of host-cell mRNAs. As polyadenylation of influenza A virus mRNAs is independent of cellular 3'-end processing factors, viral mRNAs are not affected by CPSF30 inhibition. Furthermore, the interaction of Ud/NS1 with PABPII may specifically block the nuclear export of fully processed mRNAs that partially escape 3'-end formation inhibition. Viral mRNAs must overcome this global block on nucleo-cytoplasmic transport; however, it is still unclear how this occurs. NS1 can directly block the function of two cytoplasmic antiviral proteins: 2'-5' OAS (Min & Krug 2006), and the dsRNA-dependent serine/threonine PKR (Min et al. 2007). A predominant function of the NS1 RNA-binding domain is to out-compete OAS for interaction with dsRNA, thereby inhibiting this host antiviral strategy. Given the role of RNase L in augmenting the production of IFN-β (Silverman 2007), it is possible that NS1-mediated OAS inactivation also contributes to suppression of IFN-β

synthesis (Talon et al. 2000). NS1 binds to a linker region in PKR, and prevents a conformational change that is normally required for release of PKR auto-inhibition. Such a mechanism allows NS1 to circumvent both dsRNA- and PACT-mediated inhibition of translation by PKR (Li et al. 2006). NS1 has been proposed to inhibit the induction of RNAi, but a functional role for NS1 in RNAi-antagonism during virus infection awaits clarification (Matskevich & Moelling 2007).

1.4. Aim of the research

Owing to the inhibitory functions exerted by the VP35 protein, EBOV is able to efficiently evade the innate immune response and replicate undisturbed. Therefore, VP35 is a key factor for EBOV virulence and pathogenicity, feature that makes it a valid drug target.

The aim of the research work presented in this thesis is focused on the development of strategies to overrun EBOV VP35 inhibitory functions of the IFN signaling cascade. In chapter 2 is presented the realization of a new miniaturized method able to reproduce the dsRNA-dependent RIG-I-mediated IFN-β induction signaling pathway, in order to evaluate and characterize EBOV VP35 inhibitory properties. Using this method with the aim to find new countermeasures against EBOV VP35 functions two different approaches were exploited. The first approach, described in chapter 3, is the attempt to identify VP35 target site/s suitable to design small molecules that bind VP35 dsRNA binding site and inhibit this function. The second approach, described in chapter 4, is the attempt to identify small molecules (of natural and/or synthetic origins) that, not physically interacting with VP35, could potentiate or activate the IFN signalling pathway, increasing the IFN production in response to viral infections up to a level sufficient to subvert VP35 inhibition.

2.0. A LUCIFERASE REPORTER GENE ASSAY TO MEASURE EBOLA VIRUS VP35 INHIBITION OF THE DSRNA RIG-I-MEDIATED IFN-β INDUCTION

2.1. Introduction

The high EVD lethality has been attributed to the ability of the virus to efficiently suppress the host innate antiviral response, which begins with the recognition of viral dsRNA by the cytoplasmic PRR RIG-I inducing type I IFN response. As previously described in Chapter 1, this induction is prevented by EBOV VP35 protein that, in the signal cascade that leads to type I IFN production, acts *i)* binding viral dsRNA and mimicking RIG-I recognition of 5'-ppp dsRNA (Zinzula & Tramontano 2013), *ii)* interfering with the activation of IRF-3 (Basler et al. 2000; Basler et al. 2003; Hartman, Bird, et al. 2008; Prins et al. 2009) and *iii)* inhibiting PACT-induced RIG-I ATPase activity by preventing RIG-I interaction with PACT (Luthra et al. 2013). Site-directed mutagenesis studies demonstrated that EBOV VP35 is a validated drug target by being involved in several processes that are crucial for successful virus replication and propagation (Prins, Binning, et al. 2010; Mitchell & Carter 2014). To characterize the role of the single EBOV VP35 functions in inhibiting the RIG-I signaling cascade leading to IFN-β production and to identify small molecules that could interfere with VP35 properties, a cell-based system able to quantify dsRNA IFN-β induction and its inhibition by EBOV VP35 is essential. IAV NS1 protein also strongly inhibits RIG-I-mediated IFN-β induction and a luciferase reporter gene assay has been used to assess its properties (Rückle et al. 2012), even though it was not suitable for drug development. Therefore, we established a luciferase reporter gene assay to assess EBOV VP35 inhibition of RIG-I-mediated IFN-β induction. We miniaturized and characterized the assay that can be used to evaluate EBOV VP35 properties as well as the efficacy of small molecules that can act as VP35 inhibitors.

2.2. Materials and Methods

2.2.1. Cell lines

A549 and MCDK cells were grown in Dulbecco's modified Eagle's medium (DMEM) (Gibco) supplemented with 10% fetal bovine serum (FBS) (Gibco), 1% Penicillin-Streptomycin (Pen/Strept) (EuroClone). Cells were incubated at 37 °C in a humidified 5% CO_2 atmosphere.

2.2.2. Construction of EBOV VP35 mammalian expression plasmid

To introduce the EBOV VP35 gene into a mammalian expression vector, we amplified the EBOV VP35 gene Zaire species (1976 Yambuku-Mayinga strain), previously cloned in the pET45b-ZEBOV-VP35 vector (Zinzula et al. 2009), by polymerase chain reaction (PCR). Two primers were designed to amplify the gene and introduce it into the mammalian expression vector construct by BamHI and NotI restriction enzymes. Primer sequences were: 5'-TCAGCAGAGGATCCGATAATGCATCACCACCACCATCAC-3' and 5'-GTACTAATATGCGGCCGCTCAAATTTTGAGTCCAAGTGT-3'. PCR reaction was carried out in a mixture containing: pET45b-ZEBOV-VP35 plasmid (100 ng), each primer (400 µM), $MgCl_2$ (1.5 mM), each dNTP (0.2 mM) and 0.025 µl FideliTaq™ DNA Polymerase (Usb). The PCR mixtures were filled with nuclease-free water to a final volume of 50 µL and the PCR cycle consisted of: an initial denaturation at 94 °C for 2', 35 cycles of denaturation at 94 °C for 30", annealing at 55 °C for 30", extension at 68 °C for 2', and a final extension at 68 °C for 5'. The amplified EBOV VP35 gene and the pcDNA3 plasmid (Invitrogen) were digested by BamHI and NotI restriction enzymes (New England BioLabs), linear pcDNA3 plasmid was dephosphorylated with Antarctic Phosphatase (New England BioLabs) and fragments (50 ng of linear pcDNA3 and 20 ng of insert VP35) were ligated by T4 DNA ligase (New England BioLabs) to obtain the pcDNA3-ZEBOV-VP35 plasmid that

was transformed to the *E. Coli* Top 10 strain by standard heat shock protocol at 42 °C for 90". Plasmid was extracted and sequenced for control.

2.2.3. IAV PR8 propagation

MDCK cells were infected with IAV/Puerto-Rico/8/34 (IAV PR8) strain with a MOI of 0.001 in *Infectious DMEM* with 0.2% bovine serum albumin (BSA) (Sigma Aldrich), 1% Pen/Strept, 0.01% Ca/Mg solution and 3 µg/ml of trypsin at 37 °C for about 56 hours. The medium was collected in a falcon and centrifuged at 3000 x g for 10 min at 4 °C. The virus present in the supernatant is aliquoted and frozen at -80 ° C.

2.2.4. IAV PR8 titration

MDCK cells were seeded in a 6-well multiwell plate and treated with serial dilutions (1:10) of a IAV PR8 aliquot in *Infectious PBS* with 0.2% BSA, 1% Pen/Strept and 0.01% Ca/Mg solution at 37 °C for 30 min. The inoculum was aspirated and the Plaque medium with 3% Agar was added. The plate was incubated at 37 °C for about 72 hours. 1 ml of 3.6% formaldehyde is added to each well for 1 hour and then washed with water. The lysis plaques were highlighted by Crystal violet staining.

2.2.5. IAV PR8 RNA extraction

For production of viral RNA (vRNA), A549 cells were infected with IAV PR8 with a MOI of 5 in *Infectious PBS* for 30 min. The inoculum was aspirated and the *Infectious DMEM* was added. 5 hours post infection the total RNA was isolated using the RNeasy Kit (Qiagen).

2.2.6. Luciferase reporter gene assay

A549 cells (5 x 10^4 per well) were transfected in 48-well plates with T-Pro P-Fect Transfection Reagent (T-Pro Biotechnology) with the construct pGL IFN-β luc kindly provided by Prof. Stephan Ludwig (Institute of Molecular Virology, Münster, Germany). Twenty-four hours after transfection cells were additionally transfected with IAV PR8 vRNA and incubated for further 6 hours at 37 °C with 5% CO_2. Cells were harvested with lysis buffer (50 mM Na-MES pH 7.8, 50 mM Tris-HCl pH 7.8, 1 mM dithiothreitol, 0.2% Triton X-100). The crude cell lysates were cleared by centrifugation and 50 µL of cleared lysates were added to 50 µL of luciferase assay buffer (125 mM Na-MES pH 7.8, 125 mM Tris-HCl pH 7.8, 25 mM magnesium acetate, 2.5 mg/ml ATP) in a white 96-well plate. Immediately after addition of 50 µL 1 mM D-luciferin into each well, the luminescence was measured in Victor^3 luminometer (Perkin Elmer). The relative light units (RLU) were normalized as the fold activity of the unstimulated control. Each assay was carried out in triplicate.

2.2.7. EBOV VP35 luciferase reporter gene inhibition assay

The above described luciferase reporter gene assay was used with the co-transfection of the pGL IFN-β luc plasmid with the pcDNA3-ZEBOV-VP35. When IAV NS1 was used as control, the mammalian expression plasmid pcDNA3-NS1, kindly provided by Prof. Stephan Ludwig (Institute of Molecular Virology, Münster, Germany) was co-transfected with the pGL IFN-β luc plasmid. Inhibition of luciferase expression was indicated as percentage of induced control. Each assay was carried out in triplicate.

2.3. Results

2.3.1. Miniaturization of the luciferase reporter gene assay in 48-well plates

When viral 5'-ppp dsRNA is accumulated into the cytoplasm of infected cells, its presence is recognized by RIG-I that induces a signaling cascade finally leading to the expression of IFN-β. This cytokine acts then in both autocrine and paracrine manner to induce the expression of a number of proteins coded by the ISGs that, in turn, suppress viral propagation. EBOV VP35 inhibits the RIG-I-mediated IFN-β induction (Basler et al. 2000) and this ability has been previously measured with a luciferase reporter gene assay in which IFN-β induction was stimulated by Sendai virus (SeV) infection (Basler et al. 2000; Basler et al. 2003; Hartman et al. 2004; Cárdenas et al. 2006; Prins et al. 2009; Daisy W Leung et al. 2010; Prins, Binning, et al. 2010), a method that strongly limits its range of use. Therefore, we wanted to establish a more suitable assay that could mimic the viral dsRNA IFN-β induction and could be used for drug screening. A 12-well plates method using A549 cells that were transiently transfected with a luciferase reporter gene construct (pGL IFN-β luc) driven by the IFN-β enhanceosome, a promoter element that contains all principal transcription factor binding sites of the IFN-β promoter was previously reported (Rückle et al. 2012; Hillesheim et al. 2014). In this assay, the transfection of Influenza virus A/Puerto Rico/8/1934 viral RNA (IAV PR8 vRNA) into A549 cells containing pGL IFN-β luc plasmid activates the RIG-I signaling cascade leading to a luminescent signal (System 1, Fig. 16). Such method was not suitable for drug development, therefore in order to apply this system to evaluate EBOV VP35 inhibitory functions for drug development purposes, we firstly needed to verify if we could miniaturize it. The PAMP chosen in our experiments to unleash the innate antiviral response, as mentioned above, is the vRNA of IAV PR8. To propagate this virus the MDCK cells was used to replace the conventional method which involves the use of chicken embryos. The use of this cell line derives from its ability to rapidly replicate in simple culture conditions and especially from the lack of an antiviral response which would interfere with the virus multiplication. The MDCK cells

were infected with a MOI of 0.001. The choice of a low MOI is essential for viral particles replication and propagation, which occurs at 37 °C during about 56 hours, until the cytopathic effect (CPE) shows an increase of 70%. The virus that was present in the supernatant was aliquoted and frozen at -80 ° C. To determine the viral titre of the prepared stock a plaques assay was used. The MDCK were seeded in a 6-well plate and treated with serial dilutions from an IAV PR8 aliquot to quantify. The culture was incubated for about 72 hours, during which the virus cytopathic effects occurring through the plaques lysis formation highlighted by the Crystal violet addition. IAV PR8 vRNA stocks were prepared by in vitro infection of A549 cells with IAV PR8 and subsequent purification of ribonucleic acid. The A549 cell line was infected at MOI 5 for 5 hours at 37 ° C. During the 5 hours of incubation, the ssRNA genomes were replicated and accumulated inside the infected cells, also in dsRNA form as replicative intermediate. The purification of viral RNA from the cell lysate was performed with silica-membranes. Once obtained the PAMP, we evaluated the IFN-β activation by vRNA transfection in 48-well plates and performed a time-course to assess the timing to optimize RLU signaling (Fig. 17a). Results showed that a minimum of 6 hours was needed to obtain a sufficiently strong RLU signal. Secondly, we asked which was the optimal timing for an efficient vRNA transfection and performed a vRNA transfection time-course, observing that the minimum time for an efficient transfection was 3 hours (Fig. 17b). Thirdly, to further optimize the assay, we asked which were the optimal amounts of luciferase plasmid and vRNA to be transfected into each 48-well. Hence, A549 cells were initially transfected with various amount of pGL IFN-β luc (125, 250 and 500 ng per well) and after 24 hours cells were additionally transfected with various amount of IAV PR8 vRNA (75, 125, 250 and 500 ng per well). Luciferase activity was measured 6 hours post transfection. Results showed that optimal concentrations for both reporter vector and vRNA were 250 ng (Fig. 17c). We also tried to further miniaturize the assay using 96-well plates, however the RLU signal was not sufficiently consistent to allow a reproducible use (data not shown).

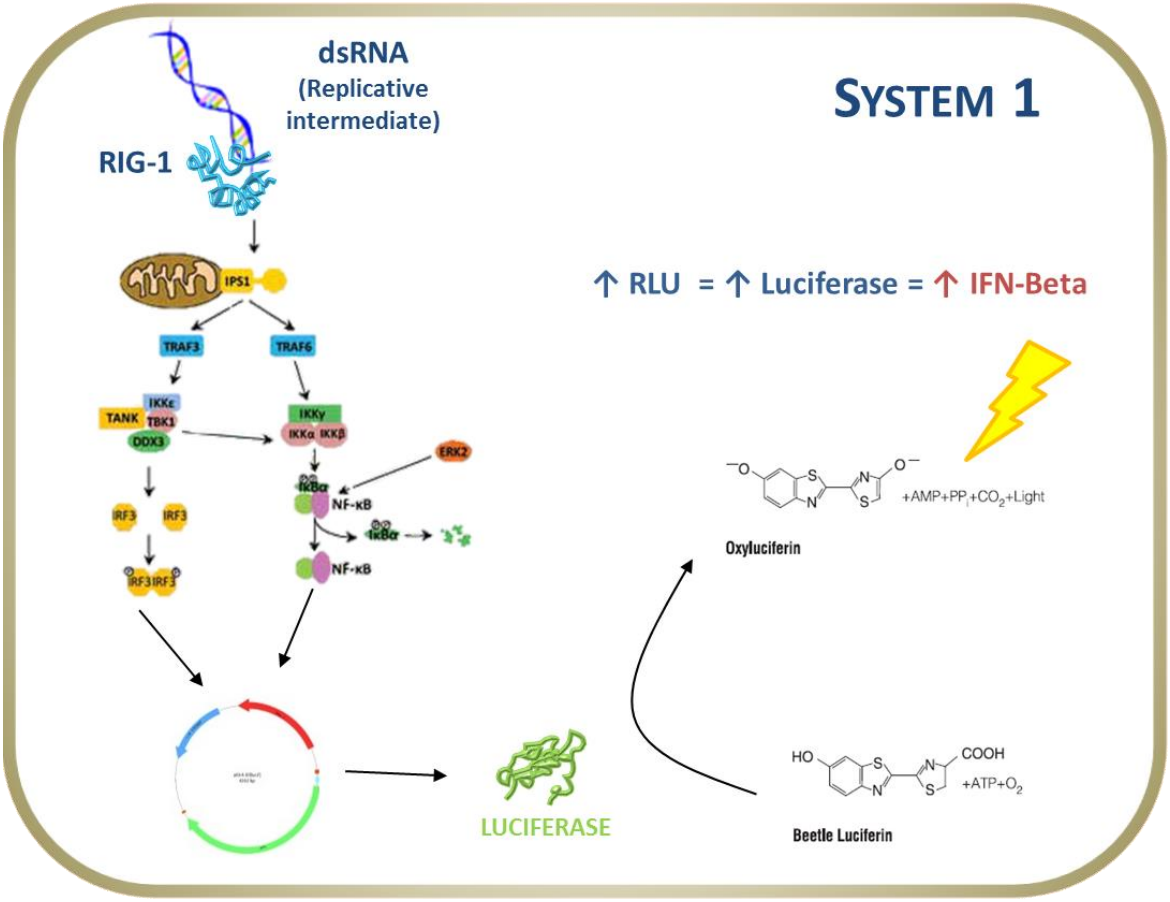

Figure 16. Stimulation of innate immune response: System 1. In *System 1*, the recognition of PAMP triggers the signal cascade that will lead to the activation of IFN-β promoter that will produce luciferase. After 6h stimulation, cells are harvested. 50 µl of cell extracts are added to 50 µl of luciferase assay buffer and immediately after injection of 50 µl 1 mM D-luciferin into each sample, the luminescence is measured with a luminometer.

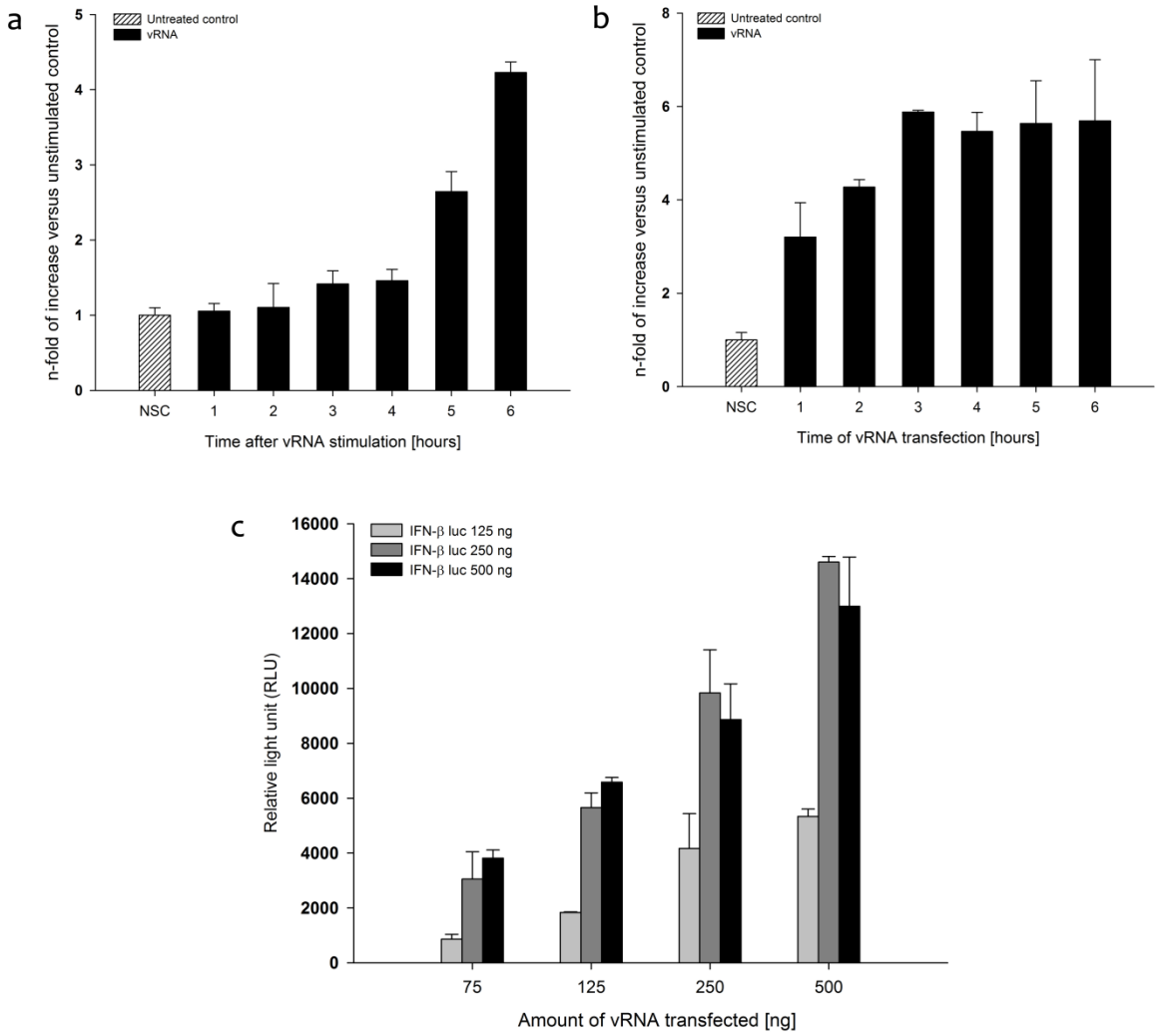

Figure 17. Miniaturization of the luciferase reporter gene assay in 48-well plates. (a) A549 cells were transfected with pGL IFN-β luc and 24 hours post transfection cells were additionally transfected with IAV vRNA. Cells were lysed respectively after 1, 2, 3, 4, 5 and 6 hours and the luciferase activity was measured. (b) A549 cells were transfected with pGL IFN-β luc and 24 hours post transfection cells were additionally transfected with IAV vRNA and the medium was changed respectively after 1, 2, 3, 4, 5 and 6 hours and luciferase activity was measured. (c) A549 were transfected with 125 ng, 250 ng and 500 ng of pGL IFN-β luc and 24 hours post transfection cells were additionally transfected with 75, 125, 250 and 500 ng of IAV vRNA. 6 hours post transfection cells were lysed and luciferase activity was measured.

2.3.2. Inhibitory effect of EBOV VP35 and IAV NS1 in the luciferase reporter gene assay in 48-well plates

Once developed the system, we asked whether this 48-well assay could be used to evaluate the ability of EBOV VP35 to inhibit the RIG-I-mediated IFN-β induction as measured by a lower production of luciferase as compared to the dsRNA stimulated control. We subcloned the EBOV Zaire strain *VP35* gene from the bacterial expression vector pET45b-ZEBOV-VP35 (Zinzula et al. 2009) into the mammalian expression vector pcDNA3. Firstly, using two primers to add BamHI and NotI cleavage sites at the ends of the *VP35* gene (Fig.18a); secondly, amplifying by PCR (Fig. 18b) and finally, cutting the PCR product and the vector pcDNA3 with these enzymes and carrying out the ligase reaction. The outcome of the ligation reaction was checked by further digestion and electrophoresis (Fig.18c). Since it is known that IAV NS1 protein strongly inhibits RIG-I-mediated IFN-β production (Rückle et al. 2012) we used IAV NS1 as control. The reporter vector was co-transfected with various amounts of pcDNA3-VP35 or pcDNA3-NS1 (10, 45, 180, 750 and 3000 ng) leading to different levels of viral protein expressions inside the cells (data not shown) (System 2, Fig. 19). Results showed a dose-dependent inhibition of the dsRNA stimulated RIG-I-mediated IFN-β production by both EBOV VP35 and IAV NS1 (Fig. 20). It is worthwhile to note that, at all plasmid concentrations, EBOV VP35 showed an inhibitory effect higher than the one shown by IAV NS1, suggesting that EBOV VP35 could be more efficient than IAV NS1 in inhibiting innate immune activation.

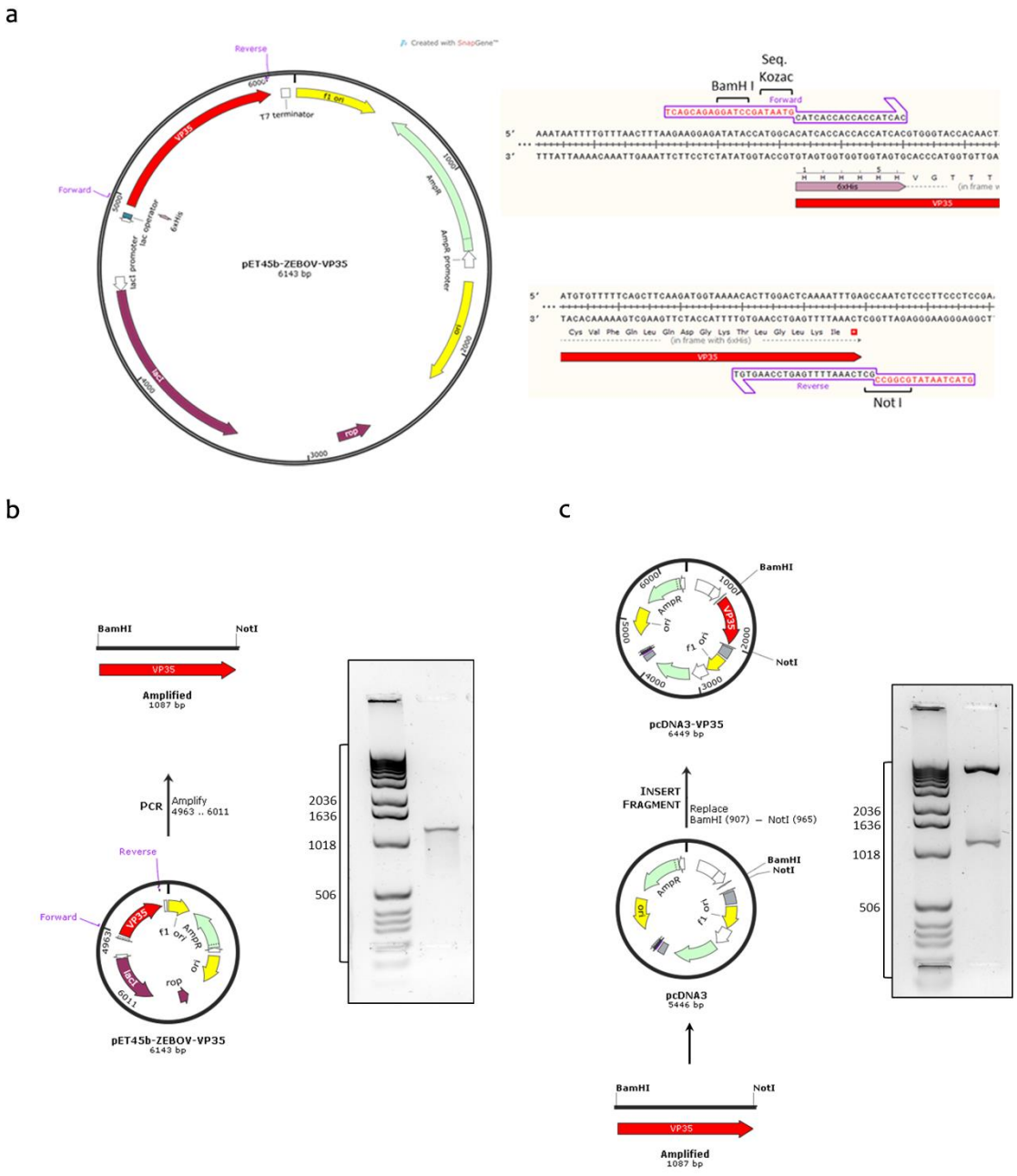

Figure 18. EBOV *VP35* gene subcloning into mammalian expression vector. (a) To add the BamHI and NotI cleavage site at the 5'- and 3'-ends of the *VP35* gene respectively, two primers were designed. (b) The *VP35* gene was amplified by PCR. (c) The amplified product and the pcDNA3 vector were cut with the restriction enzymes and were subjected to ligation reaction. After ligated product transformation in *E. coli* and extraction of the amplified plasmid, it was digested with the same restriction enzymes to check the *VP35* gene insertion in the plasmid.

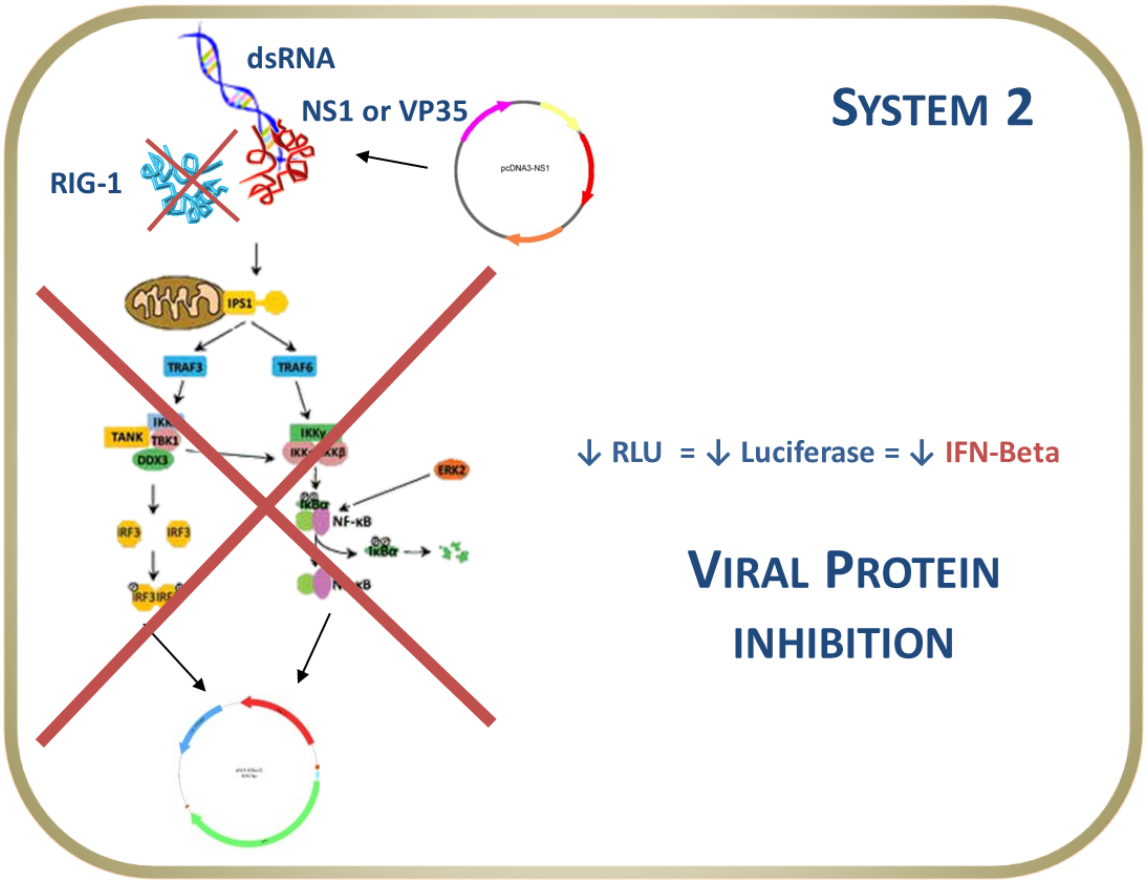

Figure 19. Stimulation inhibition of innate immune response: System 2. In *System* 2, the response will be inhibited by the presence of the viral proteins, NS1 or VP35, produced through transfected plasmid. After 6h stimulation, cells are harvested. 50 µl of cell extracts are added to 50 µl of luciferase assay buffer and immediately after injection of 50 µl 1 mM D-luciferin into each sample, the luminescence is measured with a luminometer.

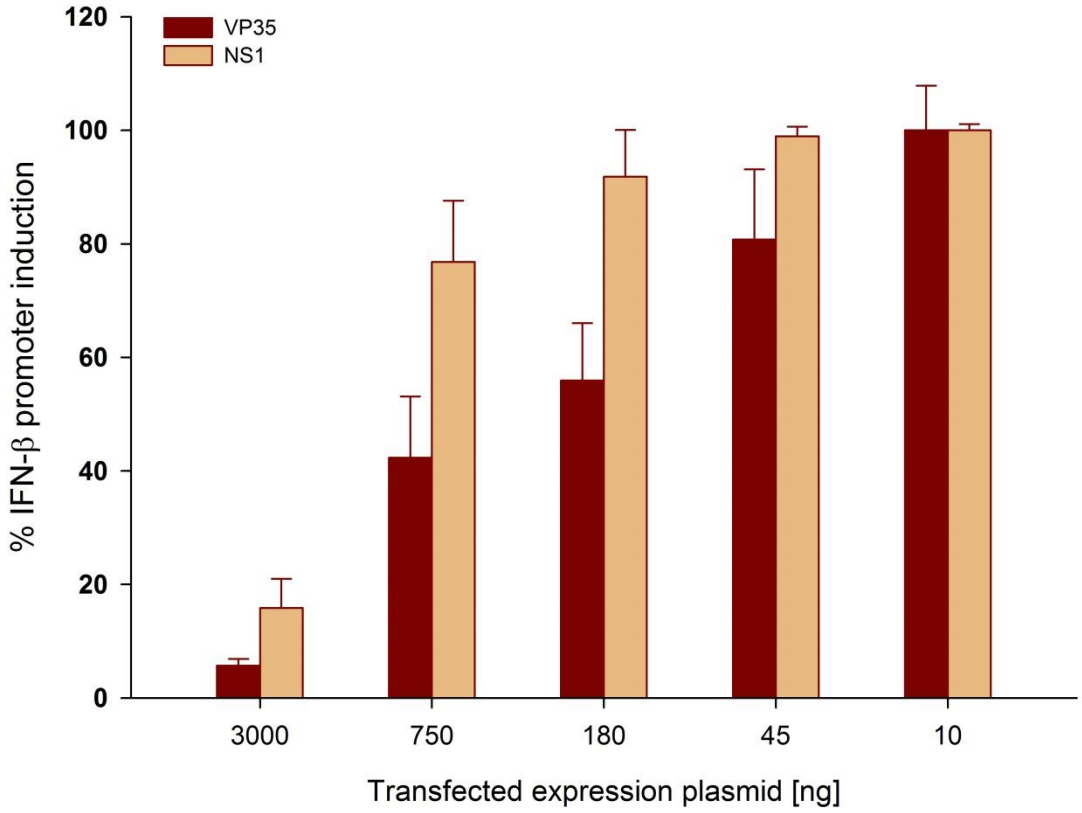

Figure 20. Inhibitory effect of EBOV VP35 and IAV NS1 in the luciferase reporter gene assay in 48-well plates. A549 cells were co-transfected with 250 ng of pGL IFN-β luc and various amount (10, 45, 180, 750 and 3000 ng) of pcDNA3-VP35 or pcDNA3-NS1. 24 hours post transfection cells were additionally transfected with 250 ng of IAV vRNA and after additional 6 hours cells were lysed and luciferase activity was measured.

2.4. Discussion.

In 2014 the largest Ebola outbreak in West Africa resulted in tens of thousands of victims and raised great concerns as it compromised public health systems and led to social disruptions. Cases of EVD have also been reported in both USA and Europe, further increasing the level of public awareness for EVD diffusion threat. Development of drugs that can inhibit EBOV replication and counteract EVD progression is therefore a global health priority. EBOV VP35 is a valid drug target, since it is one of the most potent weapons that EBOV uses to evade the innate immune antiviral response (Basler et al. 2003; Hartman, Bird, et al. 2008; Prins, Binning, et al. 2010; Daisy W. Leung et al. 2010). In fact, EBOV VP35 interferes at various levels of the RIG-I-mediated signaling cascade that leads to the type I IFN production, allowing undisturbed viral multiplication. We have previously obtained a full-length recombinant version of the EBOV VP35 protein (Zinzula et al. 2009) and have characterized its dsRNA binding function using a newly established in vitro magnetic pull down dsRNA binding assay (Zinzula et al. 2012). However, to assess the specific role that each VP35 function has in inhibiting the RIG-I-mediated signaling cascade as well as to screen for potential inhibitors, it was required the establishment of a robust and reproducible cellular assay that could measure the dsRNA induced RIG-I signaling pathway activation. Until now, methods used to analyze VP35 effects on IFN-β promoter activation utilized cellular infection with SeV as innate immunity stimulus (Basler et al. 2000; Basler et al. 2003; Hartman et al. 2004; Cárdenas et al. 2006; Prins et al. 2009; Daisy W Leung et al. 2010; Prins, Binning, et al. 2010). This technique requires up to 24 hours of stimulation to measure the luminescence signal and a more complex experimental approach, including virus manipulation. In addition, SeV infection does not activate only the RIG-I-mediated signaling pathway, which is the major VP35 target, eventually leading to IFN-β promoter activation through other pathways. An alternative more manageable method used IAV dsRNA transfection as a stimulus for the activation of RIG-I signaling pathway that culminates in IFN-β production (Hillesheim et al. 2014). Therefore, we modified this assay by

miniaturizing it from 12-well to 48-well plates, a format more suitable for small molecules screening, and optimized the assay condition which only requires 6 hours of stimulation. Subsequently, we showed that EBOV VP35 expression can inhibit the dsRNA induced RIG-I-mediated IFN-β activation dose-dependently, demonstrating that the assay can be used to identify EBOV VP35 inhibitors. Noteworthy, when compared with NS1, EBOV VP35 inhibitory efficacy was greater at higher transfected plasmid concentrations. More studies however should be performed to assess if EBOV can suppress innate immunity activation more effectively than IAV. Overall, we described the establishment of a new cell-based method to characterize EBOV VP35 properties related to its inhibition of the RIG-I-mediated IFN-β induction and to identify small molecules that can interfere with these properties.

3.0. Definition of Key Residues in dsRNA Recognition and IFN-Antagonism of Ebola Virus VP35 for Drug Development

3.1. Introduction

As described in Chapter 1, EBOV VP35 IID forms an asymmetric dimer held together by a network of hydrogen bonds with dsRNA-end independently of the nucleotide sequence: one monomer binds the sugar-phosphate backbone of both dsRNA strands and the second binds to dsRNA terminal bases and the proximal phosphate backbone. Together, the backbone-binding and the end-capping binding VP35 monomers mimic the RLRs shape and hide their recognition site at 5'-ppp dsRNA ends (Cárdenas et al. 2006; Leung et al. 2009; Daisy W Leung et al. 2010; Kimberlin et al. 2010; Ramanan et al. 2012; Bale et al. 2013; Zinzula & Tramontano 2013). The crystallographic structures provide structural basis to understand dsRNA binding-mediated inhibition of IFN response by EBOV VP35, also revealing the relative contribution of several amino acids for this function, showing differences in contribution between the two RBD/IIDs. For instance, side chains of amino acid residues R312 and R322 (EBOV numbering) are in the backbone-binding RBD/IID monomer involved in protein-protein interactions at the dimer interface, whereas the same residues undertake interactions with dsRNA in the end-capping RBD/IID. Similarly, amino acid residues such as F239, Q274, I278, K339 and I340 interact with dsRNA backbone in the backbone-binding monomer, whereas they bind to dsRNA terminal bases in the end-capping one (Daisy W Leung et al. 2010; Kimberlin et al. 2010). Moreover, the importance of VP35 RBD/IID residues like R305, K309, R312, K319, R322, F239 and K339 has been highlighted by previous mutagenesis studies, which showed decrease or loss of dsRNA binding function (Cárdenas et al. 2006; Leung et al. 2009; Daisy W Leung et al. 2010; Prins, Delpeut, et al. 2010; Zinzula et al. 2012) as well as diminished or abolished suppression of IFN-β induction (Hartman et al. 2004; Cárdenas et al. 2006; Hartman, Bird, et al. 2008; Hartman, Ling, et al. 2008; Leung et al. 2009; Daisy W Leung et al. 2010;

Prins, Delpeut, et al. 2010). In addition to end-capping, total coat of dsRNA has been described in three more recent crystallographic structures of EBOV VP35 RBD/IID and the one of closely related Marburg virus (MARV) (Bale et al. 2012; Ramanan et al. 2012; Bale et al. 2013). Shielding all available RLRs activation sites along the nucleic acid helix in addition to the sole dsRNA termini amplifies the extent of VP35 anti-IFN capabilities, reinforcing the importance of VP35 dsRNA binding function as antiviral target. However, given the difficulties in inhibiting the VP35 binding to a wide and non-specific surface of dsRNA backbone, on the one hand, and the specificity of 5'-ppp recognition, on the other hand, led us to focus on targeting the small surface of VP35 end-capping site that has potentially more implications for small molecule inhibitors design. We previously developed a biochemical assay to assess dsRNA binding ability of EBOV full length recombinant VP35 (rVP35) (Zinzula et al. 2009; Zinzula et al. 2012) and a reporter gene assay that evaluates the IFN-antagonist ability of EBOV VP35 expressed in A549 cell line (Chapter 2). Hence, in order to define their impact on dsRNA end-capping, we performed a structure-based alanine scanning mutagenesis of rVP35 residues involved in this interaction. The data collected, together with computational studies, allowed the identification of a defined site, important for prospective drug design against immune suppression function of EBOV VP35.

3.2. Materials and methods

For cell lines, mammalian expression plasmids and luciferase reporter gene inhibition assay used see Materials and methods in Chapter 2.

3.2.1. EBOV VP35 wt and mutant plasmids

Cloning of the EBOV VP35 gene into pET45b(+) vector (Novagen) to obtain the pET45b-ZEBOV-VP35 plasmid was previously described (Zinzula et al. 2009). The QuickChange II Site-Directed Mutagenesis kit (Agilent technologies) was used to obtain corresponding mutant plasmids by

introducing in the EBOV cDNA VP35 gene sequence previously described single point mutations R305A, K309A, R312A (Zinzula et al. 2012) and new mutations F239A, S272A, Q274A, L277A, I278A, Q279A, I280A, T281A, K282A, K319A, R322A, K319A/R322A and K339A.

3.2.2. Expression and purification of full-length wt and mutants EBOV rVP35

Full-length, wt and mutants, bacterially-expressed rVP35s were obtained as previously described (Zinzula et al. 2009). Briefly, protein expression was carried out on transformed *E. coli* BL21AI (Invitrogen) cultured in LB media at 37 °C and induced at an optical density of 0.6 OD at 600 nm with 0.4% L-arabinose (Sigma-Aldrich). rVP35s were IMAC purified with Ni-Sepharose High Performance (GE Healthcare) beads by using a BioLogic LP FPLC system (Biorad), and dialyzed in desalting buffer (50 mM sodium phosphate pH 7.5, 300 mM NaCl, 10% glycerol, 0.014% β-mercaptoethanol). As previously published (41), rVP35 full-length proteins were purified at ≈95% homogeneity, their integrity was assessed by PAGE analysis and their concentration was calculated using the Protein Quantification kit-Rapid (Fluka).

3.2.3. Differential scanning fluorimetry analysis

Differential scanning fluorimetry (DSF) analysis was carried out in a MiniOpticon real-time PCR instrument (BioRad) by using the Protein Thermal Shift Dye kit (Life technologies) according to manufacturer's instructions. Measurements were performed using excitation λ = 470-505 nm and emission λ = 540-700 nm and data were acquired on a temperature gradient from 25 °C to 95 °C with increments of 0.5 °C. Samples contained 2 µg rVP35 protein, 1X SYPRO Orange (Life technologies), 50 mM sodium phosphate pH 7.5, 150 mM NaCl and 20 mM $MgCl_2$ in a 20 µL final volume. Fluorescence data were analyzed, and the derivative of the curve representing melting temperature (T_m) of wild type and mutants rVP35 was obtained by using the CFX manager software v.2.1 (BioRad) tool for protein thermal shift assays protocols.

3.2.4. dsRNA in vitro transcription and dsRNA labeling

Heterologous 500 bp dsRNA was produced by in vitro transcription using the T7 MEGAscript RNAi kit (Ambion) from the linearized DNA provided with the kit, according to manufacturer's instructions. The 500 bp labeled dsRNA was generated by supplementing the in vitro transcription reaction with 0.15 µCi of ^{3}HGTP (35.5 Ci/mmol) (Perkin–Elmer). The DNA control template provided by Ambion was used to generate, by standard PCR protocols, other two linearized DNA templates to in vitro transcribe the 150 and 50 bp dsRNA as above. All in vitro transcribed (IVT) dsRNA molecules were purified from transcription reaction with the MEGAclear kit (Ambion) or with Quick Spin G25 columns (Roche), and quantified by spectrophotometry. The integrity of DNA templates and IVT dsRNA molecules was assessed by agarose-gel electrophoresis.

3.2.5. Magnetic pull down assay

The rVP35-dsRNA complex formation was assessed exploiting the properties of the TALON paramagnetic Dynabeads (Invitrogen). Firstly, 1 µg of rVP35 was conjugated to 50 µL TALON beads in a volume of 700 µL of binding/washing buffer (50 mM sodium phosphate pH 7.5, 150 mM NaCl, 0.05% Tween-20) for 15 min at 23 °C under gentle rotating agitation (20 rpm). Unconjugated rVP35 was removed by magnetic field application, supernatant removal and further washing with binding/washing buffer. Pellets with conjugated rVP35 were re-suspended in a 100 µL volume of binding/washing buffer containing 20 mM $MgCl_2$ and 1.5 nM 500 bp ^{3}H-dsRNA (0.1 Ci/mmoles), then incubated for 60 min at 37 °C (20 rpm). Unbound ^{3}H-dsRNA was separated by the conjugated rVP35-dsRNA complex by magnetic field application and supernatant removal. A further washing step was performed to completely remove unbound ^{3}H-dsRNA. ^{3}H-dsRNA elution was performed by incubation of the beads pellet in 300 µl elution buffer (binding/washing buffer plus 1 M imidazole pH 7.5) for 10 min at 23 °C (20 rpm), subsequent magnetic field application and

supernatant removal. The supernatant was transferred to vials and radioactivity was determined with a Beckman LS 6500 beta-counter (Beckman-Coulter).

3.2.6. Molecular Systems Preparation

The coordinates of VP35-dsRNA homodimer structure were taken from the RCSB Protein Data Bank (PDB ID: 3L25) (Daisy W Leung et al. 2010). The protein was prepared by using the Maestro GUI Protein Preparation Wizard module (Schrödinger LLC. 2014. Maestro GUI, New York, NY, USA). Bond orders and formal charges were added for hetero groups, and all the hydrogen atoms were added in the structure. After preparation, the structures were refined to optimize the hydrogen-bond network by using OPLS2005 force field (Banks et al. 2005). The minimization was terminated once the energy converged or the RMSD reached a maximum cut off of 0.30 Å. Wild type (wt) model was generated introducing 5'-ppp dsRNA as terminal portion using build module in Maestro GUI available in Schroedinger Suite 2014 (Schrödinger LLC. 2014. Maestro GUI, New York, NY, USA). The protein was then minimized Polak-Ribiere conjugate gradient minimization allowing 10000 iteration and a convergence threshold of 0.01 in GB/SA implicit water (Still et al. 1990). Since the model misses the coil-coil tail portion and dsRNA is likely to be open during the simulation, force constraints were applied around residue Asp218 and dsRNA terminal bases (C1-G8). The rest of the complex was left free to move. Minimized complex was then used as initial structure for MD simulation, where the same constraints were maintained. Mutants were generated based on wild type structure by mutating the corresponding residues.

3.2.7. Molecular Dynamics Simulations and MM-GBSA Calculations

MacroModel of Schrödinger Suite Software (Mohamadi et al. 1990) was applied to carry out molecular dynamics simulations (3ns) including the energy minimization and equilibration protocols (200ps). The production phase runs 3ns. The binding free energy calculations were

performed by MM/GBSA (Kollman et al. 2000) method using extracted snapshots from equilibrated trajectories. Binding free energy was computed:

$\Delta G_{bind} = G_{complex} - G_{protein} - G_{RNA}$

The free energy G, can be calculated using the scheme as follows:

$\Delta G = \Delta E_{MM} + \Delta G_{sol} - T\Delta S, \Delta G_{sol}$

and ΔS are considered approximately similar for all similar complex therefore ΔG is proportional to ΔE:

$\Delta E_{MM} = \Delta E_{int} + \Delta E_{ele} + \Delta E_{vdw}$

The average energies of MD simulation are listed in Table 4 while Fig. 26 shows DE and the most important contributions to the energy of binding: electrostatic (ΔE_{ele}) and van der Walls (ΔE_{wdw}). The resulting complexes were considered for the binding modes graphical analysis with Maestro (Schrödinger LLC. 2014. Maestro GUI, New York, NY, USA) and Pymol (Delano WL 2002).

3.2.8. Sample preparation for crystallization studies

The insert for VP35 I278A mutant IID was generated by amplifying the coding region for VP35 IID (residues 215-340) from the full length VP35 I278A mutant sequence. The amplified PCR product was cloned into a modified pMAL vector (New England Biolabs) containing a 6x Histidine tag, a maltose binding protein (MBP) fusion tag and a tobacco etch virus (TEV) protease recognition site N-terminal to the multiple cloning site. The HisTag-MBP-VP35 I278A IID plasmid was transformed into *E. coli* BL21 (DE3) cells (Novagen). VP35 1278A IID was expressed as previously described (Leung et al. 2009). Briefly, the transformed cells were grown in LB medium with 50 µg/ml of Ampicillin at 37 °C until they reached an OD_{600} of 0.4-0.6. The cells were then induced with 0.5 mM IPTG overnight at 22 °C and harvested by centrifugation at 16700 x g for 25 min The cell pellets were stored at -80 °C. The cells were thawed and resuspended in lysis buffer (25 mM sodium phosphate pH 7.0, 1 M NaCl, 5 mM β-mercaptoethanol) with 50 µg/ml of DNase, and 1 tablet of Complete EDTA-free protease inhibitor (Roche). After being lysed by sonication on ice, the cells

were clarified by centrifugation at 30000 x g for 45 min. The clarified lysate was loaded onto a 5 ml HisTrap HP column (GE Healthcare), pre-equilibrated with binding buffer containing 25 mM sodium phosphate pH 7.0, 150 mM NaCl, 10 mM imidazole, 5 mM β-mercaptoethanol. The protein was eluted with a 40% linear gradient from Buffer A (25 mM Sodium phosphate pH 7.0, 150 mM NaCl, 20 mM Imidazole, 5 mM β-mercaptoethanol) to Buffer B (25 mM Sodium phosphate pH 7.0, 150 mM NaCl, 1 M Imidazole, 5 mM β-mercaptoethanol). Affinity tag removal was performed by adding 3 mg of TEV protease to the elution fractions and dialysing overnight at 4 °C against 25 mM Sodium phosphate pH 7.0, 150 mM NaCl, 5 mM Imidazole, 5 mM β-mercaptoethanol. Digestion efficiency was assessed by SDS-PAGE. In order to effectively remove the HisTag-MBP contamination, the digested protein was loaded onto a 5 ml HisTrap HP column connected in series with a 5 ml MBPTrap HP column (GE Healthcare), both pre-equilibrated with binding buffer, collecting the unbound protein. A final purification step was performed by size-exclusion chromatography (SEC) on a HiPrep 16/60 Sephacryl S-100 HR column (GE Healthcare) in crystallization buffer (10 mM HEPES pH 7.0, 150 mM NaCl, 2 mM TCEP). The purest fractions (> 90% purity), as assessed by SDS-PAGE, were concentrated to 9 mg/ml, flash frozen and stored at -80 °C.

3.2.9. Crystallization and structure determination

Crystallization trials were set up on INTELLI-PLATE low profile 96 well plates (Art Robbins Instruments) using the sitting drop method on a Crystal Gryphon Liquid Handling System (Art Robbins Instruments). Each crystallization drop contained 150 nl or 350 nl of protein at 9 mg/ml and 150 nl of crystallization buffer from commercially available screens. The crystallization plates were incubated at 20 °C. One high-resolution dataset (1.9 Å) was collected in house at 100 K on a Rigaku-MSC Micromax-007 X-ray generator and Saturn 944+ CCD detector. The crystal was grown under condition H2 of the Index Screen (Hampton Research). The crystal was previously mounted on a CryoLoop (Hampton Research) and cryo-protected by sequentially submerging the loop in

crystallization buffer (0.2 M potassium sodium tartrate tetrahydrate, 20% polyethylene glycol 3350) with 10% and 20% glycerol. Data collection and refinement statistics are shown in Table 5. The dataset consisted of 360 images and was processed with iMOSFLM (Leslie 2006). The space group was reindexed from P222 to P212121 in Reindex (Bernardinelli & Flack 1985), in the CCP4 suite (Winn et al. 2011). Model building and initial structure refinement were performed with Phaser (McCoy et al. 2007) and REFMAC5 (Winn et al. 2011; Murshudov et al. 1997). Structure determination was obtained by molecular replacement using the wild-type VP35 IID structure (PDB entry: 3FKE) as a search model. The water molecules were previously removed from the search model using CHAINSAW (Winn et al. 2011; Stein 2008). After several cycles of rigid body and restrained refinement in REFMAC5, further structure refinement was performed with Phenix (Adams et al. 2002), alternated with model inspection and manual refinement in Coot (Emsley & Cowtan 2004). The resulting model was validated with Coot and MolProbity (Lovell et al. 2003). The structure images were generated with PyMOL (Delano WL 2002).

3.3. Results

3.3.1. dsRNA binding property of Ebola VP35 end-capping mutants

In agreement with the VP35 RBD/IID dimeric complex model present in literature (Daisy W Leung et al. 2010; Kimberlin et al. 2010), a more recent work described a kinetic in which dsRNA binding by the end-capping RBD/IID monomer constitutes the earliest binding event, to which attachment of backbone-binding RBD/IID monomers all along the dsRNA helix follows (Bale et al. 2013). Within this picture, it is the small area interacting with dsRNA terminal bases in the concave surface of the end-capping RBD/IID monomer that represents the most suitable target for small molecule inhibitors design. Moreover, selected amino acid residues laying in this area, like F239, or surrounding it, such as R312, K319, R322 and K339 were found critical for RBD/IID dsRNA binding and IFN inhibition, as their mutation into alanine resulted in decrease, or even total loss, of those

functions (Hartman et al. 2004; Cárdenas et al. 2006; Hartman, Ling, et al. 2008; Hartman, Bird, et al. 2008; Leung et al. 2009; Daisy W Leung et al. 2010; Zinzula et al. 2012; Prins, Delpeut, et al. 2010; Bale et al. 2012). In our previous effort to characterize a bacterially-expressed full length EBOV rVP35 (Zinzula et al. 2009), we also investigated the impact of rVP35 mutants at residues involved in dsRNA backbone interactions, namely R305A, K309A and R312A, on dsRNA binding ability (Zinzula et al. 2012). Here, we wanted to explore the effect of alanine substitutions at residues involved in dsRNA end-capping and, to this aim, we performed alanine-scanning in vitro site-directed mutagenesis of rVP35 residues F239, L277, I278, I280 (hydrophobic), S272, Q274, Q279, T281 (polar uncharged), K282, K319, R322, K319/R322 and K339 (polar charged) (Fig. 21).

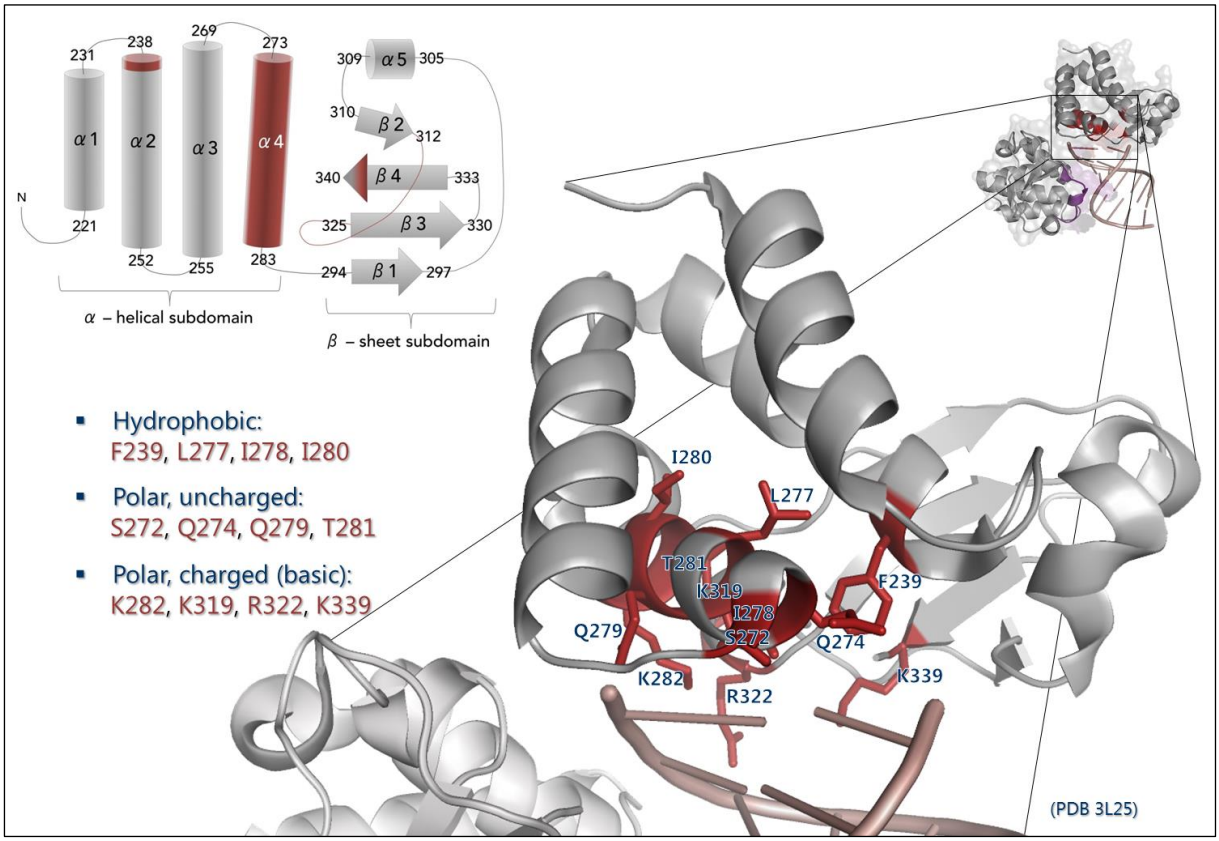

Figure 21. Important residues in end-capping interface. VP35 residues involved in end-capping interaction which can be subjected to structure-based alanine scanning.

Firstly, once all rVP35 mutants were purified as previously described (Fig. 22b) (Zinzula et al. 2009), to assess their proper folding and exclude that any difference in dsRNA binding might have been imputable to major structural perturbations, we performed a DSF analysis comparing

the thermal stability of full length wt and mutants rVP35 (Fig. 22a). Interestingly, all rVP35 mutants showed melting temperature (T_m) values comparable to wt rVP35 (59.4 ± 0.6 °C), which suggests maintenance of proper folding and no structural perturbations beyond the minimal local change (Table 2). Secondly, by using a previously described magnetic pull down assay (Zinzula et al. 2012), we assessed the dsRNA binding activity of rVP35 mutants through an homologous-competition binding curve titration with an in vitro transcribed (IVT) 500 bp dsRNA as ligand. Results showed that EBOV rVP35 end-capping mutants were impaired in dsRNA binding function, having no measurable K_d values or even poorly detectable activity with percentages ranging from 0.8% to 6% of bound dsRNA with respect to wt rVP35 (Fig. 23a). Only exceptions were, Q274A, R322A and K319A/R322A rVP35 mutants, which were able to bind the IVT 500 bp dsRNA but showed lower affinity with increased K_d values with respect to wt rVP35 (Fig. 23b). In particular, K_d values for Q274A, R322A and K319A/R322A rVP35 mutants were 5.23 ± 1.8 nM, 9.13 ± 1.5 nM and 15.62 ± 2.0 nM, respectively. According to these data, rVP35 dsRNA binding activity was seriously compromised by the change of a single amino acid residue in the end-capping binding surface. Next, to assess repercussion of those mutations on VP35 IFN-antagonism, we asked whether these residues would play a critical role in the IFN-inhibition activity of EBOV VP35 in cell cultures.

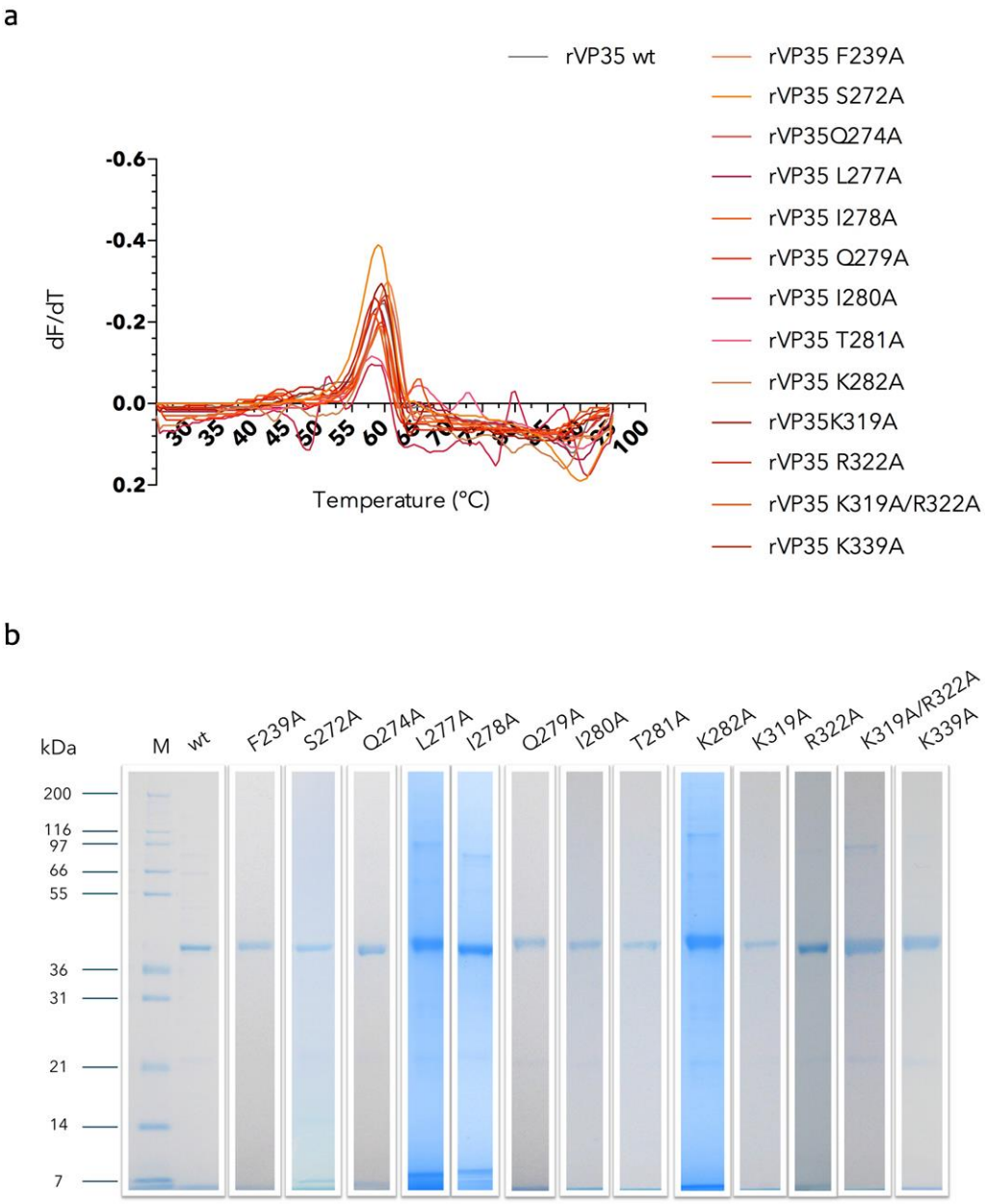

Figure 22. Assessment of thermal stability and folding state of rVP35 wt and mutants. (a) Melting curves featuring low initial fluorescence and a sigmoidal shape indicative of protein unfolding transition and first derivative of fluorescence emission data for the DSF analysis of wt and mutants rVP35. The maximum value of the curves, which represent the midpoint of the unfolding transition, or T_m, reveal that all rVP35 proteins share comparable thermal stability and folding state. (b) Coomassie blue-stained 12% SDS-PAGE analysis showing that IMAC purified full length rVP35 wt and mutants were all expressed at similar levels.

Table 2. Thermal stability of wt and mutants rVP35. T_m values obtained by DSF analysis on rVP35 wt and mutants. Data shown are the mean ± SD of three independent experiments performed in triplicate samples.

VP35 protein	T_m [°C]
wt	59.4 ± 0.6
F239A	59.7 ± 0.2
S272A	59.0 ± 0.4
Q274A	60.6 ± 0.6
L277A	58.8 ± 0.5
I278A	61.3 ± 1.2
Q279A	60.0 ± 0.6
I280A	56.5 ± 0.9
T281A	58.3 ± 0.6
K282A	59.4 ± 0.3
K319A	58.2 ± 0.6
R322A	60.3 ± 1.0
K319A/R322A	58.0 ± 0.4
K339A	59.2 ± 0.5

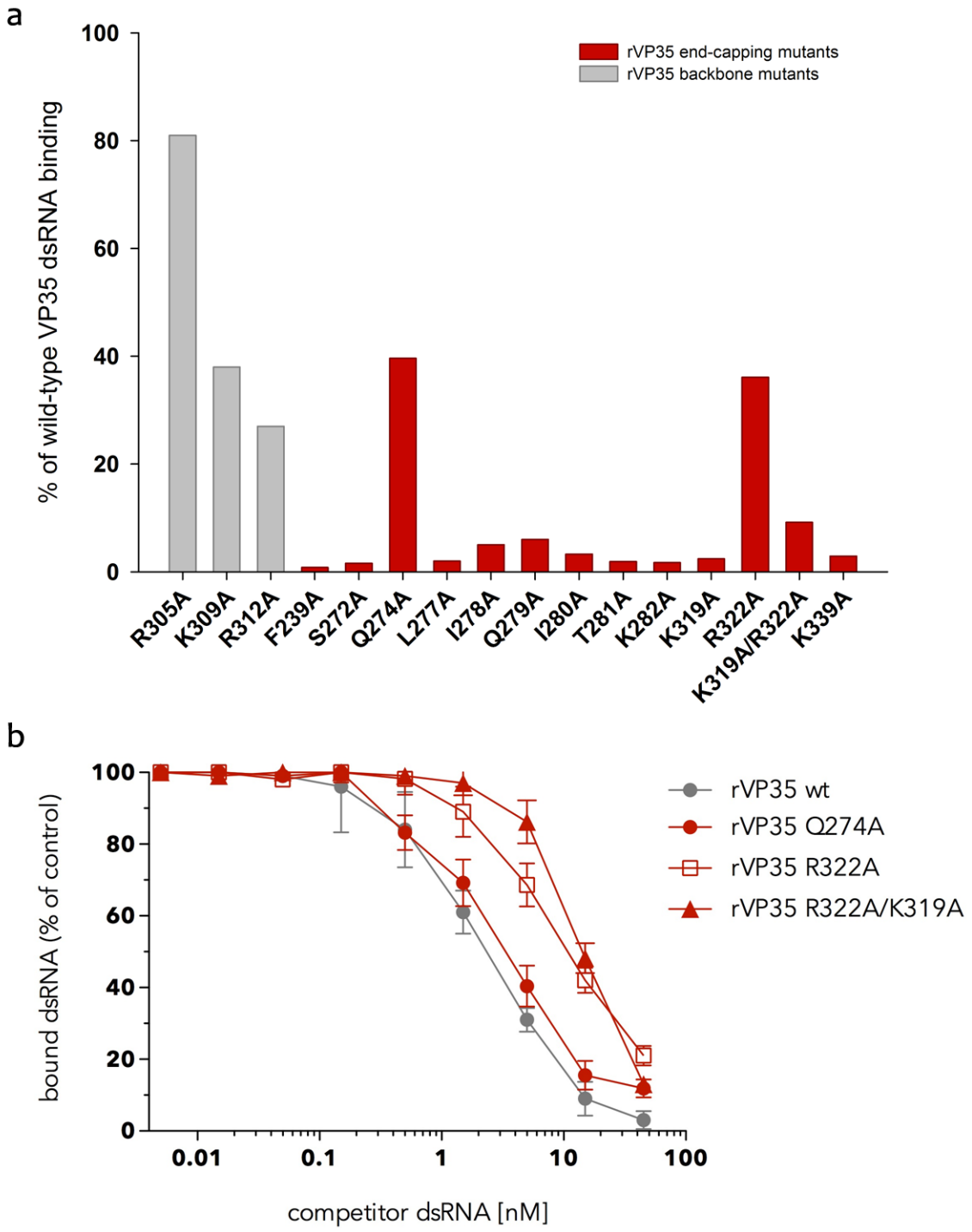

Figure 23. dsRNA binding ability of EBOV rVP35 backbone and end-capping mutants. (a) Relative dsRNA binding activity of rVP35 backbone (white dotted) and end-capping (black dotted) mutants expressed as percentage of the total amount of dsRNA bound by wt rVP35: R305A, 81.0%; K309A, 38.0%; R312A, 27.0%; F239A, 0.8%; Q274A, 39,6%; I278A, 5.0%; Q279A, 6.0%; K319A, 2.4%; R322A, 36.1%; K319A/R322A, 9.2%; K339A, 2.9%. (b) Homologous-competition binding, performed with the magnetic pull down assay at 37 °C with optimal biochemical conditions, showed that Q274A (red circle), R322A (empty red square) and K319A/R322A rVP35 (red triangle) bind to 500 bp IVT dsRNA with lower affinity with respect to wt rVP35 (full grey circle). Concentration of unlabelled competitor dsRNA is plotted versus the bound percentage of the radiolabeled dsRNA ligand, each experimental point is the mean ± SD of specific bound dsRNA from three independent experiment.

3.3.2. IFN-β inhibition property of EBOV VP35 end-capping mutants

EBOV VP35 interferes at various levels the RIG-I-mediated signaling cascade that leads to the type I IFN production, ultimately allowing uncontrolled viral replication (Zinzula & Tramontano 2013). To assess the effect of end-capping mutations on the ability of EBOV VP35 in suppress type I IFN induction in cellular systems, we used the reporter gene assay described in Chapter 2 that uses IAV dsRNA transfection as a stimulus for RIG-I signaling pathway culminating in the activation of the IFN-β promoter. As described in chapter 2, when A549 cells were co-transfected with IFN-β reporter vector and increasing amounts of plasmid expressing EBOV VP35 wt or mutants there is a dose-dependent inhibition of the dsRNA-stimulated, RIG-I-mediated IFN-β production by EBOV VP35 wt (Fig. 24). Hence, we tested the IFN-antagonism ability of EBOV VP35 end-capping mutants transfecting the VP35 carrying plasmids at different concentration to assess the relative impairment of the mutant VP35s IFN-antagonism function. Since the assay herein used is different from those previously described, we firstly assayed VP35 mutants R305A, K309A and R312A to properly compare our results with those previously reported (Hartman et al. 2004; Cárdenas et al. 2006; Leung et al. 2009; Hartman, Ling, et al. 2008). The obtained results on these three mutants showed that K309A have a moderate and R312A a significant reduction in IFN-antagonist activity, while R305A does not affect this function, confirming previous reports (Hartman et al. 2004; Cárdenas et al. 2006) (Fig. 25). Secondly, we tested all other VP35 mutants showing that F239A, S272A, Q274A, L277A and Q279A VP35 mutants substantially maintained an IFN-antagonist ability comparable to the one showed by wt VP35 (Fig. 25). Differently, I278A, I280A, T281A, K319A, K339A mutants exhibit a strong reduction in IFN-antagonism ability, particularly statistically significant at lower VP35 mutant plasmid concentrations, suggesting that these VP35 mutants can compensate dsRNA binding affinity reduction at higher protein concentrations. Most relevantly, similarly to R312A VP35, K282A and R322A VP35s showed the strongest reduction in VP35 IFN-antagonist ability, statistically significant even at the highest tested VP35 plasmid concentration

transfected (Fig. 25). An exception case is the one of K319A/R322A VP35 mutant that showed a reduction of the IFN-antagonist ability only at the intermediate plasmid concentrations. The dose dependent inhibition of the vRNA RIG-I pathway activation allowed to determine the plasmid concentration required to reduce the IFN-β promoter induction by 50%, ICp_{50} value, for all tested VP35s. Given the wt VP35 ICp_{50} value of 110 ± 4.9 ng, I278A, I280A, T281A, K319A, and K339A VP35s exhibited a significant increase in their ICp_{50} values comprised in the range of 150-170 ng ($p < 0.05$), while R312A, K282A and R322A mutants exhibited higher ICp_{50} values (517 ± 28.2 ng, 584 ± 49.4 ng and 663 ± 60.3 ng respectively) with $p < 0.05$, demonstrating the criticality of these three single amino acid mutations for the inhibitory activity of the protein (Table 3). It is worth to note that 2 out of 3 VP35 mutants that showed the strongest reduction in IFN-antagonist efficacy in cell-based assays, R312A and R322A, maintained an although reduced capability of binding dsRNA in biochemical assays. Differently, other VP35 mutants such as F239A, S272A, Q274A, L277A, I278A, I280A, T281A, K319A, and K339A that showed no or limited reduction of their IFN-antagonist efficacy in cell-based assays almost completely lost their dsRNA binding ability in biochemical assays. A number of reasons could be involved to explain these observations: *i)* some of the mutated VP35 amino acid residues, such as F239, Q274, I278 and K339, participate in both end-capping and backbone-binding VP35 monomers; *ii)* it is not clear at the moment if the magnetic binding assay with rVP35 involves monomeric, dimeric, multimeric (or a mixture of them) VP35 forms, and whether these forms have different responses to alanine scanning mutagenesis; *iii)* some of the mutated VP35 amino acid residues participate in both protein–RNA and protein–protein interactions with cellular proteins involved in the RIG-I pathway and the loss of one of the two functions is not sufficient to impair the VP35 inhibition. In any case, since the overall biochemical and cellular analysis of the results showed that a number of the selected VP35 amino acid residues such as I278A, I280A, T281A, K282A, K319A, K319A/R322A and K339A significantly reduced VP35 ability to inhibit vRNA induced RIG-I pathway activation, we asked whether it could be possible to integrate these data with a computational study to analyze the effect of mutations

in a molecular basis to identify a site potentially useful to the basis for further drug development. In particular we wanted to investigate the contribution of these mutations on the two VP35 monomeric binding surfaces, to select residues more selectively involved in the EBOV VP35 dsRNA binding function.

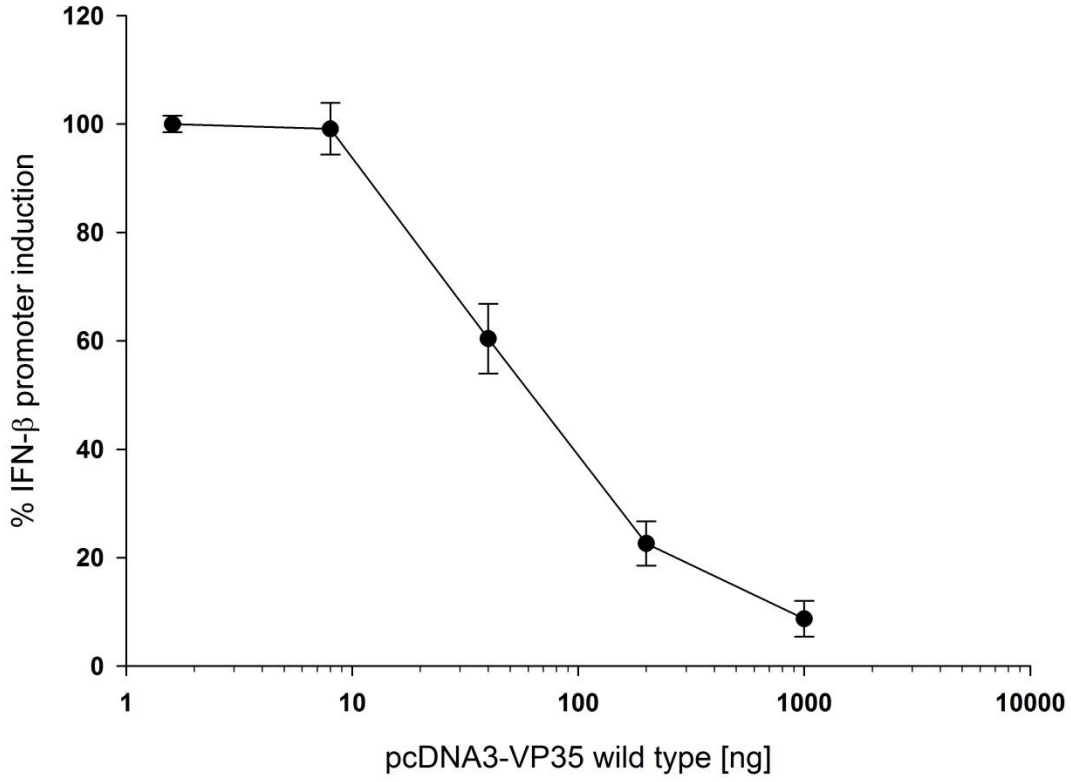

Figure 24. The dose dependent inhibition of the vRNA RIG-I pathway activation by EBOV VP35 wild type. A549 cells were co-transfected with 250 ng of pGL IFN-β luc and various amount (1.6, 8, 40, 200 and 1000 ng) of pcDNA3-ZEBOV-VP35 wild type. 24 hours post transfection cells were additionally transfected with 250 ng of IAV vRNA and after additional 6 hours cells were lysed and luciferase activity was measured. Inhibition of luciferase expression was indicated as percentage of induced control. The error bars indicate standard deviation from three independent experiments.

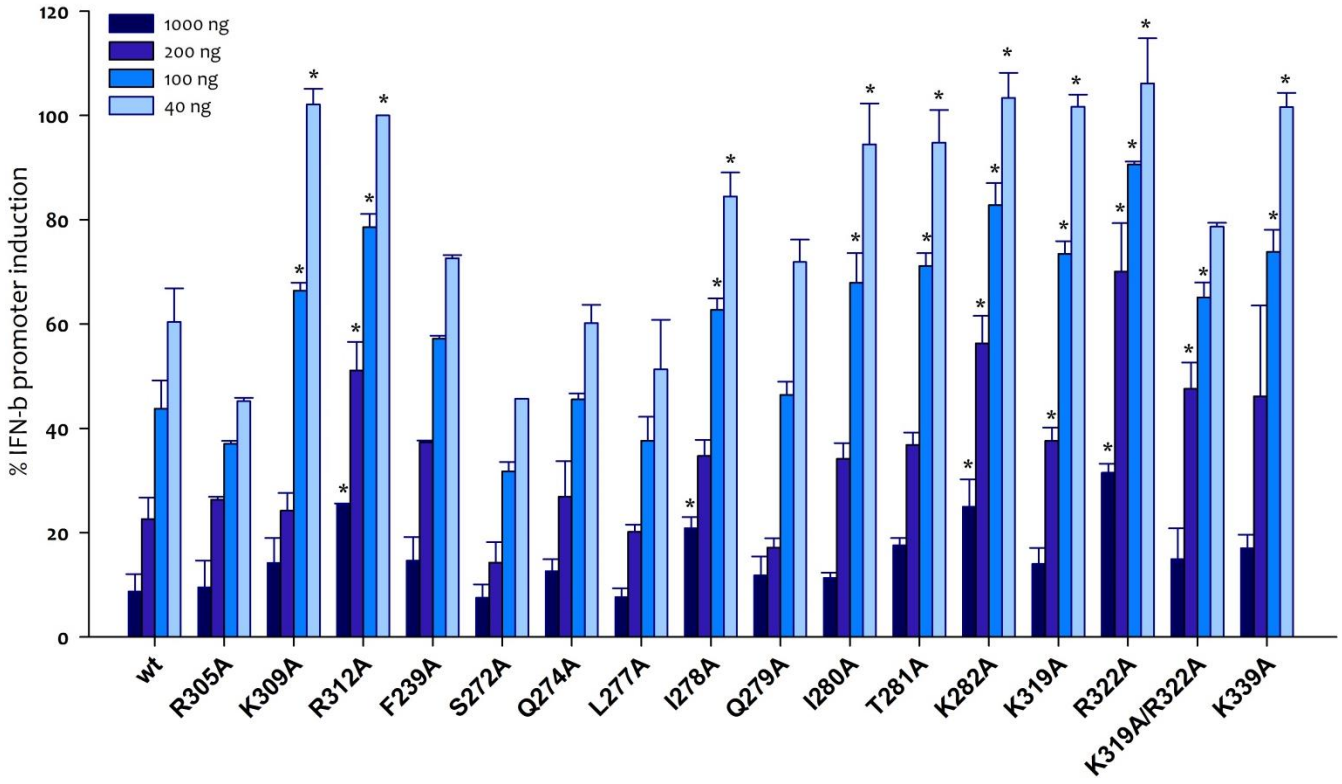

Figure 25. Luciferase reporter RIG-I-mediated IFN-β activation gene assay inhibition of EBOV VP35 wild type and mutants. A549 cells were co-transfected with 250 ng of pGL IFN-β luc and 1000, 200, 100 and 40 ng of pcDNA3-ZEBOV-VP35 wild type and end-capping mutants. 24 hours post transfection cells were additionally transfected with 250 ng of IAV vRNA and after additional 6 hours cells were lysed and luciferase activity was measured. Inhibition of luciferase expression was indicated as percentage of induced control. Data are average of three independent experiments, with error bars representing standard deviation (* p value < 0.05).

Table 3. wt and mutant EBOV VP35s IFN-β promoter induction inhibition.

VP35 protein	*[a]ICp_{50} [ng]*
wt	110 ± 4,9
R305A	88 ± 15,5
K309A	146 ± 4,8
R312A	517 ± 28,2
F239A	143 ± 1,9
S272A	59 ± 8,1
Q274A	89 ± 1,8
L277A	85 ± 9,4
I278A	151 ± 0,5
Q279A	100 ± 8,2
I280A	157 ± 11,4
T281A	166 ± 6,2
K282A	584 ± 49,4
K319A	169 ± 6,3
R322A	663 ± 60,3
K319A/R322A	177 ± 16,8
K339A	173 ± 17,3

[a]Transfected plasmid concentration required to reduce the IFN-β promoter induction by 50%.

3.3.3. Computational studies

In recent years, molecular dynamics (MD) simulations combined with binding free energy calculations have been applied successfully to understand the behavior of protein complex structures in solution (protein-ligand, protein-protein, protein-RNA interactions) and guide the drug design (Liu & Yao 2010). Therefore we investigated with computational studies - performed with the support of Dr. Simona Distinto, Department of Life and Environmental Sciences, University of Cagliari - the molecular basis of the effects of selected amino acid mutations. We have first investigated the effect of 5'-ppp portion. We add the triphosphate moiety to the crystallographic model (Daisy W Leung et al. 2010). Once minimized, the complex VP35-dsRNA was subject to MD simulation finding the formation of a more stable complex compared to the original one without 5'-ppp portion (-197 kcal/mol vs -175 kcal/mol) that confirms previous experimental studies that reveal the importance of 5'-ppp (Zinzula & Tramontano 2013). In fact, 5'-ppp during the simulation appears stabilized by an array of hydrophobic, H bonds and ionic interactions. Given that this modified model could properly assess EBOV VP35 selectivity for 5'-ppp-dsRNA versus dsRNA, we was used it as starting point for all successive MD simulations where single amino acids (except double mutated K319A/K322A) have been mutated in alanine. During a MD simulation the molecular dynamics trajectories was monitored from the convergence of the root-mean square deviation of all atoms of EBOV VP35-dsRNA complexes. All systems resulted stable during MD simulation (Fig. 26). The overall Root-Mean Square Deviation (RMSD) fluctuated in a range of 0.5 nm, indicating that the system was stabilized. All mutants maintained the backbone conformation of wt EBOV VP35 free and in complex with dsRNA. This confirmed the observations done by crystallographic experiments reported in PDB [K312A, PDB: 3L27; K339A, PDB:3L28 (Daisy W Leung et al. 2010); K319A/R322A, PDB:3L29 (Prins, Delpeut, et al. 2010)]. MD analysis showed, for all VP35 mutants, a decreased energetic stability of the complexes, given the energy increase with respect to wt (Table 4). Decomposing the binding free

energy into different items we found that electrostatic component provides the main driving force of binding affinity (Fig. 27).

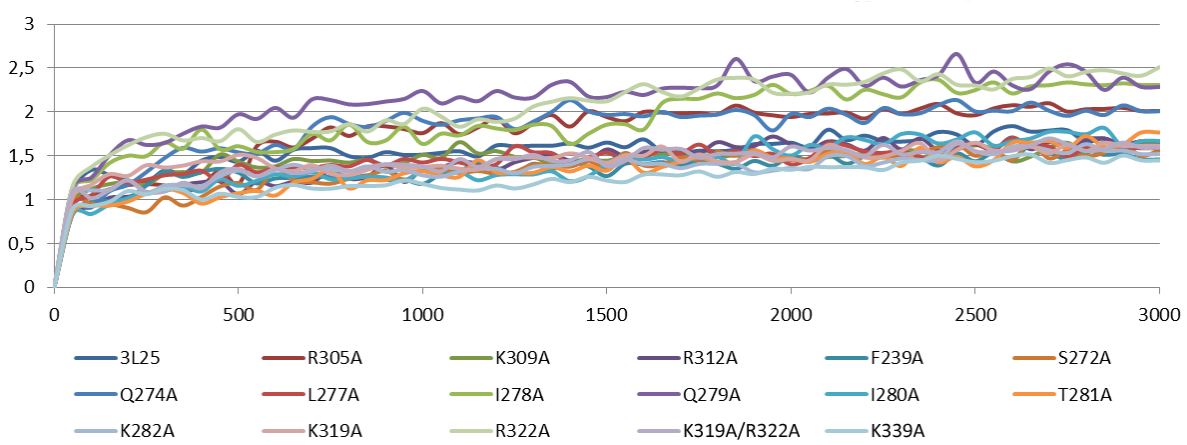

Figure 26. MD simulations. Root-Mean Square Deviation (RMSD) of VP35–dsRNA complexes during MD simulations. All systems resulted stable during MD simulation.

Table 4. Energetic stability of wt and mutants EBOV VP35-dsRNA complexes. All mutations showed a decreased energetic stability of the complexes, given the energy increase with respect to wt.

	ΔE (kcal/mol)	**$\Delta E_{mut} - \Delta E_{wt}$**
Wild-type	-197,20	
I278A	-195,79	-1,41
L277A	-193,87	-3,32
T281A	-190,23	-6,96
R312A	-190,22	-6,98
K319A	-188,56	-8,64
S272A	-182,84	-14,36
F239A	-170,47	-26,73
K339	-168,92	-28,28
K319A/R332A	-167,48	-29,72
Q274A	-164,11	-33,09
R305A	-163,68	-33,52
R322A	-157,58	-39,62
I280A	-155,31	-41,89
K309A	-148,88	-48,32
K282A	-143,18	-54,02
Q279A	-140,81	-56,39

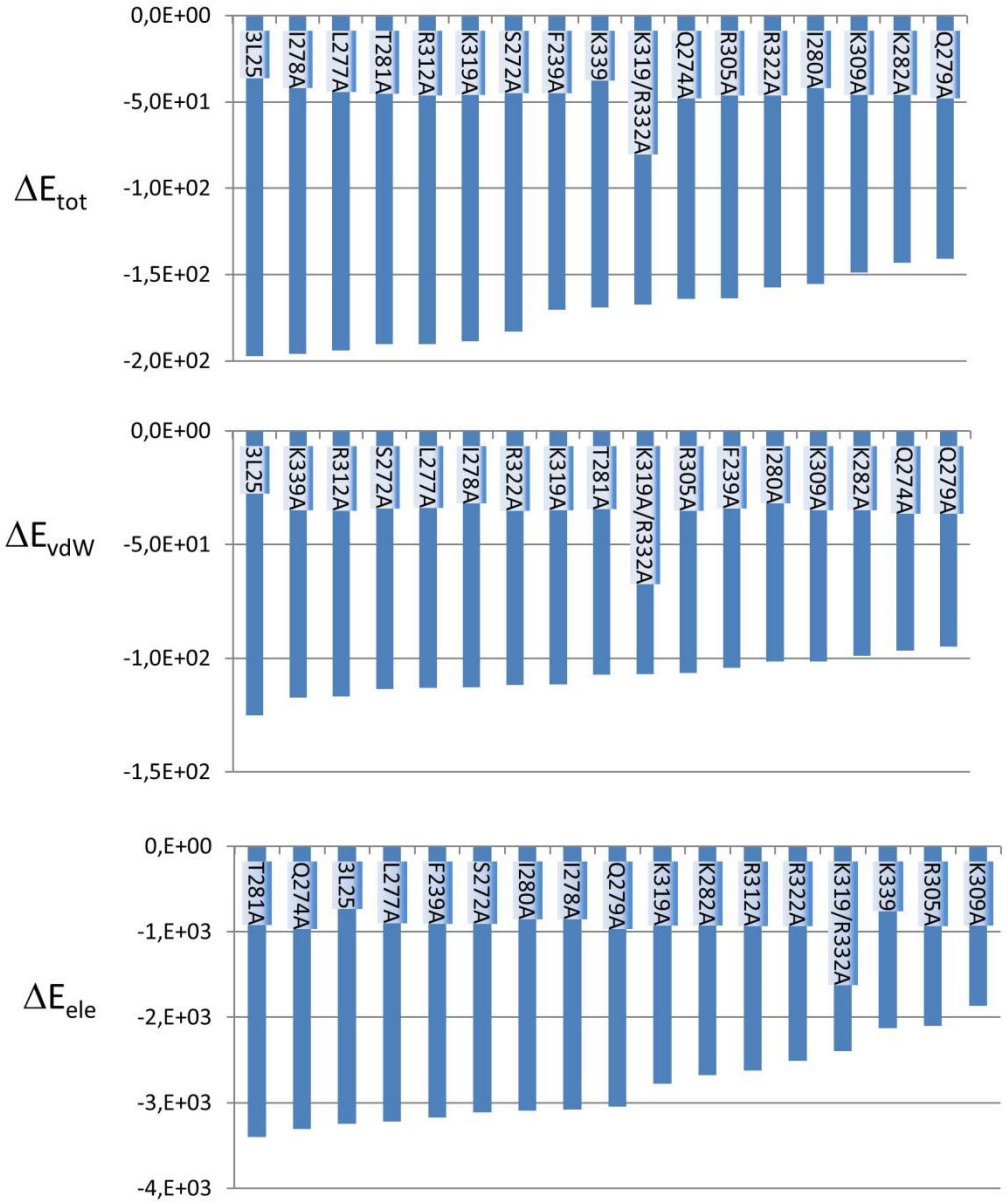

Figure 27. Decomposition of the binding free energy (ΔE). Calculated averages of ΔE and its components (Δ_{vdw} and Δ_{ele}) expressed in kcal/mol of the wild type and mutated VP35–dsRNA complexes, based on the snapshots of MD trajectories.

This could be easily interpreted since most of the mutated important residues have electrically charged side chains. The only exceptions are I278A, I280A and T281A. These three mutants are not associated to particular electrostatic changes and MD simulations showed only subtle differences in side chain conformations. Therefore their importance must be attributed to the loss of contacts with dsRNA. Hence, we investigated *i)* the contacts loss between the mutant VP35s and the whole dsRNA (Fig. 28a), *ii)* the loss of contact between the single mutated amino acid in both

chains A and B together (Fig. 28b) and *iii)* for single chain A (backbone binding, Fig. 28c) and chain B separately (end-capping binding, Fig. 28d). The analysis of the overall loss of contacts showed that all mutations are associated to detrimental of contacts with dsRNA (Fig. 28a). The decomposition analysis between the loss of contacts of backbone vs end-capping binding monomers did not show a univocal behavior for all residues. However, for K282A and K322A VP35 mutants the loss of affinity for dsRNA is surely due to loss of contacts between these two residues in Chain B and dsRNA (Fig. 28d). In addition MD analysis showed that other residues that impaired VP35 affinity for dsRNA such as K319, I280 and T281 were not involved directly with interactions with dsRNA; however, their localization in chain B was closer to dsRNA with respect to chain A, therefore their mutations in end-capping position appear to be more important that in backbone-binding. Overall, we can conclude that the effects of mutation of B-chain residues involved in end-capping binding is more important than the effect of the same residues involved in backbone binding.

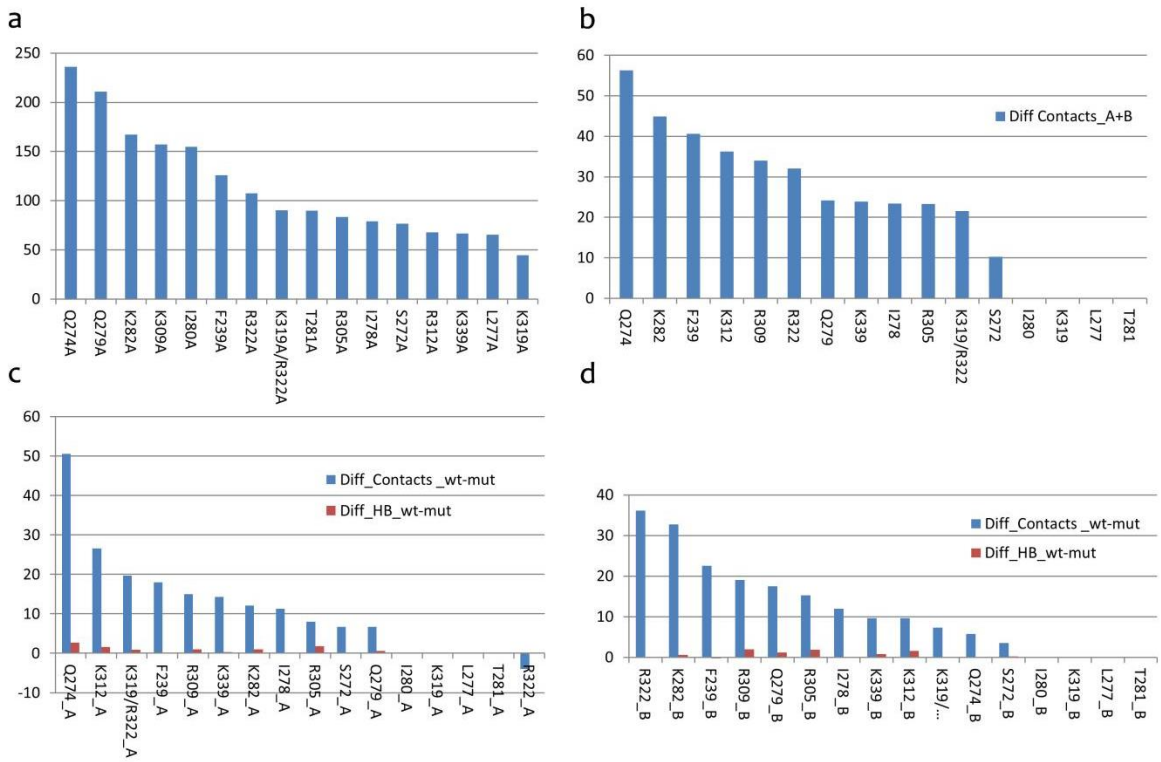

Figure 28. Number of contacts loss between the mutated enzyme and dsRNA. (a) Loss of good contacts with dsRNA for specific MD. (b) Loss of good contacts with dsRNA for specific residue mutated. (c) VP35 RBD loss of good contacts with dsRNA for specific residues mutated in chain A (backbone-binding). (d) VP35 RBD loss of good contacts with dsRNA for specific residues mutated in chain B (end-capping-binding).

3.3.4. Crystallographic structure of EBOV VP35 I278A mutant

The effect of mutations of charged VP35 residue (K312, K319/K322 and K339) was studied also by crystallographic analyses. These studies showed that their mutation do not modify the conformation of the protein but the loss of affinity for dsRNA is due to changes in the electrostatic surface potential (Daisy W Leung et al. 2010). Since our alanine scanning study showed that some important residues are not charged (I278, I280 and T281), we decided to crystallize the RDB of the I278A VP35 mutant - with the collaboration of Dr. Valeria Fadda of School of Biology, University of St Andrews, UK - to verify what could be the effect of this mutation in terms of conformational aspect. The crystallographic structure of the I278A VP35 mutant RBD was solved to 1.9 Å and compared to the previously published structures of the wt RDB VP35 (Leung et al. 2009; Daisy W Leung et al. 2010). The structure of the I278A VP35 mutant and the wt VP35, with or without dsRNA (PDB entry: 3L25 and 3FKE respectively), were superimposed in order to examine any changes in the overall structure and in the end-capping surface. Overall, the I278A VP35 mutant RBD alone did not exhibit significant structural changes when compared to wt VP35 RDB alone (Fig. 29, 30a), with a C-alpha RMSD of 0.2 Å between I278A RBD and the wt RDB. However, when comparing the I278A VP35 mutant RBD structure with the wt one in complex with dsRNA (RMSD = 0.6 Å), it is clear that most of the changes in the side chains of residues involved in dsRNA-binding (e.g. R305, K309, R312, K319 and R322) occur upon ligand binding, as similar changes are noticeable when comparing the wt unliganded structure with the dsRNA complex. However, when focusing the attention on the end-capping surface (Fig. 30b), it was possible to observe a shift in the position of the C275 side chain of the I278A VP35 mutant. F239 also appeared to be shifted in the I278A VP35 mutant in comparison to wt VP35. C275 and F239 did not show any side chain alteration when comparing the wt VP35 RBD unliganded structure to the VP35 RDB structure in complex with dsRNA (Fig. 30c). These changes in the end-capping surface, in particular the shift in the C275 side chain that could cause steric hindrance and loss of contact with the dsRNA end, partially support the data from the dsRNA-

binding and RIG-I-mediated IFN-β production inhibition assays. Finally, we confirmed that the I278A mutation does not produce any major conformational change in the protein and that its importance is due to the loss of contacts with dsRNA associated to the missing side chain.

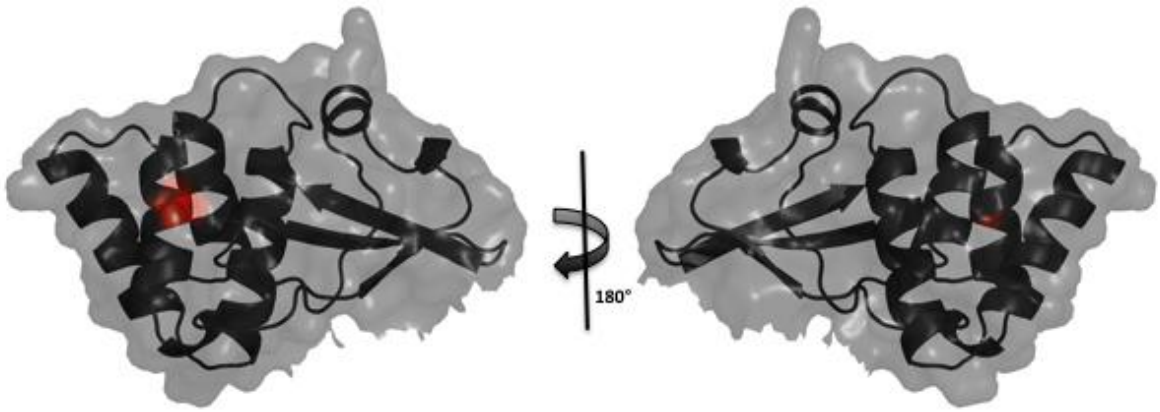

Figure 29. Crystallographic structure of VP35 I278A mutant. Crystallographic structure of I278A VP35 mutant dsRNA binding domain, with the point mutation highlighted in red.

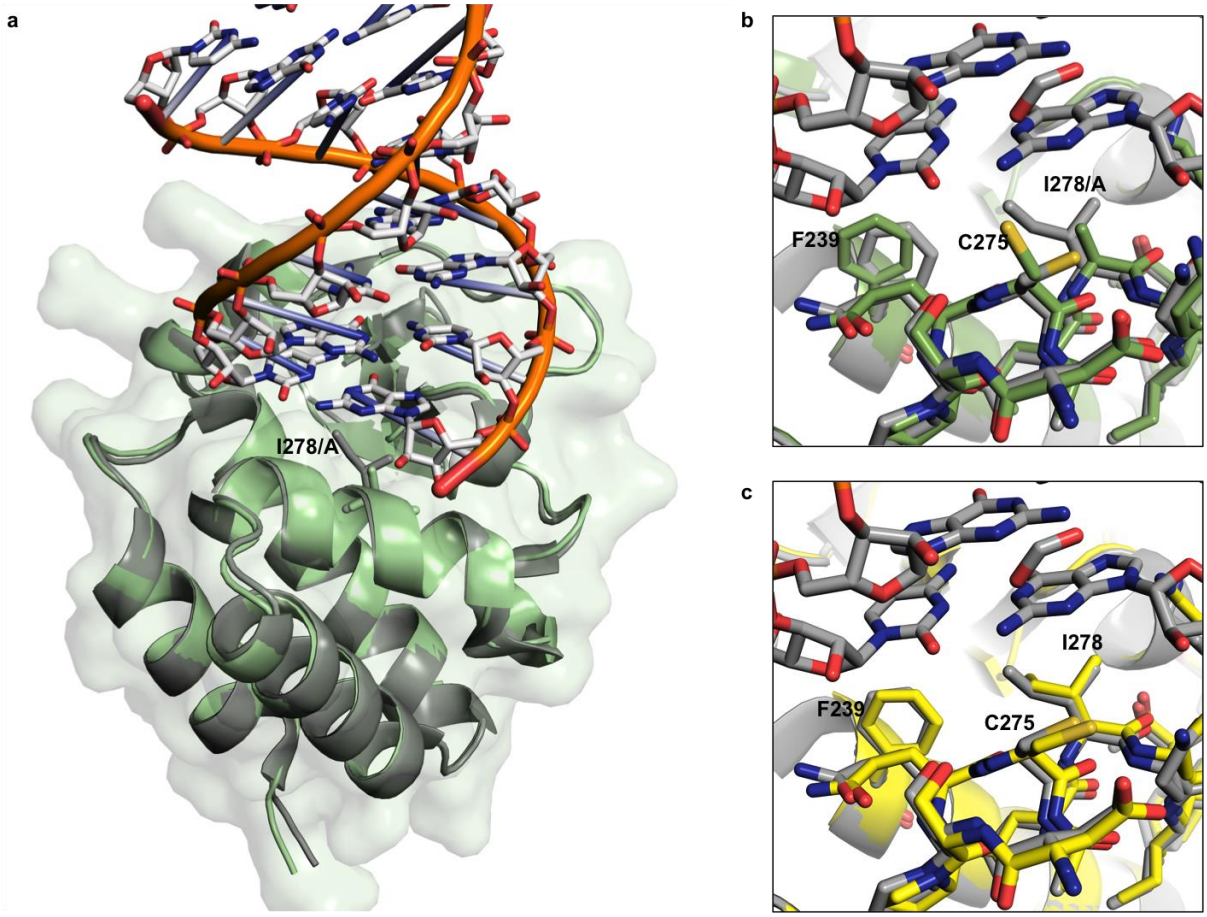

Figure 30. Structure alignment of VP35 I278A IID. Structure alignment (a) of I278A VP35 RBD (green) and wt VP35 RBD in complex with dsRNA (grey, dsRNA in stick representation; PDB accession code: 3L25), showing the location of the point mutation (sticks) in the end-capping region. A closed up view (b) of the same alignment around residues F239, C275, I278, revealed side chain shifts on the I278 VP35 RBD that could compromise the dsRNA binding function. F239 and C275 did not show significant changes in position upon dsRNA binding, as shown in the structure alignment (c) of VP35 RBD (yellow; PDB accession code: 3FKE) and VP35 RBD in complex with dsRNA (grey).

Table 5. Data collection and refinement statistics.

Data collection [a]

X-ray wavelength (Å)	1.542
Resolution range (Å)	13.9 - 1.952 (2.022 - 1.952)
Space group	P 21 21 21
Unit cell parameters (Å, °)	a = 51.75 b = 65.66 c = 72.02 α = β = γ = 90
No. observations	122680 (13760)
Completeness (%)	99.92 (99.22)
Multiplicity	6.7 (5.2)
R_{merge} *(%)* [b]	10.4 (28.1)
Average I/σI	11.80 (4.39)

Refinement

No. atoms	4188
protein atoms	1946
water molecules	263
Protein residues	247
Average B-Factor (Å)	20.9
protein	20.0
solvent	28.0
R-factor [c]	0.1802 (0.2264)
R-free [d]	0.2184 (0.2720)
RMSD bond lengths	0.007
RMSD bond angles	1.03
Ramachandran favoured (%)	99
Ramachandran outliers (%)	0
Clashscore	5.35

[a]Values in brackets correspond to the highest resolution cell

[b]Rmerge =$\sum hkl \sum i |Ihkl, i - \langle Ihkl \rangle| / \sum hkl \langle Ihkl \rangle$

[c-d]*R-factor* and *R-free* = $(\Sigma \, | \, |Fo| - |Fc| \, |)/(\Sigma \, |Fo|)$, where the *Rfree* was calculated from 5% of reflections excluded from refinement.

3.4. Discussion

As widely discussed until now, the multifunctional viral protein EBOV VP35 is a validate drug target since it is one of the most potent weapons that EBOV uses to evade the innate immune antiviral response. In the context of EBOV infection, loss of VP35 dsRNA binding and IFN-antagonist functions results in severely impaired virus replication in cells capable of mounting an IFN-α/β response and also fully attenuates the virus in vivo (Hartman, Bird, et al. 2008; Prins, Delpeut, et al. 2010). Previous studies reported that some residues comprised in the end-capping domain have critical roles in dsRNA binding wt EBOV VP35 (Leung et al. 2009; Daisy W Leung et al. 2010) and mutational studies have confirmed their implication in loss of dsRNA binding ability (Cárdenas et al. 2006; Leung et al. 2009; Daisy W Leung et al. 2010; Prins, Binning, et al. 2010; Zinzula et al. 2012) as well as in suppression of IFN-β induction (Hartman et al. 2004; Cárdenas et al. 2006; Hartman, Bird, et al. 2008; Hartman, Ling, et al. 2008; Leung et al. 2009; Daisy W Leung et al. 2010; Prins, Binning, et al. 2010). Binding experiments performed with the magnetic pull down assay show that minimal changes on the surface electrostatic charge in the pocket of full-length VP35 that houses the dsRNA terminus – such as those that may come from the alanine substitution of residues that interact with terminal bases or phosphate groups – may result in significant decrease, if not in total loss, of dsRNA binding activity in biochemical assay. In fact, while Q274 rVP35 mutant showed a 2-fold decreased binding affinity with respect to wt rVP35, for most of the tested end-capping mutants, including F239A, I278A, Q279A, I280A, T281A, K319A and K339A rVP35, the amount of bound dsRNA was barely detectable. Interestingly, and in substantial agreement with what was observed for the backbone binding R312A mutant, the absence of dsRNA binding activity previously reported for the R322A and K319A/R322A VP35 RBD (Daisy W Leung et al. 2010; Prins, Delpeut, et al. 2010) was partially restored in our full length rVP35 proteins that bear the same mutations, even though with affinities that were respectively 3-fold and 5-fold lower when compared to wt rVP35. Possibly, this greater efficiency in dsRNA binding

displayed by full length VP35s with respect to the RBD alone may reflect the critical contribution of regions lacking in the sole RBD that might have a role in stabilizing or strengthening other domains of the protein during exertion of their function. Afterwards, through an assay that evaluates the dsRNA-dependent activation of RIG-I signaling pathway we found that the mutations I278A, I280A, R312A, K282A, T281A, K319A, R322A and K339A seems to heavily affect the EBOV VP35 IFN-antagonist activity, and among these the mutants R312A, K282A and R322A seems to exhibit a critical importance for the protein inhibitory function. Comparing the biochemical and cellular data, it is clear that the loss of dsRNA binding capacity by some mutants is not necessarily manifested in a loss of VP35 IFN-antagonism. In fact, it is known that VP35 also interact with the kinase domain of the TBK-1/IKK-ε complex suppressing the activation of IRF-3 (Prins et al. 2009) and it was reported that, when the IFN-β production is activated by a dsRNA-independent mechanism, the mutated R312A, R322A and K339A VP35 showed reduced suppression of IFN-β production (Cárdenas et al. 2006; Daisy W Leung et al. 2010). On the contrary, the mutated F239A VP35, that lost the dsRNA-binding function, preserved the dsRNA-independent IFN-inhibitory property (Daisy W Leung et al. 2010). These results suggest that the loss of the dsRNA binding ability by such amino acid substitution may not impair the IRF-3 activation inhibitory capacity, which explains the discrepancy between our biochemical and cellular data. Overall, therefore, we can classify these VP35 mutants in 3 categories: *i)* VP35 mutants that show a reduced dsRNA binding ability in biochemical assay but retain IFN-antagonism in cell culture assay such as F239A, S272A, Q274A, L277A and Q279A; *ii)* VP35 mutants that show a reduced dsRNA binding ability in biochemical assay as well as a reduced IFN-antagonism in cell culture assay at lower level of protein expression but they retain IFN-antagonism functions at higher level of protein expression such as I278A, I280A, T281A, K309A, K319A, K319A/R322A and K339A; *iii)* VP35 mutants that show a reduced dsRNA binding ability in biochemical assay and show a reduced IFN-antagonism in cell culture assay even at higher level of protein expression such as R312A, K282A and R322A.

Computational studies have become necessary to investigate the molecular basis of the effects of selected amino acid mutations. Our studies, firstly, have confirmed the possibility of modeling the VP35 interaction with dsRNA by showing the importance of 5'-ppp portion for a more stable VP35:dsRNA complex compared to the original one without 5'-ppp and, secondly, have showed that - investigating the contacts loss between the mutant VP35s and the whole dsRNA - the effects upon mutation on the monomer involved in end-capping binding seems to be more important than the one involved in backbone binding monomer. Moreover, it was determined that the electrostatic component provides the main driving force of binding affinity. In fact, the most of important mutated residues have electrically charged side chains with the exception of I278A, I280A and T281A residues that showed only subtle differences in side chain conformations. The high resolution crystallographic structure of VP35 I278A RBD, chosen to see the effects of this mutation in terms of conformational aspect, revealed some minor local changes in the dsRNA end-capping pocket when compared to the wt RBD, indicating that the effects of the mutation on dsRNA binding and IFN activation were not the result of longer range distortion of the protein. This further highlights the sensitivity of VP35 function to small changes in the end-capping domain. Overall, the set of data obtained with mutational studies with the three methods (biochemical, cellular and computational) allowed us to highlight the importance of some residues involved in end-capping binding and are localized in a delimitated area (Fig. 31), where the most important appear to be the R312, K282 and R322 residues. Noteworthy, the overall data analysis suggest that this site could be involved not only in VP35 dsRNA binding but also in VP35 interaction with other cellular proteins involved in the RIG-I pathway. Therefore, this site seems to be an attractive target to develop drugs that can impede the VP35 impairment of the IFN activation and will be used in future virtual screening studies in order to find small molecules able to inhibit selectively EBOV VP35.

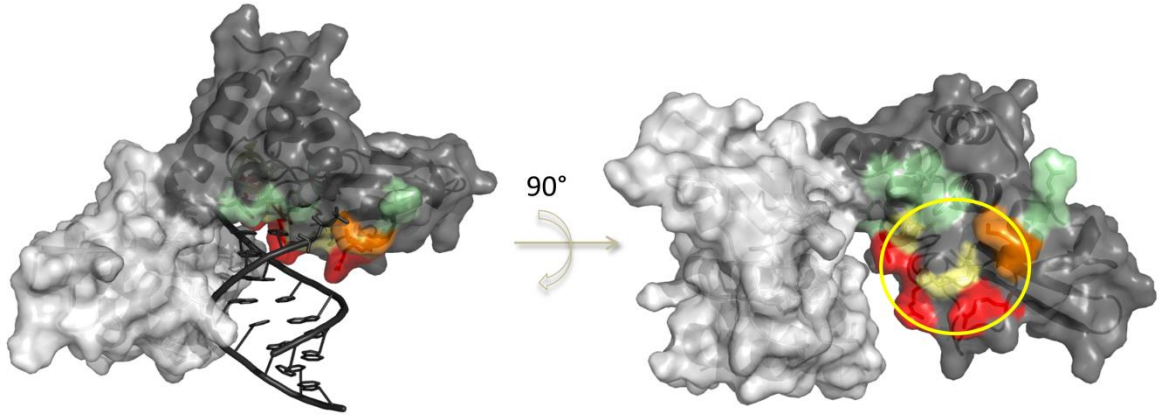

Figure 31. Hot spots of VP35 surface. Residues are colored in order of importance red (R312, K282 and R322) > orange (I278, I280, T281, K319 and K339) > yellow (K309 and K319/R322) > green (R305, F239, S272, Q274, L277 and Q279) according to p value. It is possible to highlight a binding site useful for drug design delimited by yellow circle.

4.0. Plant Extracts and Synthetic Compounds as Antagonist of VP35 IFN-β Inhibition Function.

4.1. Introduction

A first approach to overrun EBOV VP35 inhibitory functions of the IFN signaling cascade is to develop small molecules that bind to VP35 inhibiting its functions, as discussed in Chapter 3. A second approach is to identify small molecules that could potentiate or activate the IFN signalling pathway, increasing IFN production in response to viral infections to a level able to subvert VP35 inhibition not by physically interacting with it. Plants have always been known for their medicinal properties and have been used since ancient times as main healing remedy and have been often recently disregarded as the folk medicine traditions has lost attractions. Over the last years the interest for plant originated constituents is increased considerably in the attempt of identify new active substances with therapeutic properties. While no antiviral drug coming from plant constituents have been approved so far, a number of small molecules extracted from plants are known for their antiviral effects. Just as an example, flavonoids and anthraquinones which showed inhibitory activity against Herpes Simplex virus types 1 and 2 (HSV-1 and HSV-2), the Varicella Zooster virus (ZVZ), Hepatitis C virus (HCV) (Xiong et al. 2011; Yarmolinsky et al. 2012; Wahyuni et al. 2013) and HIV (Esposito et al. 2013). Among the flavonoids, also quercetin that is present in the *Hypericum hircinum L.*, a plant that grows in Sardinia (an Italian Island) is able to inhibit the HIV-1 integrase (Vandegraaff et al. 2001). As an island, Sardinia offers the greatest variety of endemic plants in Europe that, due to its geographical isolation, present significant variations in their genetic and molecular characteristics as compared to plants grown in other regions. Etnopharmacological studies have shown that a number of them were used until less than 100 years ago in folk medicine, and some of them were reported to have therapeutic effects on inflammations and immune system reinforcements. Examples are *Plagius flosculosus* which is

known for its anti-inflammatory activity associated with NF-κB inhibition (Calzado et al. 2005) and *Salvia desoleana*, whose leaves are still used for the anti-inflammatory properties (Atzei Domenico 2009) and have also showed antimicrobial activities (Peana et al. 1999). Since an increase in stimulus-dependent IFN response or a inhibition of EBOV VP35 IFN-antagonism can lead to a therapeutic action of the infection itself, in collaboration with Professor Mauro Ballero and his research team of the Botany section, Department of Life and Environment Sciences, University of Cagliari, we tested extracts of *Helichrysum microphyllum ssp. Thyrrenicum* and *Myrtus communis* plants to assess their anti-VP35 properties. Myrtle and Helichrysum are two Mediterranean taxa, present in Sardinia with different species and subspecies. Helichrysum extracts showed antiallergic properties derived from sterol and triterpene components. Moreover, the extracts showed anti-inflammatory and antimicrobial properties and were used in traditional medicine to treat skin diseases, eczemas, psoriasis and to encourage the epidermal regeneration process (Maffei Facino et al. 1988; Facino et al. 1990). The presence in Helichrysum of a phloroglucinol α-pyrone, called Arzanol, exerts a potent inhibitory action of the HIV-1 replication and show a strong anti-inflammatory action (Appendino et al. 2007). Myrtle extracts showed antibacterial activity and its leaves were used to prepare antibiotic formulations. The main secondary metabolites contained in Myrtle leaves are: myrtucommulone A, a phloroglucinol with antibiotic, antibacterial (Appendino et al. 2002) and anti-inflammatory (Feisst et al. 2005) activity; the myrtucommulone B employed in the treatment of psoriasis and as antioxidant (Rosa et al. 2003); the semimyrtucommulone with antioxidant activity (Appendino et al. 2002). In addition, we also tested the biological properties of a series of compounds synthesized by the research team of Professor Roberto Di Santo, University of Rome "La Sapienza", developed as potential broad range antiviral agents.

4.2. Materials and Methods

For cell lines and mammalian expression plasmid used, see Materials and methods in Chapter 2.

4.2.1. Cytotoxicity assay of extracts and compounds tested

For cytotoxicity tests, cell lines were seeded in 96-well plates (Spectra Plate, PerkinElmer) at an initial density of 10^5 cells/ml in DMEM, containing 10% FBS, 1% Pen/Strept, in the absence or presence of serial dilutions of extracts (from 100 µg/ml to 0,03 µg/ml) or compounds (from 100 µM to 0,03 µM), along with Camptothecin, used as positive control. Plates were incubated for 72 h at 37 °C in a humidified 5% CO_2 atmosphere. Cell viability was determined adding PrestoBlue™ Cell Viability Reagent (Invitrogen). After 1 h at 37 °C, relative fluorescence was read with a Victor^3 (Perkin Elmer). The percentages of cell viability were based on the amount of living cells in compound-treated cells relative to untreated control cells (defined as 100% viability). Cytotoxicity graphs were then generated by plotting percentage of cell viability versus concentration of extracts/compounds. Using regression analysis of cytotoxicity curves (in Microsoft excel), a trend line that best suited the curve was selected and the corresponding equation was used to calculate the concentration required to reduce cell growth by 50% (CC_{50} value).

4.2.2. IFN response induction and EBOV VP35 inhibition assays

In order to test compounds and extracts, the luciferase reporter gene assay and the same inhibition assay was performed as previously described in Chapter 2. In addition, the day of stimulation, compounds and extracts were added to cells at known concentrations and the cells were transfected with IAV PR8 vRNA and incubated for 6 hours at 37 °C with 5% CO_2. The results are shown in n-fold compared to unstimulated control (when was tested the induction increase of IFN-β production) or as percentage of induced control (in the inhibition assay).

4.3. Results

4.3.1. Cytotoxicity of Myrtle and Helichrysum extracts

The Myrtle and Helichrysum extracts were screened for cellular toxicity in order to determine appropriate concentrations for the following luciferase reporter IFN-β gene assays. From Myrtle and Helichrysum total ethanolic extracts were obtained (Helichrysum ET and Myrtle ET) from the laboratory of Botany of the Department of Life and Environment Sciences, University of Cagliari, and the volatile component was extracted by steam distillation (essential oils). Regarding the Helichrysum essential oil extraction, biomass was collected in two different moments: before (Helichrysum 1) and during (Helichrysum 2) flowering, since the volatile component is more sensitive to seasonal variations and can contain quali-quantitative variations of the secondary metabolites during plant ontogenetic cycle. These extracts were first dissolved in 100% DMSO at 5 mg/ml stock concentration. Serial dilutions ranging from 100 to 0.03 µg/ml were tested for cytotoxicity assay. As detailed in Table 6, the essential oils (Helichrysum 1, Helichrysum 2 and Myrtle EO) of the two plants showed no cytotoxic effects on A549 cells with a CC50 > 100 µg/ml. Instead, the Myrtle and Helichrysum ethanolic extracts (Myrtle ET and Helichrysum ET) showed minimal cytotoxicity with a CC50 > 50 µg/ml. Considering these results, the initial concentration of 30 µg/ml was chosen to investigate the effects of a possible increase of the dsRNA RIG-I-mediated IFN-β induction.

Table 6. Cell growth inhibition of A549 cell line by plant extracts. CC_{50} values were obtained in A549 cell line. Camptothecin was used as positive control. Data shown are the mean ± SD of three independent experiments performed in duplicate samples.

Extract	*[a]CC_{50} (µg/ml)*
Helichrysum 1 *(Helichrysum microphyllum ssp. Thyrrenicum 1)*	> 100
Helichrysum 2 *(Helichrysum microphyllum ssp. Thyrrenicum 2)*	> 100
Helichrysum ET *(Helichrysum microphyllum ssp. Thyrrenicum EtOH)*	91 ± 15
Myrtle EO *(Myrtus communis)*	> 100
Myrtle ET *(Myrtus communis)*	66 ± 17
Camptothecin	0,3 ± 0,2

[a]Extract concentration required to reduce cell growth by 50%.

4.3.2. Helichrysum and Myrtle extracts effects on IFN-β induction

Sardinia provides a large variety of endemic plant species that have significant genetic and molecular characteristics as well as metabolites that differ from the one of plants grown in other areas. In particular, Myrtle and Helichrysum present particular immunogenic property, as mentioned previously. In that context, it becomes interesting to assess the extracts components effects on the IFN signaling cascade. As reported before, the extracts were assayed with serial dilutions starting from 30 µg/ml concentration, to ensure that marginal cytotoxic effects could not influence the data. Results showed that 3 µg/ml of Helichrysum 1 and 10 µg/ml of Helichrysum 2 significantly increase the dsRNA-dependent IFN-β production from 7.2 to 8.7 folds (p value < 0.05) (Fig. 32a) and 8.4 folds respectively (p value < 0.01) (Fig. 32b), while 3 and 1 µg/ml of ethanolic extract Helichrysum ET from 7.2 to 8.5 and 8.3 folds respectively (p value < 0.05) (Fig. 32c) when compared to unstimulated control. Myrtle ET at 1 µg/ml concentration also increased the IFN-induction from 6.7 to 8.5 folds (p value < 0.05) (Fig. 33b), while Myrtle essential oil, Myrtle EO, had no impact on the system (Fig. 33a). Next, to assess repercussion of IFN-induction increase

on VP35 IFN-antagonism, we asked whether these extract would revert the dsRNA-dependent IFN-β induction inhibited by EBOV VP35.

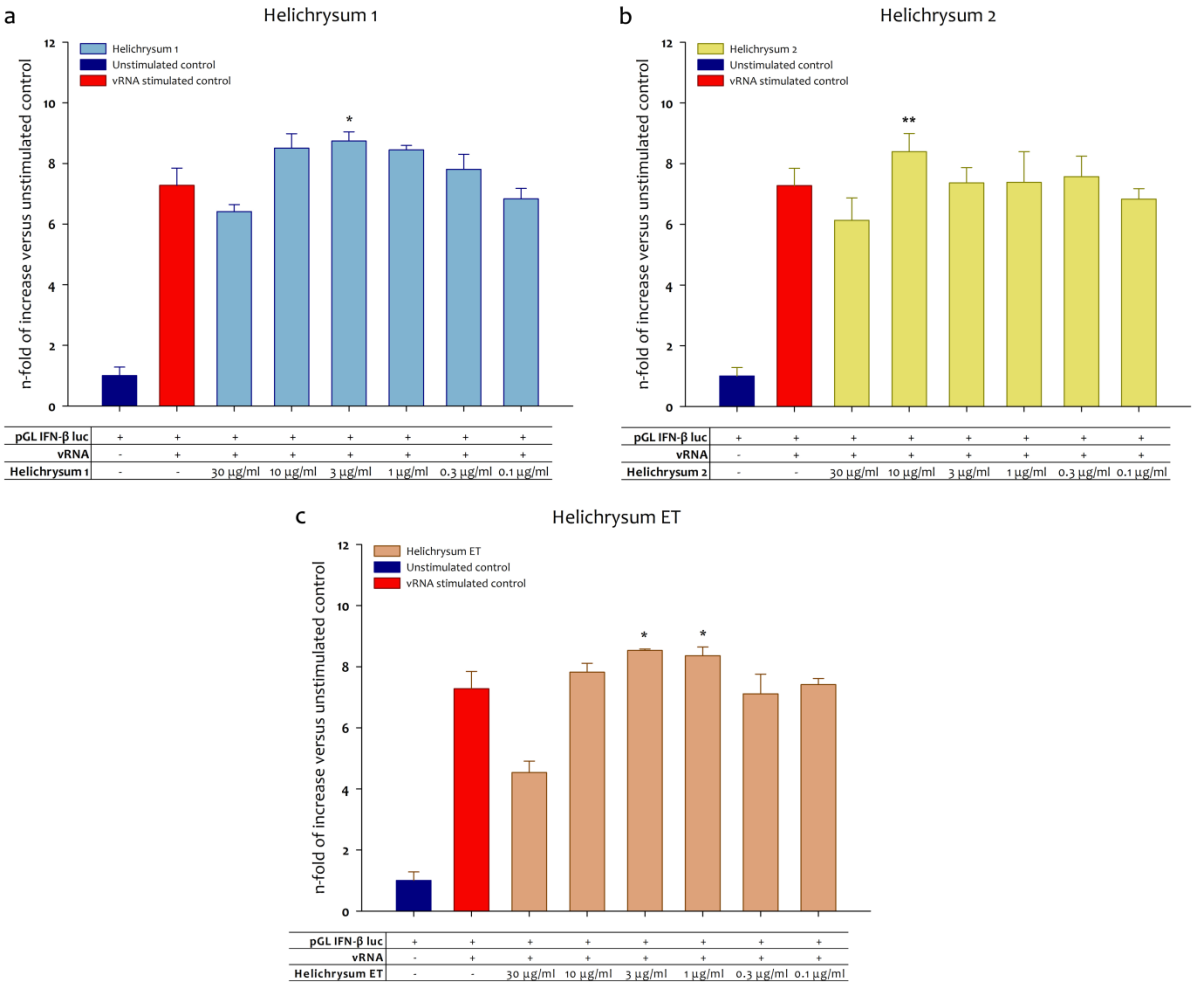

Figure 32. Helichrysum extracts effects on dsRNA RIG-I-mediated IFN-β induction. A549 cells were co-transfected with 250 ng of pGL IFN-β luc. 24 hours post transfection cells were additionally transfected with 250 ng of IAV vRNA and were added various concentrations (30, 10, 3, 1, 0.3, 0.1 µg/ml) of extracts. After additional 6 hours cells were lysed and luciferase activity was measured. Results are shown in n-fold compared to unstimulated control (* p value < 0.05, ** p value < 0.01).

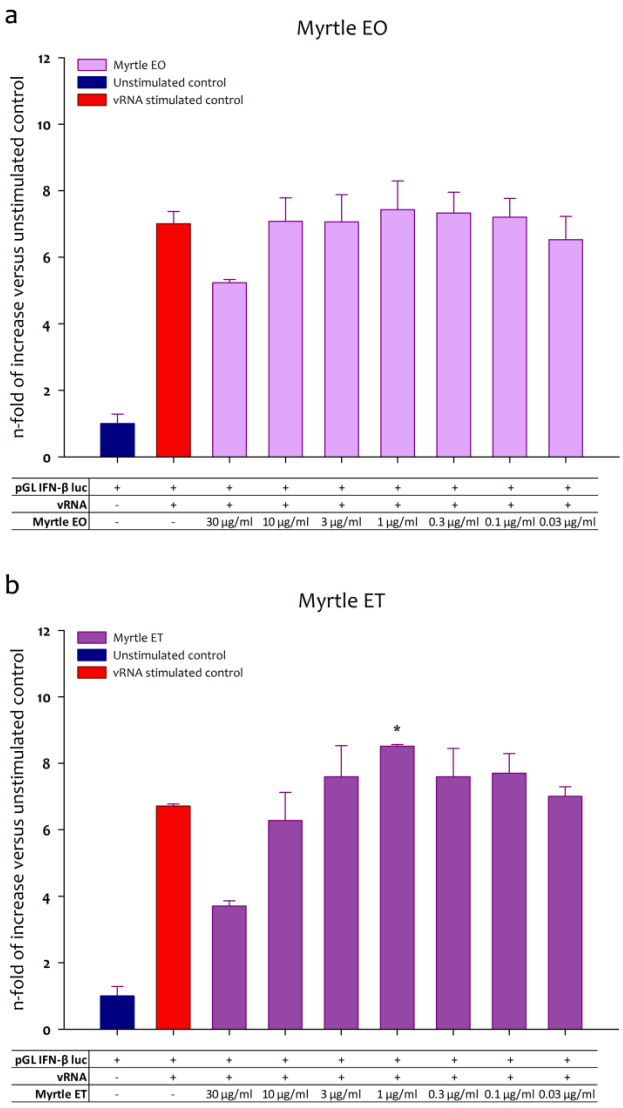

Figure 33. Myrtle extracts effects on dsRNA RIG-I-mediated IFN-β induction. A549 cells were co-transfected with 250 ng of pGL IFN-β luc. 24 hours post transfection cells were additionally transfected with 250 ng of IAV vRNA and were added various concentrations (30, 10, 3, 1, 0.3, 0.1, 0.03 µg/ml) of extracts. After additional 6 hours cells were lysed and luciferase activity was measured. Results are shown in n-fold compared to unstimulated control (* p value < 0.05).

4.3.3. Helichrysum and Myrtle extracts effects on the IFN-β induction inhibition of EBOV VP35

Given the data obtained, we investigated whether the increase of IFN-induction was sufficient to subvert the blockade of the signalling cascade operated by EBOV VP35. For this reason, the active concentrations of each of the 2 extracts were tested in dsRNA-dependent RIG-I-mediated IFN-β induction system in the presence of EBOV VP35. Results showed that, in the presence of VP35

(Fig. 34) the extracts concentrations tested did not significant affect the VP35 inhibition of the vRNA induced IFN response.

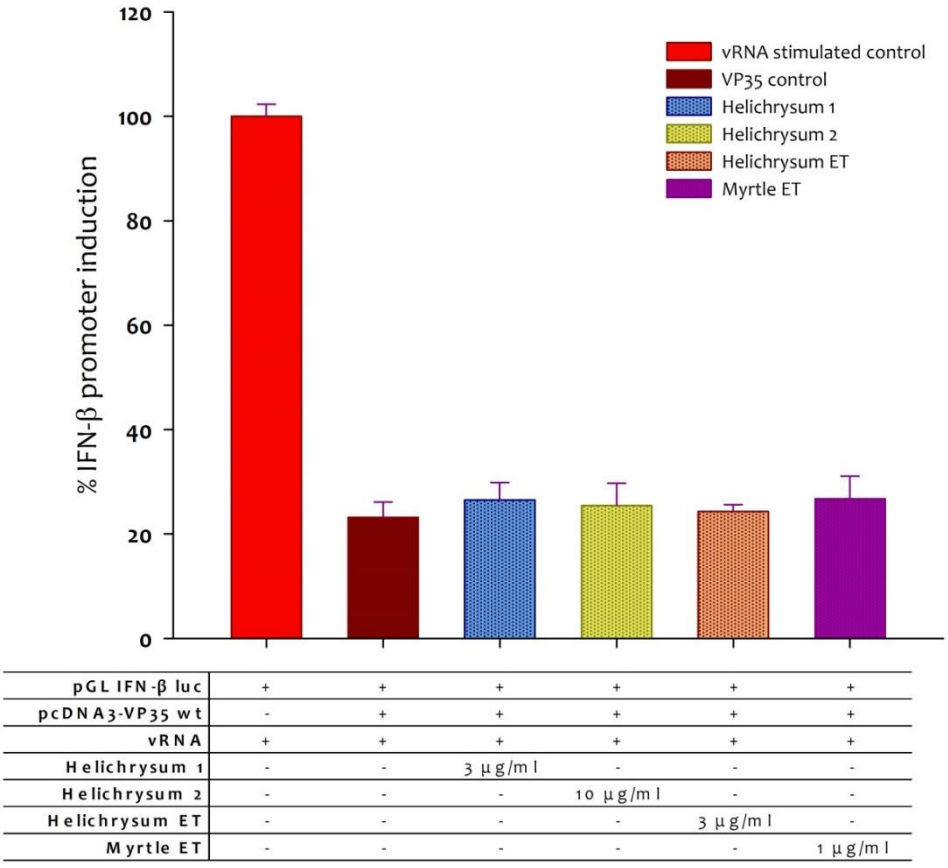

pGL IFN-β luc	+	+	+	+	+	+
pcDNA3-VP35 wt	-	+	+	+	+	+
vRNA	+	+	+	+	+	+
Helichrysum 1	-	-	3 µg/ml	-	-	-
Helichrysum 2	-	-	-	10 µg/ml	-	-
Helichrysum ET	-	-	-	-	3 µg/ml	-
Myrtle ET	-	-	-	-	-	1 µg/ml

Figure 34. Helichrysum and Myrtle extracts effects on the IFN-β induction inhibition by EBOV VP35. A549 cells were co-transfected with 250 ng of pGL IFN-β luc and 100 ng of pcDNA3-EBOV-VP35. 24 hours post transfection cells were treated with plant extracts and additionally transfected with 250 ng of IAV vRNA. After additional 6 hours cells were lysed and luciferase activity was measured. Inhibition of luciferase expression was indicated as percentage of induced control. Error bars indicate standard deviation from three independent experiments.

4.3.4. Cytotoxicity of synthetic compounds

The eight synthetic compounds (*a-h*) obtained from the research team of Professor Roberto Di Santo, University of Rome "La Sapienza", were first dissolved in 100% DMSO at 100 mM stock concentration and assayed with serial dilutions ranging from 100 to 0.03 µM. Some compounds (*a*, *e* and *g*) showed CC_{50} values > 100 µM, while the others > 90 µM (*b* and *c*) and > 70 µM (*d*, *f* and *h*) (Table 7). Considering these results, in following assays was chosen the initial concentration of 30 µg/ml and 30 µM for extracts and compounds, respectively, to investigate the effects of a possible increase of the dsRNA RIG-I-mediated IFN-β induction.

Table 7. Cell growth inhibition of A549 cell line by synthetic compounds. CC_{50} values were obtained in A549 cell line. Camptothecin was used as positive control. Data shown are the mean ± SD of three independent experiments performed in duplicate samples.

Compound	***[a]CC$_{50}$ (µM)***
a	> 100
b	92,9 ± 4,8
c	93,1 ± 1,7
d	78,1 ± 1,3
e	> 100
f	72,8 ± 1,5
g	> 100
h	79,5 ± 0,8
Camptothecin	0,3 ± 0,2

[a]Compound concentration required to reduce cell growth by 50%.

4.3.5. Synthetic compounds effects on IFN-β induction

The *a-h* compounds series was synthesized by the research group of Prof Roberto Di Santo, University of Rome "La Sapienza", as potential broad spectrum antiviral drugs. These compounds were tested on dsRNA-dependent RIG-I-mediated IFN-β induction, using 30, 10 and 3 µM

concentrations. Data showed that only compound *a* induced a significant increase of the dsRNA-dependent RIG-I-mediated IFN-β induction at 10 and 3 μM concentrations from 5.8 to 7.9 and 7.5 folds respectively, as compared to unstimulated control ($p < 0.01$ and $p < 0.05$, respectively), while the others compounds did not show any increase (Fig. 35a,b). Subsequently, in order to verify if compound *a* was able to induce by itself the IFN signalling cascade (even in the absence of a vRNA stimulus), it was tested in the same system but in the absence of the IAV RNA stimulation. Results showed that compound *a* alone does not induce the IFN response (Fig. 36). The fact that compound *a* was not able to induce IFN response by itself is very important; in fact, the identification of possible antiviral drugs that enhance the IFN response only during infection, avoiding the harmful effects of uncontrolled IFN stimulation, is a priority in the perspective of drug development. Next, we investigated the compound *a* capacity to subvert the EBOV VP35 inhibition.

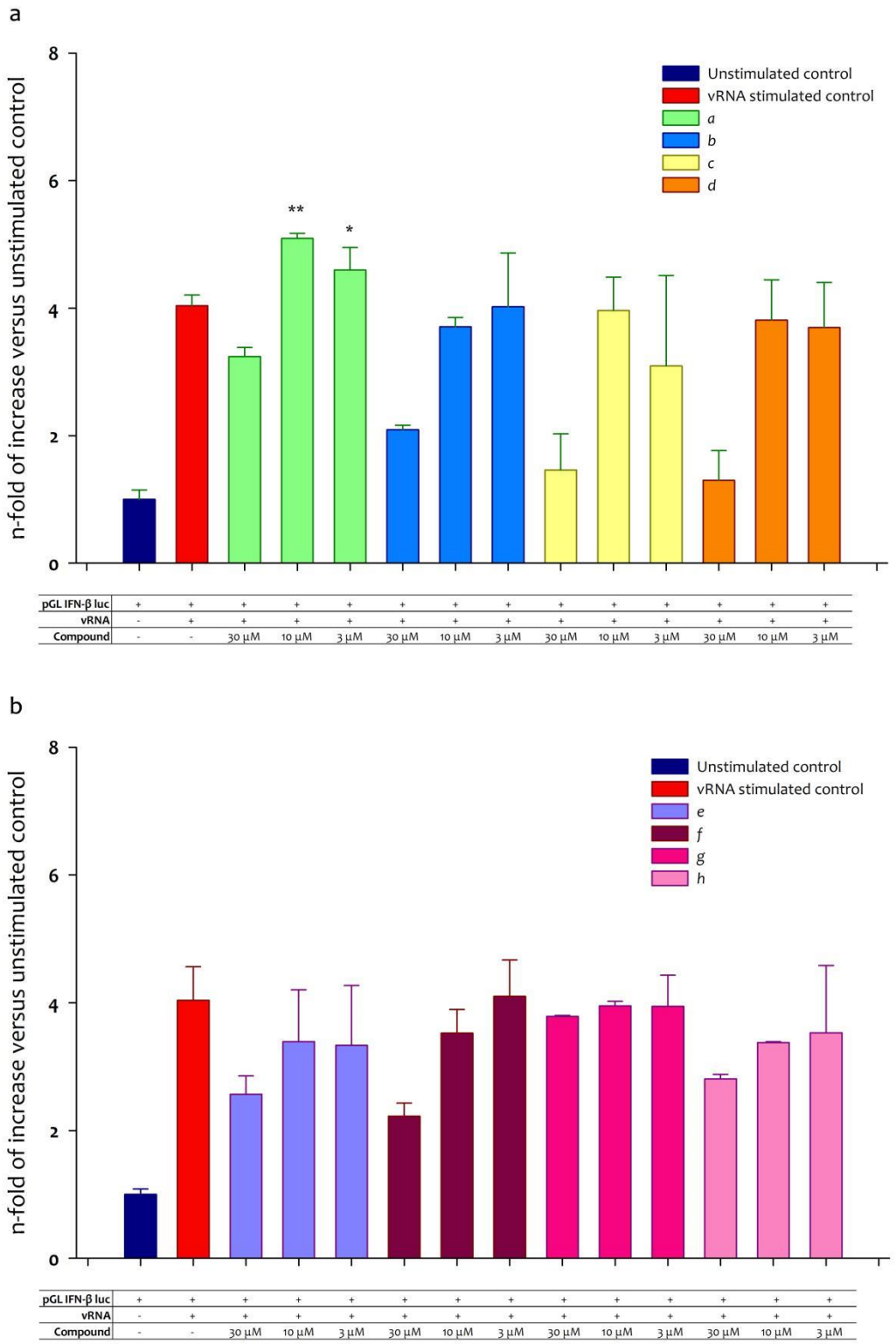

Figure 35. Effects of compounds *a-h* on IFN-β induction. Data show the effects of compound *a*, *b*, *c*, *d* (Fig. 34a), *e*, *f*, *g* and *h* (Fig. 34b) on dsRNA RIG-I-mediated IFN induction. A549 cells were co-transfected with 250 ng of pGL IFN-β luc. 24 hours post transfection cells were additionally transfected with 250 ng of IAV vRNA and were added various concentrations (30, 10, 3 µM) of compounds. After additional 6 hours cells were lysed and luciferase activity was measured. The results are shown in n-fold compared to unstimulated control. Only compound *a* showed significant effects (* p value < 0.05, ** p value < 0.01).

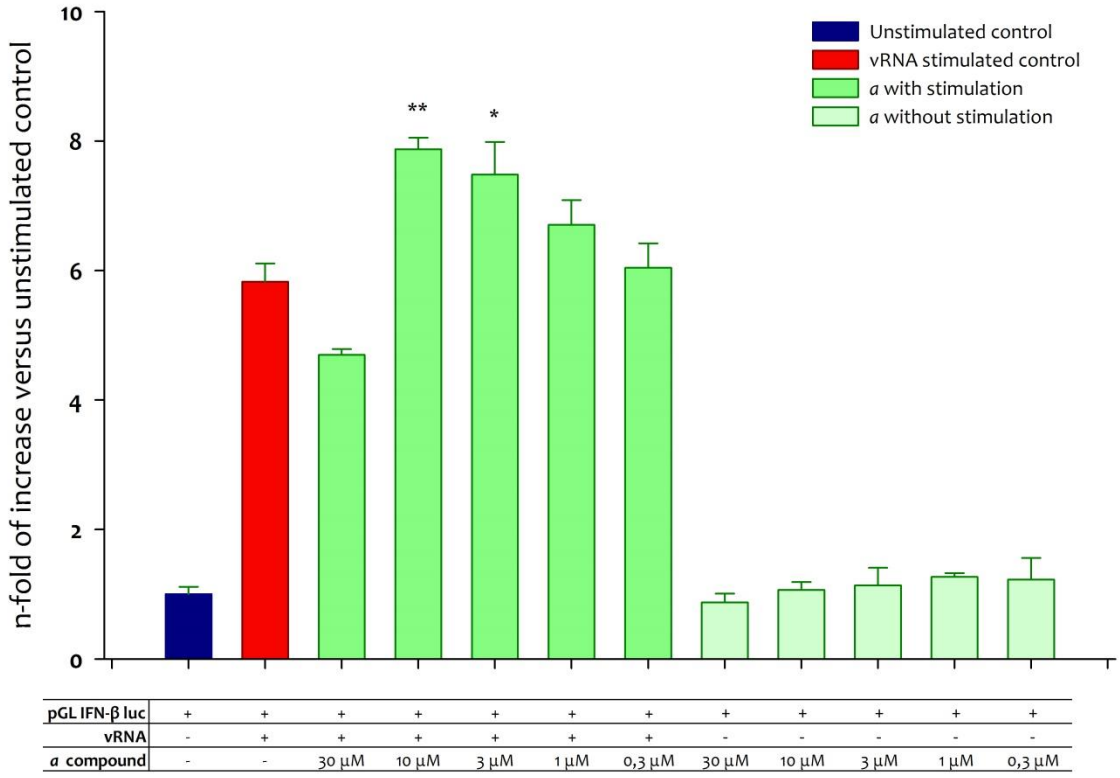

Figure 36. Compound *a* effects on IFN-β induction. Compound *a* was tested in RIG-I-mediated IFN-β induction system with and without dsRNA stimulation. A549 cells were co-transfected with 250 ng of pGL IFN-β luc. 24 hours post transfection cells were additionally transfected with 250 ng of IAV vRNA, or not transfected, and were added various concentrations (30, 10, 3, 1, 0.3 µM) of compound *a*. After additional 6 hours cells were lysed and luciferase activity was measured. Results are shown in n-fold compared to unstimulated control (* p value < 0.05, ** p value < 0.01).

4.3.6. Effects of compound a on the IFN-β induction inhibition of VP35

To assess whether the IFN-I response induction by compound *a* was able to counteract the EBOV VP35 inhibitory functions, the compound was tested on A549 cells stimulated with dsRNA in the presence of the viral protein. Observed data demonstrated that at 10 and 3 µM concentrations of compound *a* determined a significant percentage increase from 31.5 % of VP35 inhibited control to 44.5% and 44.4% respectively (p value < 0.05) (Fig. 37). Hence, compound *a* concentrations that increase the IFN-response induction also showed a subverting effect against EBOV VP35 inhibition.

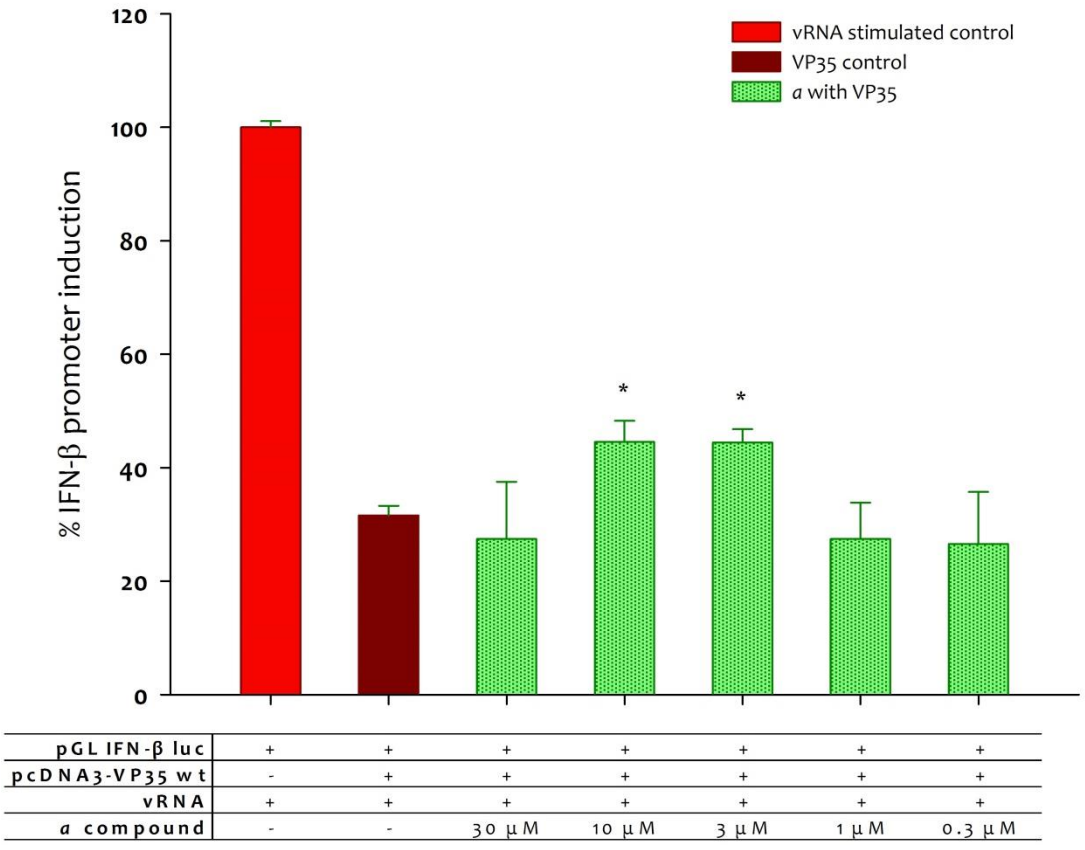

Figure 37. Compound *a* effects on the IFN-β induction inhibition of VP35. A549 cells were co-transfected with 250 ng of pGL IFN-β luc and 100 ng of pcDNA3-EBOV-VP35. 24 hours post transfection cells were treated with compound *a* (30, 10 3, 1, 0.3 µM) and additionally transfected with 250 ng of IAV vRNA. After additional 6 hours cells were lysed and luciferase activity was measured. Inhibition of luciferase expression was indicated as percentage of induced control. The error bars indicate standard deviation from three independent experiments (* p value < 0.05).

4.4. Discussion

The discovery of a small molecule that is able to act on the innate antiviral response, reinforcing it when under viral attack, represents a different approach against the inhibitory strategies operated by EBOV through its VP35 protein. For this purpose, we tested in our system the effects of two Sardinian plants extracts with particular properties, such as Myrtle and Helichrysum, and a series of synthetic compounds developed as potential antiviral drugs. In the system that evaluates the IFN induction increase, the Helichrysum and Myrtle ethanolic extracts and essential oils of Helichrysum, but not of Myrtle, increased the IFN-I induction. However, this IFN production induction did not appear to be powerful enough to overturn VP35 inhibition.

Among the synthesized compounds *a-h*, only compound *a* showed a significant effect in increasing IFN-I vRNA induced production. Noteworthy, it did not stimulate the innate antiviral response when tested in the absence of a vRNA stimulus. Very significantly, when compound *a* was tested on VP35 inhibition it showed to be able to overcome its effects, although not completely. This VP35 overcoming activity, along with the fact compound *a* acts only under antiviral response induction, makes this molecule very attractive for the development of an antiviral drug. Further studies will need to be performed to determine the compound *a* target that, presumably, is situated in one or more components belonging to RIG-I-mediated IFN signaling pathway, and if its VP35 inhibition is sufficient to induce an innate immune response that could be effective in EVD.

5.0. CONCLUSIONS

The largest Ebola outbreak in West Africa has so far caused thousands of victims raising a great health and social global concern. As widely discussed until now, the success of EBOV replication is dependent on viral inhibition of the initial innate immune responses to infection. Therefore, EBOV VP35 protein is a validate drug target since it is one of the most potent weapons owned by EBOV. In fact, EBOV VP35, interfering at various levels with the RIG-I-mediated signaling cascade that leads to the type I IFN production, prevents the establishment of an effective antiviral immune response. In order to find novel countermeasures against EBOV VP35 functions our work started with the establishment of a new miniaturized cell-based method to characterize EBOV VP35 properties related to its inhibition of the dsRNA-dependent RIG-I-mediated IFN-β induction. The development of this method was the starting point for the exploitation of two different approaches against the inhibitory strategies operated by EBOV VP35.

The first approach focused on setting the basis for the development of small molecules that bind to VP35 and inhibit its functions. Therefore, it was important to identify sensitive sites on the protein to be used as drug target. Given that EBOV VP35 forms an asymmetric dimer on dsRNA terms with two different binding surfaces (backbone and end-capping), through mutational studies performed with three methods (biochemical, cellular and computational) we obtained a set of data that allowed us to highlight the importance of residues R312, K282 and R322 that are involved in end-capping binding. These residues are localized in a delimitated area that could be involved not only in VP35 dsRNA binding but also in VP35 interaction with other cellular proteins involved in the RIG-I pathway. Therefore, the identification of this site will be used in future virtual screening studies in order to find small molecules able to inhibit selectively EBOV VP35.

The second approach focused on the identification of small molecules that could potentiate or activate the IFN signalling pathway, increasing IFN production in response to viral infections up to a level able to subvert VP35 inhibition. For this purpose, were tested two Sardinian plants extracts

(Myrtle and Helichrysum) and a series of synthetic compounds developed as potential broad range antiviral drugs. On the one side, the tested extracts, even increasing IFN activation, were not able to subvert VP35 inhibition. On the other side, instead, the synthetic compound *a* increased IFN-induction only under antiviral response stimulation and was able to subvert VP35 inhibition, proving to be very attractive base for the development of an antiviral agent. These two different strategies are an interesting starting point for further studies that should focus on: *i)* the design and synthesis of molecules to test as selective inhibitors of EBOV VP35; *ii)* the study of the mechanism of action of compound *a* and its derivatives inside the dsRNA-dependent RIG-I-mediated IFN signaling pathway, in order to potentiate the IFN response and the anti-VP35 inhibition towards the realization of new effective countermeasures against EVD.

ACKNOWLEDGEMENTS

First of all, I would like to express my special appreciation and thanks to Professor Enzo Tramontano who supported me with his great experience and knowledge during these three years of work, especially for his precious encouragement expressed in the hardest moments.

I would like to thank also Professor Stephan Ludwig and his staff of Institute of Molecular Virology of Münster, Germany, for the kind support and insider tips that allowed me to develop this project. Moreover, this research was performed thanks to the precious work of Dr. Luca Zinzula, Dr. Simona Distinto and Professor Elias Maccioni of the Department of Life and Environmental Sciences, University of Cagliari, and the cooperation of Professor Garry Taylor and Dr. Valeria Fadda, School of Biology, University of St Andrews, UK, the research groups of Professor Roberto Di Santo and Professor Roberta Costi, University of Rome "La Sapienza", and of Professor Mauro Ballero, Botany section, Department of Life and Environment Sciences, University of Cagliari.

I would also like to thank Dr. Francesca Esposito, Dr. Angela Corona and the Ph.D. students Gian Luca Daino, Nicole Grandi, Marta Cadeddu and Aldo Frau who always supported me during ordinary laboratory life. I would especially like to thank Laura Vargiu, who was the first to introduce me to the cell cultures world, and the Master degree students Gianfranca Mastroni, Stefania Musinu and Luisa Pinna that efficiently supported me with experiments and data collection for my Ph.D. thesis.

Finally, a special thanks to my family for all of the sacrifices that they have made on my behalf and for the unconditional support. At the end I would like to sincerely thank Gian Marco who incentivized me to strive towards my goal and was always my support in the moments when the difficulties appeared insuperable.

Heartfelt thanks to all.

Data presented in this Ph.D. thesis have been published in the following research articles:

Cannas, V., Daino, G. L., Corona, A., Esposito, F., Tramontato, E., 2015. A luciferase reporter gene assay to measure Ebola Virus VP35 inhibition of the viral dsRNA RIG-I-mediated IFN-β induction. *The Journal of infectious disease.* (Accepted)

REFERENCES

Adams, P.D. et al., 2002. PHENIX: building new software for automated crystallographic structure determination. *Acta crystallographica. Section D, Biological crystallography*, 58(Pt 11), pp.1948–1954.

Albariño, C.G. et al., 2013. Genomic analysis of filoviruses associated with four viral hemorrhagic fever outbreaks in Uganda and the Democratic Republic of the Congo in 2012. *Virology*, 442(2), pp.97–100.

Amblard, J. et al., 1997. Identification of the Ebola virus in Gabon in 1994. *Lancet*, 349(9046), pp.181–182.

Amman, B.R. et al., 2012. Seasonal pulses of Marburg virus circulation in juvenile Rousettus aegyptiacus bats coincide with periods of increased risk of human infection. *PLoS pathogens*, 8(10), p.e1002877.

Ank, N., West, H. & Paludan, S.R., 2006. IFN-lambda: novel antiviral cytokines. *Journal of interferon & cytokine research : the official journal of the International Society for Interferon and Cytokine Research*, 26(6), pp.373–379.

Appendino, G. et al., 2007. Arzanol, an anti-inflammatory and anti-HIV-1 phloroglucinol alpha-Pyrone from Helichrysum italicum ssp. microphyllum. *Journal of natural products*, 70(4), pp.608–612.

Appendino, G. et al., 2002. Oligomeric acylphloroglucinols from myrtle (Myrtus communis). *Journal of natural products*, 65(3), pp.334–338.

Ascenzi, P. et al., 2008. Ebolavirus and Marburgvirus: insight the Filoviridae family. *Molecular aspects of medicine*, 29(3), pp.151–185.

Atzei Domenico, A., 2009. *Le piante nella tradizione popolare della Sardegna*,

Baize, S. et al., 1999. Defective humoral responses and extensive intravascular apoptosis are associated with fatal outcome in Ebola virus-infected patients. *Nature medicine*, 5(4), pp.423–426.

Baize, S. et al., 2014. Emergence of Zaire Ebola Virus Disease in Guinea. *New England Journal of Medicine*, 371(15), pp.1418–1425.

Bale, S. et al., 2013. Ebolavirus VP35 coats the backbone of double-stranded RNA for interferon antagonism. *Journal of virology*, 87(18), pp.10385–8.

Bale, S. et al., 2012. Marburg virus VP35 can both fully coat the backbone and cap the ends of dsRNA for interferon antagonism. *PLoS pathogens*, 8(9), p.e1002916.

Banks, J.L. et al., 2005. Integrated Modeling Program, Applied Chemical Theory (IMPACT). *Journal of computational chemistry*, 26(16), pp.1752–1780.

Baron, R.C., McCormick, J.B. & Zubeir, O.A., 1983. Ebola virus disease in southern Sudan: hospital dissemination and intrafamilial spread. *Bulletin of the World Health Organization*, 61(6), pp.997–1003.

Barrette, R.W. et al., 2011. Current perspectives on the phylogeny of Filoviridae. *Infection, Genetics and Evolution*, 11(7), pp.1514–1519.

Basler, C.F. et al., 2000. The Ebola virus VP35 protein functions as a type I IFN antagonist. *Proceedings of the National Academy of Sciences of the United States of America*, 97(22), pp.12289–94.

Basler, C.F. et al., 2003. The Ebola virus VP35 protein inhibits activation of interferon regulatory factor 3. *Journal of virology*, 77(14), pp.7945–56.

Basler, C.F. & Aguilar, P. V, 2008. Progress in identifying virulence determinants of the

1918 H1N1 and the Southeast Asian H5N1 influenza A viruses. *Antiviral research*, 79(3), pp.166–178.

Basler, C.F. & Amarasinghe, G.K., 2009. Evasion of interferon responses by Ebola and Marburg viruses. *Journal of interferon & cytokine research : the official journal of the International Society for Interferon and Cytokine Research*, 29(9), pp.511–20.

Baum, A. & García-Sastre, A., 2010. Induction of type I interferon by RNA viruses: cellular receptors and their substrates. *Amino acids*, 38(5), pp.1283–99. Available at: http://www.pubmedcentral.nih.gov/articlerender.fcgi?artid=2860555&tool=pmcentrez&rendertype=abstract [Accessed July 6, 2011].

Bausch, D.G. & Schwarz, L., 2014. Outbreak of ebola virus disease in Guinea: where ecology meets economy. *PLoS neglected tropical diseases*, 8(7), p.e3056.

Beniac, D.R. et al., 2012. The organisation of Ebola virus reveals a capacity for extensive, modular polyploidy. *PLoS ONE*, 7(1).

Berke, I.C. & Modis, Y., 2012. MDA5 cooperatively forms dimers and ATP-sensitive filaments upon binding double-stranded RNA. *The EMBO journal*, 31(7), pp.1714–1726.

Bernardinelli, G. & Flack, H.D., 1985. Least-squares absolute-structure refinement. Practical experience and ancillary calculations. *Acta Crystallographica Section A*, 41(5), pp.500–511. Available at: http://dx.doi.org/10.1107/S0108767385001064.

Bharat, T. a M. et al., 2012. Structural dissection of Ebola virus and its assembly determinants using cryo-electron tomography. *Proceedings of the National Academy of Sciences of the United States of America*, 109(11), pp.4275–80.

Biedenkopf, N. et al., 2013. Phosphorylation of Ebola virus VP30 influences the composition of the viral nucleocapsid complex: impact on viral transcription and replication. *The Journal of biological chemistry*, 288(16), pp.11165–11174.

Borchert, M. et al., 2011. Ebola haemorrhagic fever outbreak in Masindi District, Uganda: outbreak description and lessons learned. *BMC Infectious Diseases*, 11(1), p.357.

Bornholdt, Z.A. & Prasad, B.V.V., 2006. X-ray structure of influenza virus NS1 effector domain. *Nature structural & molecular biology*, 13(6), pp.559–560.

Bosio, C.M. et al., 2003. Ebola and Marburg viruses replicate in monocyte-derived dendritic cells without inducing the production of cytokines and full maturation. *The Journal of infectious diseases*, 188(11), pp.1630–1638.

Bowie, A.G. & Unterholzner, L., 2008. Viral evasion and subversion of pattern-recognition receptor signalling. *Nature reviews. Immunology*, 8(12), pp.911–922.

Bray, M., 2005. Pathogenesis of viral hemorrhagic fever. *Current Opinion in Immunology*, 17(4), pp.399–403.

Bray, M. & Geisbert, T.W., 2005. Ebola virus: the role of macrophages and dendritic cells in the pathogenesis of Ebola hemorrhagic fever. *The international journal of biochemistry & cell biology*, 37(8), pp.1560–1566.

Bres, P., 1978. The epidemic of Ebola haemorrhagic fever in Sudan and Zaire, 1976: introductory note. *Bulletin of the World Health Organization*, 56(2), p.245.

Briand, S. et al., 2014. The International Ebola Emergency. *New England Journal of Medicine*, 371(13), pp.1180–1183.

Burke, J., Declerq, R. & Ghysebrechts, G., 1978. Ebola haemorrhagic fever in Zaire, 1976. Report of an international commission. *Bulletin of the World Health Organization*, 56(2), pp.271–293.

Bwaka, M.A. et al., 1999. Ebola hemorrhagic fever in Kikwit, Democratic Republic of the Congo: clinical observations in 103 patients. *The Journal of infectious diseases*, 179 Suppl , pp.S1–7.

Calisher, C.H. et al., 2006. Bats: important reservoir hosts of emerging viruses. *Clinical microbiology reviews*, 19(3), pp.531–545.

Calzado, M.A. et al., 2005. Inhibition of NF-kappaB activation and expression of inflammatory mediators by polyacetylene spiroketals from Plagius flosculosus. *Biochimica et biophysica acta*, 1729(2), pp.88–93.

Cárdenas, W.B. et al., 2006. Ebola virus VP35 protein binds double-stranded RNA and inhibits alpha/beta interferon production induced by RIG-I signaling. *Journal of virology*, 80(11), pp.5168–78.

Centers for Disease Control and Prevention (CDC), 2015a. 2014 Ebola Outbreak in West Africa - Case Counts. *Atlanta, CDC*. Available at: http://www.cdc.gov/vhf/ebola/outbreaks/2014-west-africa/case-counts.html.

Centers for Disease Control and Prevention (CDC), 2001. Outbreak of Ebola hemorrhagic fever Uganda, August 2000-January 2001. *MMWR. Morbidity and mortality weekly report*, 50(5), pp.73–77.

Centers for Disease Control and Prevention (CDC), 2015b. Outbreaks Chronology: Ebola Virus Disease. *Atlanta, CDC*. Available at: http://www.cdc.gov/vhf/ebola/outbreaks/history/chronology.html.

Chang, T.-H. et al., 2009. Ebola Zaire virus blocks type I interferon production by exploiting the host SUMO modification machinery. *PLoS pathogens*, 5(6), p.e1000493.

Chen, Z., Li, Y. & Krug, R.M., 1999. Influenza A virus NS1 protein targets poly(A)-binding protein II of the cellular 3'-end processing machinery. *The EMBO journal*, 18(8), pp.2273–2283.

Chien, C. et al., 2004. Biophysical characterization of the complex between double-stranded RNA and the N-terminal domain of the NS1 protein from influenza A virus: evidence for a novel RNA-binding mode. *Biochemistry*, 43(7), pp.1950–1962.

Connolly, B.M. et al., 1999. Pathogenesis of experimental Ebola virus infection in guinea pigs. *The Journal of infectious diseases*, 179 Suppl , pp.S203–17.

Crary, S.M. et al., 2003. Analysis of the role of predicted RNA secondary structures in Ebola virus replication. *Virology*, 306, pp.210–218.

Delano WL, 2002. The PyMol molecular graphics system.

Deng, I.M., Duku, O. & Gillo, a. L., 1978. Ebola haemorrhagic fever in Sudan, 1976. Report of a WHO/International Study Team. *Bulletin of the World Health Organization*, 56(2), pp.247–270.

Diao, F. et al., 2007. Negative regulation of MDA5- but not RIG-I-mediated innate antiviral signaling by the dihydroxyacetone kinase. *Proceedings of the National Academy of Sciences of the United States of America*, 104(28), pp.11706–11711.

Dixon, M.G. & Schafer, I.J., 2014. Ebola viral disease outbreak--West Africa, 2014. *MMWR. Morbidity and mortality weekly report*, 63(25), pp.548–551.

Edson, R.S., Bundrick, J.B. & Litin, S.C., 2011. Clinical pearls in infectious diseases. *Mayo Clinic proceedings*, 86(3), pp.245–248.

Ehrhardt, C. et al., 2010. Interplay between influenza A virus and the innate immune signaling. *Microbes and infection / Institut Pasteur*, 12(1), pp.81–87.

Emsley, P. & Cowtan, K., 2004. Coot: model-building tools for molecular graphics. *Acta crystallographica. Section D, Biological crystallography*, 60(Pt 12 Pt 1), pp.2126–2132.

Esposito, F. et al., 2013. Hypericum hircinum L. Components as new single-molecule inhibitors of both HIV-1 reverse transcriptase-associated DNA polymerase and ribonuclease H activities. *Pathogens and Disease*, 68, pp.116–124.

Fabozzi, G. et al., 2011. Ebolavirus proteins suppress the effects of small interfering RNA by direct interaction with the mammalian RNA interference pathway. *Journal of virology*, 85(6), pp.2512–2523.

Facino, R.M. et al., 1990. Phytochemical characterization and radical scavenger activity of flavonoids from Helichrysum italicum G. Don (Compositae). *Pharmacological research : the official journal of the Italian Pharmacological Society*, 22(6), pp.709–721.

Fauci, A.S., 2014. Ebola--underscoring the global disparities in health care resources. *The New England journal of medicine*, 371(12), pp.1084–1086.

Feder, H.M.J., Nelson, R. & Reiher, H.W., 1997. Bat bite? *Lancet*, 350(9087), p.1300.

Feisst, C. et al., 2005. Identification of molecular targets of the oligomeric nonprenylated acylphloroglucinols from Myrtus communis and their implication as anti-inflammatory compounds. *The Journal of pharmacology and experimental therapeutics*, 315(1), pp.389–396.

Feldmann, H. et al., 2004. Ebola virus ecology: a continuing mystery. *Trends in microbiology*, 12(10), pp.433–437.

Feldmann, H. et al., 1996. Filovirus-induced endothelial leakage triggered by infected monocytes/macrophages. *Journal of virology*, 70(4), pp.2208–2214.

Feng, Z. et al., 2007. The VP35 protein of Ebola virus inhibits the antiviral effect mediated by double-stranded RNA-dependent protein kinase PKR. *Journal of virology*, 81(1), pp.182–92.

Fisher-Hoch, S.P. et al., 1992. Pathogenic potential of filoviruses: role of geographic origin of primate host and virus strain. *The Journal of infectious diseases*, 166(4), pp.753–763.

Formenty, P. et al., 1999. Human infection due to Ebola virus, subtype Cote d'Ivoire: Clinical and biologic presentation. *Journal of Infectious Diseases*, 179(SUPPL. 1), pp.S48–S53.

Formenty, P. et al., 2003. Outbreak of Ebola haemorrhagic fever in the Republic of Congo, 2003. *Medecine Tropicale*, 63(3), pp.291–295.

Fowler, R.A. et al., 2014. Caring for critically ill patients with ebola virus disease. Perspectives from West Africa. *American journal of respiratory and critical care medicine*, 190(7), pp.733–737.

Foy, E. et al., 2005. Control of antiviral defenses through hepatitis C virus disruption of retinoic acid-inducible gene-I signaling. *Proceedings of the National Academy of Sciences of the United States of America*, 102(8), pp.2986–2991.

Furuta, Y. et al., 2013. Favipiravir (T-705), a novel viral RNA polymerase inhibitor. *Antiviral research*, 100(2), pp.446–454.

Gaajetaan, G.R., Bruggeman, C.A. & Stassen, F.R., 2012. The type I interferon response

during viral infections: a "SWOT" analysis. *Reviews in medical virology*, 22(2), pp.122–137.

Gack, M.U. et al., 2009. Influenza A virus NS1 targets the ubiquitin ligase TRIM25 to evade recognition by the host viral RNA sensor RIG-I. *Cell host & microbe*, 5(5), pp.439–449.

Geisbert, T.W., Young, H.A., et al., 2003. Mechanisms underlying coagulation abnormalities in ebola hemorrhagic fever: overexpression of tissue factor in primate monocytes/macrophages is a key event. *The Journal of infectious diseases*, 188(11), pp.1618–1629.

Geisbert, T.W., Hensley, L.E., et al., 2003. Pathogenesis of Ebola hemorrhagic fever in cynomolgus macaques: evidence that dendritic cells are early and sustained targets of infection. *The American journal of pathology*, 163(6), pp.2347–2370.

Geisbert, T.W. et al., 2010. Postexposure protection of non-human primates against a lethal Ebola virus challenge with RNA interference: a proof-of-concept study. *Lancet*, 375(9729), pp.1896–1905.

Georges, A.J. et al., 1998. [Ebola virus: what the practitioner needs to know]. *Medecine tropicale : revue du Corps de sante colonial*, 58(2), pp.177–186.

Gerlier, D. & Lyles, D.S., 2011. Interplay between innate immunity and negative-strand RNA viruses: towards a rational model. *Microbiology and molecular biology reviews : MMBR*, 75(3), pp.468–90, second page of table of contents.

Goeijenbier, M. et al., 2014. Ebola virus disease : a review on epidemiology , symptoms , treatment and pathogenesis. , (9), pp.442–448.

Gonzalez, J.P., Pourrut, X. & Leroy, E., 2007. Ebolavirus and other filoviruses. *Current topics in microbiology and immunology*, 315, pp.363–387.

Goodsell, D.S., 2014. Ebola Virus Proteins. *RCSB PDB Molecule of the Month*, 17, p.403.

Grard, G. et al., 2011. Emergence of divergent Zaire ebola virus strains in Democratic Republic of the Congo in 2007 and 2008. *The Journal of infectious diseases*, 204 Suppl , pp.S776–84.

Groseth, A., Feldmann, H. & Strong, J.E., 2007. The ecology of Ebola virus. *Trends in microbiology*, 15(9), pp.408–416.

Le Guenno, B. et al., 1995. Isolation and partial characterisation of a new strain of Ebola virus. *The Lancet*, 345(8960), pp.1271–1274.

Gupta, M., Spiropoulou, C. & Rollin, P.E., 2007. Ebola virus infection of human PBMCs causes massive death of macrophages, CD4 and CD8 T cell sub-populations in vitro. *Virology*, 364(1), pp.45–54.

Haasnoot, J. et al., 2007. The ebola virus VP35 protein is a suppressor of RNA silencing. *PLoS Pathogens*, 3(6), pp.0794–0803.

Hale, B.G. et al., 2008. Structure of an avian influenza A virus NS1 protein effector domain. *Virology*, 378(1), pp.1–5.

Hale, B.G. et al., 2008. The multifunctional NS1 protein of influenza A viruses. *Journal of General Virology*, 89, pp.2359–2376.

Haller, O. & Kochs, G., 2002. Interferon-induced mx proteins: dynamin-like GTPases with antiviral activity. *Traffic (Copenhagen, Denmark)*, 3(10), pp.710–717.

Haller, O., Kochs, G. & Weber, F., 2006. The interferon response circuit: induction and suppression by pathogenic viruses. *Virology*, 344(1), pp.119–30. Available at: http://www.ncbi.nlm.nih.gov/pubmed/16364743 [Accessed June 16, 2011].

Harcourt, B.H., Sanchez, A. & Offermann, M.K., 1998. Ebola virus inhibits induction of genes by double-stranded RNA in endothelial cells. *Virology*, 252(1), pp.179–188.

Harcourt, B.H., Sanchez, A. & Offermann, M.K., 1999. Ebola virus selectively inhibits responses to interferons, but not to interleukin-1beta, in endothelial cells. *Journal of virology*, 73(4), pp.3491–3496.

Hartlieb, B. et al., 2003. Oligomerization of Ebola virus VP30 is essential for viral transcription and can be inhibited by a synthetic peptide. *The Journal of biological chemistry*, 278(43), pp.41830–41836.

Hartman, A.L., Bird, B.H., et al., 2008. Inhibition of IRF-3 activation by VP35 is critical for the high level of virulence of ebola virus. *Journal of virology*, 82(6), pp.2699–704.

Hartman, A.L. et al., 2006. Reverse genetic generation of recombinant Zaire Ebola viruses containing disrupted IRF-3 inhibitory domains results in attenuated virus growth in vitro and higher levels of IRF-3 activation without inhibiting viral transcription or replication. *Journal of virology*, 80(13), pp.6430–6440.

Hartman, A.L., Ling, L., et al., 2008. Whole-genome expression profiling reveals that inhibition of host innate immune response pathways by Ebola virus can be reversed by a single amino acid change in the VP35 protein. *Journal of virology*, 82(11), pp.5348–58.

Hartman, A.L., Towner, J.S. & Nichol, S.T., 2004. A C-terminal basic amino acid motif of Zaire ebolavirus VP35 is essential for type I interferon antagonism and displays high identity with the RNA-binding domain of another interferon antagonist, the NS1 protein of influenza a virus. *Virology*, 328, pp.177–184.

Hastie, K.M. et al., 2012. Hiding the evidence: two strategies for innate immune evasion by hemorrhagic fever viruses. *Current opinion in virology*, 2(2), pp.151–156.

Hayward, J.A. et al., 2013. Identification of diverse full-length endogenous betaretroviruses in megabats and microbats. *Retrovirology*, 10, p.35.

Heald, A.E. et al., 2014. Safety and pharmacokinetic profiles of phosphorodiamidate morpholino oligomers with activity against ebola virus and marburg virus: results of two single-ascending-dose studies. *Antimicrobial agents and chemotherapy*, 58(11), pp.6639–6647.

Hensley, L.E. et al., 2002. Proinflammatory response during Ebola virus infection of primate models: possible involvement of the tumor necrosis factor receptor superfamily. *Immunology letters*, 80(3), pp.169–179.

Hillesheim, A. et al., 2014. β-catenin promotes the type I IFN synthesis and the IFN-dependent signaling response but is suppressed by influenza A virus-induced RIG-I/NF-κB signaling. *Cell communication and signaling : CCS*, 12(1), p.29.

Hornung, V. et al., 2006. 5'-Triphosphate RNA is the ligand for RIG-I. *Science (New York, N.Y.)*, 314(5801), pp.994–997.

Huggins, J.W., 1989. Prospects for treatment of viral hemorrhagic fevers with ribavirin, a broad-spectrum antiviral drug. *Reviews of infectious diseases*, 11 Suppl 4, pp.S750–61.

Isaacs, A. & Lindenmann, J., 1957. Virus interference. I. The interferon. *Proceedings of the Royal Society of London. Series B, Containing papers of a Biological character. Royal Society (Great Britain)*, 147(927), pp.258–267.

Jahrling, P.B. et al., 2007. Ebola hemorrhagic fever: evaluation of passive immunotherapy in nonhuman primates.

The Journal of infectious diseases, 196 Suppl , pp.S400–3.

Jahrling, P.B. et al., 1999. Evaluation of immune globulin and recombinant interferon-alpha2b for treatment of experimental Ebola virus infections. *The Journal of infectious diseases*, 179 Suppl , pp.S224–34.

Johnson, E. et al., 1995. Lethal experimental infections of rhesus monkeys by aerosolized Ebola virus. *International journal of experimental pathology*, 76(4), pp.227–236.

Johnson, N., Arechiga-Ceballos, N. & Aguilar-Setien, A., 2014. Vampire bat rabies: ecology, epidemiology and control. *Viruses*, 6(5), pp.1911–1928.

Kang, D. et al., 2002. mda-5: An interferon-inducible putative RNA helicase with double-stranded RNA-dependent ATPase activity and melanoma growth-suppressive properties. *Proceedings of the National Academy of Sciences of the United States of America*, 99(2), pp.637–642.

Kash, J.C. et al., 2006. Global suppression of the host antiviral response by Ebola- and Marburgviruses: increased antagonism of the type I interferon response is associated with enhanced virulence. *Journal of virology*, 80(6), pp.3009–3020.

Kato, H. et al., 2005. Cell type-specific involvement of RIG-I in antiviral response. *Immunity*, 23(1), pp.19–28.

Kato, H. et al., 2006. Differential roles of MDA5 and RIG-I helicases in the recognition of RNA viruses. *Nature*, 441(7089), pp.101–105.

Kawai, T. & Akira, S., 2007. TLR signaling. *Seminars in immunology*, 19(1), pp.24–32.

Khan, A.S. et al., 1999. The reemergence of Ebola hemorrhagic fever, Democratic Republic of the Congo, 1995. *Journal of Infectious Diseases*, 179(SUPPL. 1), pp.S76–S86.

Kim, Y.-M. et al., 2008. UNC93B1 delivers nucleotide-sensing toll-like receptors to endolysosomes. *Nature*, 452(7184), pp.234–238.

Kimberlin, C.R. et al., 2010. Ebolavirus VP35 uses a bimodal strategy to bind dsRNA for innate immune suppression. *Proceedings of the National Academy of Sciences of the United States of America*, 107(1), pp.314–9.

Kollman, P.A. et al., 2000. Calculating structures and free energies of complex molecules: combining molecular mechanics and continuum models. *Accounts of chemical research*, 33(12), pp.889–897.

Komuro, A. & Horvath, C.M., 2006. RNA- and virus-independent inhibition of antiviral signaling by RNA helicase LGP2. *Journal of virology*, 80(24), pp.12332–12342.

Kortepeter, M.G., Bausch, D.G. & Bray, M., 2011. Basic clinical and laboratory features of filoviral hemorrhagic fever. *The Journal of infectious diseases*, 204 Suppl , pp.S810–6.

Kubo, M., Hanada, T. & Yoshimura, A., 2003. Suppressors of cytokine signaling and immunity. *Nature immunology*, 4(12), pp.1169–1176.

Kuhn, J.H., 2008. Filoviruses. A compendium of 40 years of epidemiological, clinical, and laboratory studies. *Archives of virology. Supplementum*, 20, pp.13–360.

Kuhn, J.H. et al., 2010. Proposal for a revised taxonomy of the family Filoviridae: Classification, names of taxa and viruses, and virus abbreviations. *Archives of Virology*, 155, pp.2083–2103.

Kuo, R.-L. & Krug, R.M., 2009. Influenza a virus polymerase is an integral component of the CPSF30-NS1A protein complex in

infected cells. *Journal of virology*, 83(4), pp.1611–1616.

Lamunu, M. et al., 2004. Containing a haemorrhagic fever epidemic: the Ebola experience in Uganda (October 2000–January 2001). *International Journal of Infectious Diseases*, 8(1), pp.27–37.

Leroy, E.M. et al., 2009. Human Ebola outbreak resulting from direct exposure to fruit bats in Luebo, Democratic Republic of Congo, 2007. *Vector borne and zoonotic diseases (Larchmont, N.Y.)*, 9(6), pp.723–728.

Leslie, A.G.W., 2006. The integration of macromolecular diffraction data. *Acta crystallographica. Section D, Biological crystallography*, 62(Pt 1), pp.48–57.

Leung, D.W. et al., 2010. Ebolavirus VP35 is a multifunctional virulence factor. *Virulence*, 1(6), pp.526–531.

Leung, D.W. et al., 2010. Structural basis for dsRNA recognition and interferon antagonism by Ebola VP35. , 17(2), pp.165–172.

Leung, D.W. et al., 2009. Structure of the Ebola VP35 interferon inhibitory domain. , 106(2), pp.411–416.

Li, S. et al., 2006. Binding of the influenza A virus NS1 protein to PKR mediates the inhibition of its activation by either PACT or double-stranded RNA. *Virology*, 349(1), pp.13–21.

Lin, D., Lan, J. & Zhang, Z., 2007. Structure and function of the NS1 protein of influenza A virus. *Acta Biochimica et Biophysica Sinica*, 39(3), pp.135–162.

Liu, H. & Yao, X., 2010. Molecular basis of the interaction for an essential subunit PA-PB1 in influenza virus RNA polymerase: insights from molecular dynamics simulation and free energy calculation. *Molecular pharmaceutics*, 7(1), pp.75–85.

Liu, P. et al., 2007. Retinoic acid-inducible gene I mediates early antiviral response and Toll-like receptor 3 expression in respiratory syncytial virus-infected airway epithelial cells. *Journal of virology*, 81(3), pp.1401–1411.

Lovell, S.C. et al., 2003. Structure validation by Calpha geometry: phi,psi and Cbeta deviation. *Proteins*, 50(3), pp.437–450.

Ludwig, S. et al., 2002. The influenza A virus NS1 protein inhibits activation of Jun N-terminal kinase and AP-1 transcription factors. *Journal of virology*, 76(21), pp.11166–11171.

Ludwig, S. & Wolff, T., 2009. Influenza A virus TRIMs the type I interferon response. *Cell host & microbe*, 5(5), pp.420–421.

Luthra, P. et al., 2013. Mutual antagonism between the Ebola virus VP35 protein and the RIG-I activator PACT determines infection outcome. *Cell Host Microbe*, 14(1), pp.74–84.

MacNeil, A. et al., 2010. Proportion of Deaths and Clinical Features in Bundibugyo Ebola Virus Infection, Uganda. *Emerging Infectious Disease journal*, 16(12), p.1969.

Maffei Facino, R. et al., 1988. Anti-erythematous and photoprotective activities in guinea pigs and in man of topically applied flavonoids from Helichrysum italicum G. Don. *Acta Therapeutica*, 14(4), pp.323–345. Available at: http://www.scopus.com/inward/record.url?eid=2-s2.0-0024230618&partnerID=40&md5=3e25a8bcb72578c9cebb2c36ad56c534.

Mahanty, S. et al., 2003. Cutting edge: impairment of dendritic cells and adaptive immunity by Ebola and Lassa viruses. *Journal of immunology (Baltimore, Md. : 1950)*, 170(6), pp.2797–2801.

Mahanty, S. & Bray, M., 2004. Reviews Pathogenesis of filoviral haemorrhagic fevers. , 4(August), pp.487–498.

Mahendradhata, Y., 2005. *Emerging Infectious Diseases*, Elsevier Inc.

Martinez, M.J. et al., 2011. Role of VP30 phosphorylation in the Ebola virus replication cycle. *The Journal of infectious diseases*, 204 Suppl , pp.S934–40.

Matskevich, A.A. & Moelling, K., 2007. Dicer is involved in protection against influenza A virus infection. *The Journal of general virology*, 88(Pt 10), pp.2627–2635.

McCarty, C.L. et al., 2014. Response to importation of a case of Ebola virus disease--Ohio, October 2014. *MMWR. Morbidity and mortality weekly report*, 63(46), pp.1089–1091.

McCormick, J.B. et al., 1983. Biologic differences between strains of Ebola virus from Zaire and Sudan. *The Journal of infectious diseases*, 147(2), pp.264–267.

McCoy, A.J. et al., 2007. Phaser crystallographic software. *Journal of applied crystallography*, 40(Pt 4), pp.658–674.

Melchjorsen, J. et al., 2005. Activation of innate defense against a paramyxovirus is mediated by RIG-I and TLR7 and TLR8 in a cell-type-specific manner. *Journal of virology*, 79(20), pp.12944–12951.

Mibayashi, M. et al., 2007. Inhibition of retinoic acid-inducible gene I-mediated induction of beta interferon by the NS1 protein of influenza A virus. *Journal of virology*, 81(2), pp.514–524.

Min, J.-Y. et al., 2007. A site on the influenza A virus NS1 protein mediates both inhibition of PKR activation and temporal regulation of viral RNA synthesis. *Virology*, 363(1), pp.236–243.

Min, J.-Y. & Krug, R.M., 2006. The primary function of RNA binding by the influenza A virus NS1 protein in infected cells: Inhibiting the 2'-5' oligo (A) synthetase/RNase L pathway. *Proceedings of the National Academy of Sciences of the United States of America*, 103(18), pp.7100–7105.

Mitchell, W.M. & Carter, W. a, 2014. The quest for effective Ebola treatment: Ebola VP35 is an evidence-based target for dsRNA drugs. *Emerging Microbes & Infections*, 3(10), p.e77.

Mohamadi, F. et al., 1990. Macromodel—an integrated software system for modeling organic and bioorganic molecules using molecular mechanics. *Journal of Computational Chemistry*, 11(4), pp.440–467. Available at: http://dx.doi.org/10.1002/jcc.540110405.

Mohamadzadeh, M. et al., 2006. Activation of triggering receptor expressed on myeloid cells-1 on human neutrophils by marburg and ebola viruses. *Journal of virology*, 80(14), pp.7235–7244.

Mohamadzadeh, M., Chen, L. & Schmaljohn, A.L., 2007. How Ebola and Marburg viruses battle the immune system. *Nature reviews. Immunology*, 7(7), pp.556–567.

Moller, P. et al., 2005. Homo-oligomerization of Marburgvirus VP35 is essential for its function in replication and transcription. *Journal of virology*, 79(23), pp.14876–14886.

Muhlberger, E. et al., 1999. Comparison of the transcription and replication strategies of marburg virus and Ebola virus by using artificial replication systems. *Journal of virology*, 73(3), pp.2333–2342.

Mühlberger, E., 2007. Filovirus replication and transcription. *Futur V*, 2(2), pp.205–215.

Mupapa, K. et al., 1999. Treatment of Ebola hemorrhagic fever with blood

transfusions from convalescent patients. International Scientific and Technical Committee. *The Journal of infectious diseases*, 179 Suppl , pp.S18–23.

Murshudov, G.N., Vagin, A.A. & Dodson, E.J., 1997. Refinement of macromolecular structures by the maximum-likelihood method. *Acta crystallographica. Section D, Biological crystallography*, 53(Pt 3), pp.240–255.

Muyembe-Tamfum, J.J. et al., 1999. Ebola outbreak in Kikwit, Democratic Republic of the Congo: discovery and control measures. *The Journal of infectious diseases*, 179 Suppl , pp.S259–62.

Muyembe-Tamfum, J.J. et al., 2012. Ebola virus outbreaks in Africa: past and present. *The Onderstepoort journal of veterinary research*, 79(2), p.451.

Ndambi, R. et al., 1999. Epidemiologic and clinical aspects of the Ebola virus epidemic in Mosango, Democratic Republic of the Congo, 1995. *The Journal of infectious diseases*, 179 Suppl , pp.S8–10.

Negredo, A. et al., 2011. Discovery of an ebolavirus-like filovirus in europe. *PLoS pathogens*, 7(10), p.e1002304.

Nkoghe, D. et al., 2011. A limited outbreak of Ebola haemorrhagic fever in Etoumbi, Republic of Congo, 2005. *Transactions of the Royal Society of Tropical Medicine and Hygiene*, 105(8), pp.466–472.

Nkoghe, D. et al., 2005. Multiple Ebola virus haemorrhagic fever outbreaks in Gabon, from October 2001 to April 2002. *Bulletin de la Societe de Pathologie Exotique*, 98(3), pp.224–229.

Oczkowski, S., 2007. The bitten man: Reflections on international health. *Open medicine : a peer-reviewed, independent, open-access journal*, 1(3), pp.e160–3.

Oestereich, L. et al., 2014. Successful treatment of advanced Ebola virus infection with T-705 (favipiravir) in a small animal model. *Antiviral research*, 105, pp.17–21.

Olejnik, J. et al., 2011. Intracellular Events and Cell Fate in Filovirus Infection. *Viruses*, 3(8), pp.1501–1531.

Omatsu, T. et al., 2007. Biological characters of bats in relation to natural reservoir of emerging viruses. *Comparative immunology, microbiology and infectious diseases*, 30(5-6), pp.357–374.

Onoguchi, K. et al., 2007. Viral infections activate types I and III interferon genes through a common mechanism. *The Journal of biological chemistry*, 282(10), pp.7576–7581.

Onyango, C.O. et al., 2007. Laboratory diagnosis of Ebola hemorrhagic fever during an outbreak in Yambio, Sudan, 2004. *The Journal of infectious diseases*, 196 Suppl , pp.S193–8.

Palese, P. & Shaw, M.L., 2007. Orthomyxoviridae: the viruses and their replication. In Fields Virology, ed. *D. M. Knipe & P. M. Howley*. Philadelphia: Lippincott Williams & Wilkins, pp. 1647–1689.

Parra, J.M., Salmerón, O.J. & Velasco, M., 2014. The First Case of Ebola Virus Disease Acquired outside Africa. *New England Journal of Medicine*, 371(25), pp.2439–2440.

Patel, C. V et al., 2000. PACT, a stress-modulated cellular activator of interferon-induced double-stranded RNA-activated protein kinase, PKR. *The Journal of biological chemistry*, 275(48), pp.37993–37998.

Peana, A.T., Moretti, M.D. & Juliano, C., 1999. Chemical composition and antimicrobial action of the essential oils of Salvia

desoleana and S. sclarea. *Planta medica*, 65(8), pp.752–754.

Pichlmair, A. et al., 2006. RIG-I-mediated antiviral responses to single-stranded RNA bearing 5'-phosphates. *Science (New York, N.Y.)*, 314(5801), pp.997–1001.

Platanias, L.C., 2005. Mechanisms of type-I- and type-II-interferon-mediated signalling. *Nature reviews. Immunology*, 5(5), pp.375–386.

Pourrut, X. et al., 2007. Spatial and temporal patterns of Zaire ebolavirus antibody prevalence in the possible reservoir bat species. *The Journal of infectious diseases*, 196 Suppl , pp.S176–83.

Pourrut, X. et al., 2005. The natural history of Ebola virus in Africa. *Microbes and infection / Institut Pasteur*, 7(7-8), pp.1005–1014.

Prins, K.C., Binning, J.M., et al., 2010. Basic residues within the ebolavirus VP35 protein are required for its viral polymerase cofactor function. *Journal of virology*, 84(20), pp.10581–91.

Prins, K.C., Delpeut, S., et al., 2010. Mutations abrogating VP35 interaction with double-stranded RNA render Ebola virus avirulent in guinea pigs. *Journal of virology*, 84(6), pp.3004–15.

Prins, K.C., Cardenas, W.B. & Basler, C.F., 2009. Ebola virus protein VP35 impairs the function of interferon regulatory factor-activating kinases IKKepsilon and TBK-1. *Journal of virology*, 83(7), pp.3069–3077.

Qiu, X. et al., 2014. Reversion of advanced Ebola virus disease in nonhuman primates with ZMapp. *Nature*, 514(7520), pp.47–53.

Qiu, Y. & Krug, R.M., 1994. The influenza virus NS1 protein is a poly(A)-binding protein that inhibits nuclear export of mRNAs containing poly(A). *Journal of virology*, 68(4), pp.2425–2432.

Ramanan, P. et al., 2011. Filoviral immune evasion mechanisms. *Viruses*, 3(9), pp.1634–49.

Ramanan, P. et al., 2012. Structural basis for Marburg virus VP35-mediated immune evasion mechanisms. *Proceedings of the National Academy of Sciences of the United States of America*, 109(50), pp.20661–6.

Ramos, I. & Fernandez-Sesma, A., 2012. Innate immunity to H5N1 influenza viruses in humans. *Viruses*, 4(12), pp.3363–3388.

Randall, R.E. & Goodbourn, S., 2008. Interferons and viruses: An interplay between induction, signalling, antiviral responses and virus countermeasures. *Journal of General Virology*, 89, pp.1–47.

Reed, D.S. et al., 2004. Depletion of peripheral blood T lymphocytes and NK cells during the course of ebola hemorrhagic Fever in cynomolgus macaques. *Viral immunology*, 17(3), pp.390–400.

Reid, S.P. et al., 2006. Ebola virus VP24 binds karyopherin alpha1 and blocks STAT1 nuclear accumulation. *Journal of virology*, 80(11), pp.5156–5167.

Reikine, S., Nguyen, J.B. & Modis, Y., 2014. Pattern Recognition and Signaling Mechanisms of RIG-I and MDA5. *Frontiers in immunology*, 5(July), p.342.

Richman, D.D. et al., 1983. Antigenic analysis of strains of Ebola virus: identification of two Ebola virus serotypes. *The Journal of infectious diseases*, 147(2), pp.268–271.

Roddy, P. et al., 2012. Clinical Manifestations and Case Management of Ebola Haemorrhagic Fever Caused by a Newly Identified Virus Strain, Bundibugyo, Uganda, 2007–2008. *PLoS ONE*, 7(12), p.e52986.

Rosa, A. et al., 2003. Antioxidant activity of oligomeric acylphloroglucinols from

Myrtus communis L. *Free radical research*, 37(9), pp.1013–1019.

Rouquet, P. et al., 2005. Wild Animal Mortality Monitoring and Human Ebola Outbreaks, Gabon and Republic of Congo, 2001–2003. *Emerging Infectious Disease journal*, 11(2), p.283.

Rückle, A. et al., 2012. The NS1 protein of influenza A virus blocks RIG-I-mediated activation of the noncanonical NF-κB pathway and p52/RelB-dependent gene expression in lung epithelial cells. *Journal of virology*, 86(18), pp.10211–7.

Ryabchikova, E.I., Kolesnikova, L. V & Luchko, S. V, 1999. An analysis of features of pathogenesis in two animal models of Ebola virus infection. *The Journal of infectious diseases*, 179 Suppl , pp.S199–202.

Saito, T. et al., 2007. Regulation of innate antiviral defenses through a shared repressor domain in RIG-I and LGP2. *Proceedings of the National Academy of Sciences of the United States of America*, 104(2), pp.582–587.

Sanchez, A. et al., 2004. Analysis of human peripheral blood samples from fatal and nonfatal cases of Ebola (Sudan) hemorrhagic fever: cellular responses, virus load, and nitric oxide levels. *Journal of virology*, 78(19), pp.10370–10377.

Sarkar, D., Desalle, R. & Fisher, P.B., 2008. Evolution of MDA-5/RIG-I-dependent innate immunity: independent evolution by domain grafting. *Proceedings of the National Academy of Sciences of the United States of America*, 105(44), pp.17040–17045.

Satterly, N. et al., 2007. Influenza virus targets the mRNA export machinery and the nuclear pore complex. *Proceedings of the National Academy of Sciences of the United States of America*, 104(6), pp.1853–1858.

Schlee, M. et al., 2009. Recognition of 5' triphosphate by RIG-I helicase requires short blunt double-stranded RNA as contained in panhandle of negative-strand virus. *Immunity*, 31(1), pp.25–34.

Schümann, M., Gantke, T. & Mühlberger, E., 2009. Ebola virus VP35 antagonizes PKR activity through its C-terminal interferon inhibitory domain. *Journal of virology*, 83(17), pp.8993–8997.

Seth, R.B. et al., 2005. Identification and characterization of MAVS, a mitochondrial antiviral signaling protein that activates NF-kappaB and IRF 3. *Cell*, 122(5), pp.669–682.

Shoemaker, T. et al., 2012. Reemerging Sudan Ebola Virus Disease in Uganda, 2011. *Emerging Infectious Diseases*, 18(9), pp.1480–1483.

Shuai, K. & Liu, B., 2005. Regulation of gene-activation pathways by PIAS proteins in the immune system. *Nature reviews. Immunology*, 5(8), pp.593–605.

Silverman, R.H., 1994. Fascination with 2-5A-dependent RNase: a unique enzyme that functions in interferon action. *Journal of interferon research*, 14(3), pp.101–104.

Silverman, R.H., 2007. Viral encounters with 2',5'-oligoadenylate synthetase and RNase L during the interferon antiviral response. *Journal of virology*, 81(23), pp.12720–12729.

Smith, I. & Wang, L.-F., 2013. Bats and their virome: an important source of emerging viruses capable of infecting humans. *Current opinion in virology*, 3(1), pp.84–91.

Smither, S.J. et al., 2014. Post-exposure efficacy of oral T-705 (Favipiravir) against inhalational Ebola virus infection in a mouse model. *Antiviral research*, 104, pp.153–155.

Stahelin, R. V, 2014. Membrane binding and bending in Ebola VP40 assembly and egress. *Frontiers in microbiology*, 5, p.300.

Stein, N., 2008. {\it CHAINSAW}: a program for mutating pdb files used as templates in molecular replacement. *Journal of Applied Crystallography*, 41(3), pp.641–643. Available at: http://dx.doi.org/10.1107/S0021889808006985.

Stein, R. a., 2015. What is Ebola? *International Journal of Clinical Practice*, 69(March), pp.49–58.

Still, W.C. et al., 1990. Semianalytical treatment of solvation for molecular mechanics and dynamics. *J. Am. Chem. Soc.*, 112, pp.6127–6129.

Takada, A., 2012. Filovirus tropism: cellular molecules for viral entry. *Frontiers in microbiology*, 3, p.34.

Takahasi, K. et al., 2008. Nonself RNA-sensing mechanism of RIG-I helicase and activation of antiviral immune responses. *Molecular cell*, 29(4), pp.428–440.

Takeuchi, O. & Akira, S., 2008. MDA5/RIG-I and virus recognition. *Current opinion in immunology*, 20(1), pp.17–22.

Talloczy, Z., Virgin, H.W. 4th & Levine, B., 2006. PKR-dependent autophagic degradation of herpes simplex virus type 1. *Autophagy*, 2(1), pp.24–29.

Talon, J. et al., 2000. Activation of interferon regulatory factor 3 is inhibited by the influenza A virus NS1 protein. *Journal of virology*, 74(17), pp.7989–7996.

Towner, J.S. et al., 2009. Isolation of genetically diverse Marburg viruses from Egyptian fruit bats. *PLoS pathogens*, 5(7), p.e1000536.

Towner, J.S. et al., 2004. Rapid diagnosis of Ebola hemorrhagic fever by reverse transcription-PCR in an outbreak setting and assessment of patient viral load as a predictor of outcome. *Journal of virology*, 78(8), pp.4330–4341.

Uze, G. & Monneron, D., 2007. IL-28 and IL-29: newcomers to the interferon family. *Biochimie*, 89(6-7), pp.729–734.

Vandegraaff, N. et al., 2001. Specific inhibition of human immunodeficiency virus type 1 (HIV-1) integration in cell culture: putative inhibitors of HIV-1 integrase. *Antimicrobial agents and chemotherapy*, 45(9), pp.2510–2516.

Versteeg, G. a & García-Sastre, A., 2010. Viral tricks to grid-lock the type I interferon system. *Current opinion in microbiology*, 13(4), pp.508–16.

Wahyuni, T.S. et al., 2013. Antiviral activities of Indonesian medicinal plants in the East Java region against hepatitis C virus. *Virology journal*, 10, p.259.

Wamala, J.F. et al., 2010. Ebola Hemorrhagic Fever Associated with Novel Virus Strain, Uganda, 2007–2008. *Emerging Infectious Disease journal*, 16(7), p.1087.

Wang, X. et al., 2002. Functional replacement of the carboxy-terminal two-thirds of the influenza A virus NS1 protein with short heterologous dimerization domains. *Journal of virology*, 76(24), pp.12951–12962.

Warren, T.K. et al., 2010. Advanced antisense therapies for postexposure protection against lethal filovirus infections. *Nature medicine*, 16(9), pp.991–994.

Warren, T.K. et al., 2014. Protection against filovirus diseases by a novel broad-spectrum nucleoside analogue BCX4430. *Nature*, 508(7496), pp.402–405.

Weber, F., Haller, O. & Kochs, G., 2000. MxA GTPase blocks reporter gene expression of reconstituted Thogoto virus

ribonucleoprotein complexes. *Journal of virology*, 74(1), pp.560–563.

Weingartl, H.M. et al., 2012. Transmission of Ebola virus from pigs to non-human primates. *Scientific reports*, 2, p.811.

WHO Ebola Response Team, 2014. Ebola Virus Disease in West Africa — The First 9 Months of the Epidemic and Forward Projections. *New England Journal of Medicine*, 371(16), pp.1481–1495.

Williams, B.R., 1999. PKR; a sentinel kinase for cellular stress. *Oncogene*, 18(45), pp.6112–6120.

Winn, M.D. et al., 2011. Overview of the CCP4 suite and current developments. *Acta crystallographica. Section D, Biological crystallography*, 67(Pt 4), pp.235–242.

World Health Organization (WHO), 2014. Ebola virus disease. *Fact sheet N°103*. Available at: http://www.who.int/mediacentre/factsheets/fs103/en/.

World Health Organization (WHO), 2012. Outbreak news. Ebola haemorrhagic fever, Democratic Republic of the Congo. *Wkly Epidemiol Rec*, 87(36), pp.338–339.

Xiong, H.-R. et al., 2011. The effect of emodin, an anthraquinone derivative extracted from the roots of Rheum tanguticum, against herpes simplex virus in vitro and in vivo. *Journal of ethnopharmacology*, 133(2), pp.718–723.

Yamayoshi, S. et al., 2008. Ebola virus matrix protein VP40 uses the COPII transport system for its intracellular transport. *Cell host & microbe*, 3(3), pp.168–177.

Yarmolinsky, L. et al., 2012. Potent antiviral flavone glycosides from Ficus benjamina leaves. *Fitoterapia*, 83(2), pp.362–367.

Yin, C. et al., 2007. Conserved surface features form the double-stranded RNA binding site of non-structural protein 1 (NS1) from influenza A and B viruses. *The Journal of biological chemistry*, 282(28), pp.20584–20592.

Yoneyama, M. et al., 2004. The RNA helicase RIG-I has an essential function in double-stranded RNA-induced innate antiviral responses. *Nature immunology*, 5(7), pp.730–737.

Yoneyama, M. & Fujita, T., 2010. Recognition of viral nucleic acids in innate immunity. *Reviews in Medical Virology*, pp.4–22.

Yoneyama, M. & Fujita, T., 2009. RNA recognition and signal transduction by RIG-I-like receptors. *Immunological reviews*, 227(1), pp.54–65.

Zaki, S.R. & Goldsmith, C.S., 1999. Pathologic features of filovirus infections in humans. *Current topics in microbiology and immunology*, 235, pp.97–116.

Zampieri, C. a, Sullivan, N.J. & Nabel, G.J., 2007. Immunopathology of highly virulent pathogens: insights from Ebola virus. *Nature immunology*, 8(11), pp.1159–1164.

Zinzula, L. et al., 2012. dsRNA binding characterization of full length recombinant wild type and mutants Zaire ebolavirus VP35. *Antiviral research*, 93(3), pp.354–63.

Zinzula, L. et al., 2009. Purification and functional characterization of the full length recombinant Ebola virus VP35 protein expressed in E. coli. *Protein expression and purification*, 66(1), pp.113–9.

Zinzula, L. & Tramontano, E., 2013. Strategies of highly pathogenic RNA viruses to block dsRNA detection by RIG-I-like receptors: hide, mask, hit. *Antiviral research*, 100(3), pp.615–35.